Doctorado en Oceanografía y Cambio Global
Universidad de Las Palmas de Gran Canaria

DOCTORAL THESIS

Impact of recent volcanic eruptions in the Canary Islands on the physical-chemical and biological properties of the local marine environment

Author:
Alba González Vega

Supervisors:
Eugenio Fraile Nuez
Jesús M. Arrieta López de Uralde

Las Palmas de Gran Canaria, diciembre de 2023

Dª MAGDALENA SANTANA CASIANO, COORDINADORA DEL PROGRAMA DE DOCTORADO EN OCEANOGRAFÍA Y CAMBIO GLOBAL DE LA UNIVERSIDAD DE LAS PALMAS DE GRAN CANARIA

INFORMA,

De que la Comisión Académica del Programa de Doctorado, en su sesión de fecha   tomó el acuerdo de dar el consentimiento para su tramitación, a la tesis doctoral titulada "Impact of recent volcanic eruptions in the Canary Islands on the physical-chemical and biological properties of the local marine environment" presentada por la doctoranda Dª Alba González Vega, dirigida por el Doctor Eugenio Fraile Nuez y codirigida por el Doctor Jesús M. Arrieta López de Uralde

Y para que así conste, y a efectos de lo previsto en el Artº 11 del Reglamento de Estudios de Doctorado (BOULPGC 04/03/2019) de la Universidad de Las Palmas de Gran Canaria, firmo la presente en Las Palmas de Gran Canaria,

UNIVERSIDAD DE LAS PALMAS DE GRAN CANARIA
ESCUELA DE DOCTORADO

Programa de doctorado en Oceanografía y Cambio Global.

Título de la Tesis: Impact of recent volcanic eruptions in the Canary Islands on the physical-chemical and biological properties of the local marine environment.

Tesis Doctoral presentada por D/Dª Alba González Vega.

Dirigida por el Dr. D. Eugenio Fraile Nuez

Codirigida por el Dr. D. Jesús María Arrieta López de Uralde

Las Palmas de Gran Canaria, a 5 de diciembre de 2023

El Director,   El Codirector,   La Doctoranda,

A mi familia

Table of contents

Summary

Oceanic volcanism is a key process with the potential to alter all properties of the marine environment at different scales, along with a great impact on global biogeochemical budgets. The interaction between volcanoes and the ocean can occur in different forms: submarine volcanic eruptions, hydrothermal emissions, or the arrival of lava and ashes from a subaerial eruption to the ocean. However, the direct observation and instrumental monitoring of these processes is not a common occurrence, as they usually present important logistical challenges.

In the Canary Islands, an archipelago with active intraplate volcanism, two eruptions have taken place this century so far, at the two youngest and most active islands: a submarine eruption at the southern coast of El Hierro island in 2011, and a subaerial eruption at the area of Cumbre Vieja in La Palma in 2021. In the first case, the submarine volcano named Tagoro erupted during 6 months, with dramatic consequences for the surrounding marine environment. However, after the eruption ended, the volcano evolved towards a hydrothermal system with diffuse flow which remains active, and the ecosystem was completely recovered in a few years. In the case of La Palma, the lava flows emitted from the subaerial volcano during 85 days of eruption made their way downslope until they reached the ocean, forming two lava deltas; these are new emerged platforms formed by the deposition of new volcanic materials over previous oceanic seafloor.

In this thesis, we present three oceanographic studies related to these two juvenile volcanoes. The studies are presented in a chronological manner and explore the three main types of volcano-ocean interactions: the submarine eruption of Tagoro volcano (El Hierro), the posterior hydrothermal emissions from the same volcano, and the formation of lava deltas at La Palma.

First, we explore the dramatic consequences of the submarine eruption at El Hierro on the dissolved oxygen content of the surrounding oceanic area. The volcanic emissions carried important amounts of reduced chemical species which were quickly oxidized in contact with the seawater. This led to suboxic and even anoxic conditions in a wide area around the island, with decreases up to -96% in the oxygen concentration compared to normal conditions. The volcanic emissions generated plumes which were variably distributed around the island depending on local currents. These plumes of deoxygenated waters covered areas larger than 460 km² at times. Mesoscale structures such as eddies also controlled the transport of these plumes: an island-generated anticyclonic eddy was sampled 80 km south from the volcano, where a -8% oxygen decrease was still found.

The second study comprises a 7-years monitoring of the emission of dissolved inorganic nutrients from Tagoro submarine volcano, both during the eruption and during the following post-eruptive stage with hydrothermal emissions, which remains active. Inorganic nutrients were found to be highly enriched in the emitted fluids. Silicate ($Si(OH)_4$) was the most enriched, with a 325-fold increase compared to normal conditions in the area. Phosphate (PO_4) was also highly enriched (10-fold). Nitrogen was mainly emitted in the form of ammonium (NH_4^+), with an almost 100-fold increase, but the oxidized forms nitrate and nitrite (NO_3^- and NO_2^-) also presented enrichments of smaller magnitude. We calculated the yearly fluxes of these nutrients, which are in a range between 0.02 to 3.19 mol m^{-2} year^{-1}. These fluxes are comparable to some of the most important inputs of nutrients to the region, such as the NW-African upwelling.

For the third study, we move on to the 2021 subaerial eruption at La Palma. The formation of the lava deltas from this eruption generated important physical-chemical and biological anomalies in the whole water column of the surrounding oceanic environment. The turbidity levels were particularly remarkable, up to 30 times higher than normal levels. Decreases in pH and dissolved oxygen were observed, while temperature increased and salinity showed a variable behavior. The thermal and haline anomalies were observed up to 6 km distance from shore. The heat input into the water column generated a lava-induced upwelling: the heated waters ascended to surface and were replaced with deeper, colder waters. This effect was limited to the area where new volcanic sediments were present and to a distance of 1 km from the shoreline. However, the ascent of these deeper, nutrient-rich waters did not generate any phytoplankton bloom. In fact, an abrupt decrease in depth-integrated chlorophyll-*a* was observed, suggesting a negative effect on primary producers. Chlorophyll-*a* showed a -41% decrease in just two days after the first lava-seawater contact, and a -69% decrease one month later. This effect was observed at least up to 2.5 km distance from coast (not delimited).

While these three studies represent a valuable contribution to the scientific knowledge of oceanic volcanism, they also have relevant implications for crisis management during volcanic emergencies. We provide some recommendations for oceanographic sampling during a volcanic emergency, drawn from the experience gained by our working team during the two latest volcanic crises of the Canary Islands. We also highlight some important implications of this work towards understanding oceanic ecosystem resilience after volcanic eruptions. Overall, this thesis aims to help strengthen the archipelago's capability to respond effectively to future volcanic eruptions.

General introduction

1.1. Volcanoes and the ocean

Volcanism is a key planetary process transferring heat and matter between the Earth's interior and its surface (Mather, 2015). Volcanoes have played a leading role in many major events of Earth's geological, climatic, and biospheric history, either directly triggering or being involved in a variety of planetary-scale phenomena including climate changes, mass extinctions, and even the establishment of an oxygenated atmosphere (Leckie et al., 2002; Méhay et al., 2009).

Due to the variety of processes involved, volcanoes are studied from a multidisciplinary perspective. While the geological processes are a key aspect, the interaction of volcanoes with their environment calls for a much wider range of disciplines to be involved in their study. In this context, oceanography is key for a comprehensive understanding of volcanic processes, since submarine volcanism is the predominant form of volcanism on Earth (Crisp, 1984).

The interaction between oceans and volcanic outputs occurs mainly through two processes: i) direct outputs from submarine volcanoes and hydrothermal vents; and ii) lava flows from near-shore subaerial eruptions which eventually reach the ocean.

1.1.1. Submarine volcanoes and hydrothermal vents

Our knowledge of volcanic processes largely relays on the observations of subaerial (in-land) eruptions. Yet, about 85% of the Earth's volcanic output occurs beneath the ocean (Crisp, 1984).

Submarine volcanism differs from subaerial volcanism in many aspects. The role of pressure is a key factor, as pressure in the ocean increases by 1 bar for every 10 m increase in depth. These high pressures counteract the escape of volatiles from lava, such as carbon dioxide and water; this, along with the higher density of water compared to air, makes the eruptions much less explosive (Mitchell, 2012). Another important factor is the greater heat capacity and thermal conductivity of water compared to air, which results in a much faster cooling of the lava. Additionally, rates of volcanic output in oceanic areas tend to be greater than rates in continental areas, due a thinner crust among other factors (Crisp, 1984).

Most of the existing knowledge on oceanic volcanism comes from highly evolved deep-sea hydrothermal vents, particularly the high-temperature, high-flow vents known as "black-smokers" (Stetter, 1982; Karl et al., 1988; Rona and Speer, 1989; Mortlock et al., 1993). In contrast, diffuse venting is typically defined as low-

temperature (<50ºC), low-velocity venting (Baker et al., 2016). This type of venting is responsible for 90% of axial heat loss (Elderfield and Schultz, 1996) and has an upmost importance in global biogeochemical budgets, mainly due to their ability to provide important nutrients and metals in a biologically available form (Baker et al., 2016; Lough et al., 2019; Resing et al., 2015; Santana-González et al., 2017; Tilliette et al., 2022).

Regarding their location, 75% of oceanic volcanism occurs in mid-ocean ridge spreading centers (Mitchell, 2012), which are typically 1 to 4 km beneath the sea surface (Resing and Sansone, 1999). The study of mid-ocean ridge hydrothermalism was particularly fruitful during the 1980s and 1990s, which vastly advanced the knowledge of biogeochemical fluxes in the deep ocean (Von Damm et al., 1985; Baker and Massoth, 1987; Baker et al., 1987, 1995; Little et al., 1987; Karl et al., 1989; Lupton et al., 1989, 1995; Massoth et al., 1989; Speer and Rona, 1989; Butterfield et al., 1990; Johnson and Embley, 1990; Rona and Trivett, 1992; Baker, 1994; Embley et al., 1995; Sarradin et al., 1999). However, while this line has not been abandoned (Barreyre et al., 2012; Kipp et al., 2018), more recent studies have also started to pay more attention to intra-plate and shallow submarine volcanism, as the processes and consequences of volcanic outputs on shallower environments can be quite different from those in the deep sea (Wenzhofer et al., 2000; Aliani et al., 2004, 2010; Prol-Ledesma et al., 2004; McCarthy et al., 2005; Kilias et al., 2013; Buck et al., 2018; Esposito et al., 2018; Bellec et al., 2020).

Lastly, while evolved hydrothermal venting is well studied, direct observations of submarine magmatic eruptions are less common, as they usually occur in remote locations and their monitoring represents a logistical challenge (Mitchell, 2012). Submarine eruptions can produce highly corrosive plumes, explosive degassing, bubbling, and even tsunamis (Dziak et al., 2012; Fraile-Nuez et al., 2012; Kubota et al., 2022), which highly difficult their sampling. These conditions can be extremely damaging and deathly for the local ecosystem at the moment of the eruption (Staudigel et al., 2006; Fraile-Nuez et al., 2012). However, once this first impact is overcome, evolved submarine volcanic settings are known to host unique and thriving ecosystems (Karl et al., 1989; Sorokin et al., 1998; Desbruyères et al., 2001; Lam et al., 2004; Tarasov et al., 2005; Staudigel et al., 2006; Baker et al., 2012; Danovaro et al., 2017; Bellec et al., 2020).

1.1.2. Lava-ocean interactions from subaerial volcanism

Subaerial volcanism can also interact with the ocean in many ways. A common example is the effect of ash deposition, which has been shown to hold the potential for oceanic fertilization (Langmann et al., 2010; Witt et al., 2017). However, another one of the most interesting and yet less documented interaction processes is the arrival of lava flows from subaerial eruptions to the ocean.

This feature is common in intra-plate oceanic islands with volcanic activity (Carracedo et al., 2001; Soule et al., 2021; Rodriguez-Gonzalez et al., 2022). The growth of these islands is generally based on a cycle of eruptive activity and erosional periods (Carracedo et al., 1999). Erosion tends to form coastal cliffs and rocky shorelines at the edge of shore platforms; consequently, when an eruption takes place, the lava flow can easily propagate downslope and reach the coastline, spilling over cliffs and filling the shore platforms (Rodríguez-González et al., 2022). This process produces massive inputs of heat and mass to the ocean (Sansone and Resing, 1995).

Unlike submarine volcanoes, where the volcanic outputs are directly injected into the ocean, the lava from subaerial volcanoes that reaches the ocean has undergone degassing and partial solidification on its way to the coast. Still, when the lava flow meets the seawater, the temperature of both fluids can differ in hundreds or even thousands of °C (Román et al., 2022). As a consequence, the lava quickly solidifies as it fills the insular shelf, forming a new platform over previous oceanic territory. This structure is called a lava delta (Soule et al., 2021; Rodriguez-Gonzalez et al., 2022).

Lava deltas can be quite hazardous features, as they increase the submarine slope instability, which can lead to collapse and even the generation of local tsunamis (Chiocci et al., 2008; Bosman et al., 2014). Other hazards such as hydrovolcanic explosions and clouds of toxic gases can also occur (Mattox and Mangan, 1997). Therefore, studying the development of these structures is necessary to ensure the safety of the population during volcanic emergencies, along with later decisions in socioeconomic issues such as coastal planning, navigation safety, and fisheries. However, despite their importance, and precisely due to this hazardous nature, these structures have been scarcely studied, particularly the underwater processes (Soule et al., 2021).

1.2. The Canary Islands, a volcanic archipelago

The Canary Islands are an intraplate archipelago adjacent to the northwest margin of the African continent, at 27–29ºN latitude and 18–13ºW longitude. They are close to a continental margin, rooted on old crust (Jurassic, 170-150 Ma), and on a slow-moving oceanic plate (Carracedo et al., 1998).

The origin of the Canary Islands has been extensively debated over the years (Bosshard and MacFarlane, 1970; McDougall, 1971; Morgan, 1971; Anguita and Hernán, 1975; Fuster, 1975; Araña and Ortiz, 1991; Carracedo et al., 1998; Negredo et al., 2022). Originally, two main lines of thought were developed in parallel, which can broadly be categorized as: i) a hot spot origin, and ii) a series of tectonic models.

Among the tectonic models, the most relevant hypothesis was the propagating fracture model, proposed by Anguita and Hernán (1975) based on a mechanism described by McDougall (1971). This model described a fracture connecting the Canary archipelago to the Atlas Mountains in Morocco, according to which, compressional tension would lead to decompressional melting and magma escape. Other hypotheses that can be categorized as 'tectonic models' were proposed, such as: a local extensional ridge (Fuster, 1975), a set of uplifted tectonic blocks (Araña and Ortiz, 1991), or a rifted zone stretching from Cape Verde to Central Europe (Oyarzun et al., 1997).

However, the line that has received the most support over the years has been the hot spot origin (Schmincke, 1973; Holik et al., 1991; Hoernle and Schmincke, 1993; Watts, 1994; Hoernle et al., 1995; Carracedo et al., 1998). The model was originally proposed by Morgan (1971) based on Wilson's (1963) hot spot concept. They proposed an origin for several intraplate archipelagos consisting of a mantle plume located beneath a moving lithospheric plate, resulting in the upwelling of hot material with volcanic output, which generates islands in a sequenced manner as the plate moves away.

The specific mechanisms that drive this hot spot are still object of debate. Initially, the two main hypotheses proposed were the upwelling of an upper-mantle plume (Morgan, 1971) or a small-scale mantle convection at the edge of cratons (King and Ritsema, 2000). More recent models propose that the ascent of an upper-mantle plume interplays with a strong lithospheric heterogeneity; in other words, magma takes advantage of inherited oceanic fractures (Negredo et al., 2022). This was supported by León et al. (2022), who determined that submarine volcanic edifices follow a trending WNW-ESE direction which coincides with the trajectories of the zones of oceanic fracture.

The formation of each island is characterized by an initial phase of rapid growth (the 'shield-building' stage), followed by a period of quiescence and deep erosion ('erosion gap'), and a 'post-erosional' stage of activity (Carracedo et al., 1998; Negredo et al., 2022). The eastern islands, Fuerteventura and Lanzarote, are at the erosional stage. In the center, Tenerife and Gran Canaria are in the post-shield stage with rejuvenated volcanism, while La Gomera is the only island to not show evidence of recent activity. The western islands, La Palma and El Hierro, are at the most active juvenile shield-building stage (Carracedo et al., 1998; León et al., 2022; Negredo et al., 2022).

According to the existing historical records (last 600 years), there is an average of one volcanic eruption every 25-30 years in the Canary Islands (Sobradelo et al., 2011). This century so far, two eruptions have occurred within a 10-years span, in the two youngest and most active islands: a submarine eruption at El Hierro (2011) and a subaerial eruption at La Palma (2021).

1.3. El Hierro

El Hierro is the youngest of the Canary Islands, located at the south-western end of the archipelago. Its oldest subaerial rocks are dated at 1.12 Ma (Guillou et al., 1996). The island rises from 4000 m below the ocean to 1500 m above sea level and has a subaerial area of 280 km² (López et al., 2012).

The geometry of the island is shaped by three convergent rifts (NE, NW, and S) arranged at roughly 120º, separated by at least three gigantic landslides that formed wide embayments which extend offshore (Guillou et al., 1996; Masson et al., 2002; López et al., 2012). The most recent landslide, on the northwest flank of El Hierro (El Golfo failure), occurred only 15,000 years ago (Masson, 1996). The three-armed rift system is responsible for the recent volcanic eruptions of the island (Guillou et al., 1996; J. Carracedo et al., 2001; López et al., 2012).

Due to its offshore position in the SW end of the archipelago and far away from the NW African upwelling, El Hierro is surrounded by some of the most oligotrophic waters of the Canary Islands (Barton et al., 1998). However, the island holds a marine reserve at the south-west submarine valley ('Mar de las Calmas'), where fishery resources are abundant and only artisan fishing is allowed (Martín-Sosa, 2017).

Even though the island is at an active phase of shield-stage growth, a quiescent period of over 200 years had passed since the last description of an eruption in

historical records, in the year 1793 at Lomo Negro (Villasante-Marcos and Pavón-Carrasco, 2014).

1.3.1. Tagoro submarine volcano (2011)

In 2011, an underwater eruption took place at the southern coast of El Hierro island. This was not only the first known submarine eruption in the Canary region in 600 years of records, but also the first time that a volcanic eruption was fully instrumentally monitored in the archipelago (López et al., 2012).

The pre-eruptive unrest began in July 2011 with the observation of low-magnitude seismicity, initially located in the northern part of the island and subsequently migrating southwards. Since then and during the 96 days prior to the eruption, different precursory signals were exhaustively monitored. A dense multiparametric monitoring network was deployed all over El Hierro island by the Instituto Geográfico Nacional (IGN). During the whole pre-eruptive period, more than 10,000 earthquakes were located, with maximum local magnitude (M_L) of 4.3 mbLg and intensities up to V in the EMS (European Macroseismic Scale, which goes from I to XII). A maximum ground deformation of more than 5 cm was registered. The seismic crisis peaked on 21 August (454 events), but magnitudes continued to increase (López et al., 2012).

Finally, on 10 October 2011 at 05:15 (GMT), a clear volcanic tremor started to be recorded by all seismic stations on the island, with highest amplitudes in the southernmost station. All data suggested the beginning of a submarine eruption, though evidence of it was not observed on the sea surface until a couple of days later (López et al., 2012).

The eruption took place at 27° 37.178' N 17° 59.574' W, located 1.8 km offshore from La Restinga, the southernmost village of the island. The volcano was located in the western flank of the southern ridge of El Hierro, with the lava flowing south-westwards into a valley that directed the lava towards an apron at depths of >1000 m (Rivera et al., 2013).

The growth in a sloping area contributed to instability, with recurrent failures, land-sliding, and collapsing events which constantly changed the morphology and depth of the cone (Rivera et al., 2013). The eruption was occurring mainly through two vents which developed into a double cone infilling the upper part of the valley, with its summit moving gradually to the northwest. The volcano continued growing and evolving until it reached its maximum and final elevation at 88 m below sea level (Fraile-Nuez et al., 2012). The final cone consists of at least four vents aligned in a north-northwest-south-southeast direction, with a main crater

at 127 m depth (Fraile-Nuez et al., 2018). The volcano was entirely generated during the eruptive underwater phase that took place between 10 October, 2011 and 5 March, 2012 (Fraile-Nuez et al., 2018, 2023).

In the water column, discolored volcanic plumes were observed ranging from light green to milky blue and dark brown colors (Santana-Casiano et al., 2013), covering a wide area around the island often following the south-westward flow of the Canary Current, but with a very unsteady behavior strongly dependent on environmental conditions (Eugenio et al., 2014). Bubbling and degassing were often observed, with bubbles reaching 10-15 m in height, and abundant rock fragments were also found floating in surface (Santana-Casiano et al., 2013).

Extreme physical-chemical perturbations were reported, including thermal increase, water acidification, deoxygenation, and metal enrichment, which resulted in significant alterations to the activity and composition of local plankton communities and high fish mortality (Fraile-Nuez et al., 2012; Santana-Casiano et al., 2013).

This was the first time that a specific plan for volcanic emergency management and civil protection was activated in the Canary Islands, abbreviated as PEVOLCA (complete name: *Plan Especial de Protección Civil y Atención de Emergencias por Riesgo Volcánico en la Comunidad Autónoma de Canarias*). The PEVOLCA was established in 2010 and later renewed in 2018 (BOC 154/2018, decreto 112/2018). It coordinates all the different entities involved in the crisis management, including government authorities, civil protection, security forces, and scientific assessment. For the latter group, eight regional and national scientific institutions conform the PEVOLCA Scientific Committee, which provides valuable real-time data from diverse areas such as geology, meteorology, geochemistry, or oceanography.

From March 2012, after the eruption came to an end, Tagoro submarine volcano entered a post-eruptive stage which is still active, with degassing and hydrothermal activity comprising a diffuse release of heat, gases, inorganic nutrients, and metals from the main and secondary craters (Santana-Casiano et al., 2013; Fraile-Nuez et al., 2018).

Since the eruption of Tagoro volcano and to this date, an intense monitoring effort has been made to characterize the physical-chemical, biological, and geological processes that take place over the volcano. The Spanish Institute of Oceanography (IEO-CSIC) has led this task, in collaboration with the two Canary universities (ULPGC, ULL) and other national and international marine research centers and private foundations. Over 30 oceanographic cruises have been carried

out in the area (average of 2 per year) measuring more than 40 physical-chemical, geologic, and biological variables, in the context of nine different scientific projects (Fraile-Nuez et al., 2023). The cruises have not only been multidisciplinary but also diverse in techniques and instrumentation, including CTD casts, multi-sensor moorings and buoys, multibeam echosounds, and the use of remotely operated vehicles (ROVs) for both image acquisition and sample collection with custom-made devices (Fraile-Nuez et al., 2023).

The scientific knowledge obtained from both the eruption and the subsequent monitoring of the post-eruptive stage has provided one of the largest datasets of an active shallow submarine volcano in the world, producing a large number of scientific publications over the years (Fraile-Nuez et al., 2012, 2018, 2023; Santana-Casiano et al., 2013, 2016; Coca et al., 2014; Eugenio et al., 2014; Ferrera et al., 2015; Marcello et al., 2015; Danovaro et al., 2017; Santana-González et al., 2017; Álvarez-Valero et al., 2018; Sotomayor-García et al., 2019; González-Vega et al., 2020, 2022; Fernández de Puelles et al., 2021).

1.4. La Palma

La Palma is the second youngest island of the Canary Islands, located at the north-west end of the archipelago. This island is at the earliest and fastest shield-building stage of growth and is currently the fastest-growing island in the archipelago: half of all the eruptions in the Canary Islands in the last 600 years have taken place in La Palma (Anguita, 2018).

The island was formed by successive volcanic edifices and subsequent large lateral collapses (Ancochea et al., 1994). The oldest volcanic edifices, Taburiente volcano and Cumbre Nueva ridge at the northern part of the island, are dated between 1.7 and 0.5 Ma (Carracedo et al., 1999). After a period of volcanic quiescence, volcanic activity shifted towards the south of the island, constituting the Cumbre Vieja ridge (Urgeles et al., 2001).

Cumbre Vieja is a polygenetic volcanic rift, formed by a series of monogenetic volcanic fissures and vents, mostly concentrated in a north-south trend. The ridge presents a height of roughly 2000 m above sea level, and its western coastal flank has undergone significant marine erosion, resulting in vertical coastal cliffs as high as 700 m (Carracedo et al., 1999).

1.4.1. Eruption at Cumbre Vieja (2021)

(Disclaimer: at the time of writing this thesis, the 2021 volcano has yet to receive an official name, although the tentative name of Tajogaite has been proposed and already been used in some scientific literature which is cited throughout this work. For lack of an official name, the 2021 eruption will hereafter be referred to as Cumbre Vieja volcano, volcano at Cumbre Vieja, or La Palma volcano.)

Anomalous seismic activity had been registered since 2017 at the south of La Palma, in the Cumbre Vieja region. However, the last and most intense pre-eruptive seismic swarm lasted less than two weeks, starting on 11 September 2021. The earthquakes gradually grew in frequency, magnitude, and shallowness, with more than 400 events registered with a maximum magnitude of 3.2 mbLg, along with ground deformation up to 15 cm (IGN, 2022).

On 19 September 2021, at 15:12 local time, an eruption started in the area of Cabeza de Vaca (28°36'58.6"N, 17°52'0.6"W), at 900 m altitude. Volcanic tremor was registered in all seismic stations. Initially, two fissures of hundreds of meters long were observed, aligned in a NW-SE direction and separated by 200 m, with several points of emission of pyroclastics and lava flows (IGN, 2022). A main cone started to take form.

The eruption lasted 85 days. Over 7000 people were evacuated during the emergency, and the total of population whose houses were affected by the lava flow are over 2300 people, which represents a 7% of the population of the island (Cabildo de La Palma). Over 1600 edifices, 370 Ha of agricultural land, and 73 km of roads were destroyed or endangered (Cabildo de La Palma).

The eruption was fissural with a strombolian mechanism (a mixed mechanism with explosive phases that produce pyroclastic deposits and effusive phases that produce lava flows, simultaneously). Surface temperature of the lava flow was as high as 1113°C, with a thickness of 8-15 m, and the eruptive column was around 6 km height above sea level (IGN, 2022). Earthquakes continued to take place, with magnitudes up to 5.1 mbLg, and ground deformation up to 33 cm was registered (IGN, 2022).

The lava flowed westward down the slope until reaching the coast 9 days later between the Tazacorte harbor and La Bombilla, where coastal cliffs of roughly 100 m height can be found. On 28 September at 23:00 local time, the lava started to cascade down the cliff and came into contact with the ocean for the first time. During the following weeks, subsequent lava flows continued to reach the coast and fill the submarine upper slope. The result was the formation of two lava deltas:

one main lava delta of 43 Ha around the location of the first contact, formed by the merging of several smaller deltas; and another lava delta of 5.4 Ha further north (Lozano Rodríguez et al., 2023).

The underwater propagation of the lava deltas was conditioned by the presence of submarine gullies, which were filled by the propagating lava flows reaching a maximum thickness of 40 m (Lozano Rodríguez et al., 2023). Volcanic material was identified as far as 1.2 km from the original coastline at >300 m below sea level. The total volume of lava reaching the ocean was estimated as 3 Mm^3 (Lozano Rodríguez et al., 2023). Two types of underwater lava flows were identified: in the shallower and less steep surfaces, "aa" flow types were dominant; whereas along the slopes found at greater depths, pillow lavas and mega-pillows were identified, with diameters up to 2 m (Lozano Rodríguez et al., 2023).

These lava inputs, along with the deposition of ashes and the presence of fine-grained volcanic materials suspended in the seawater, caused important alterations on the physical-chemical properties of the surrounding marine environment, including water acidification, temperature increase, and high turbidity (Fraile-Nuez et al., 2021; González-Santana et al., 2022; Román et al., 2022), as well as important fish mortality (Caballero et al., 2023).

1.5. Aims of this thesis

1.5.1. Motivation

The Canary Islands are a volcanically active archipelago. After a peaceful period of 40 years without volcanic eruptions (since Teneguía volcano in 1971), the population had to face two volcanic emergencies in just 10 years (2011 and 2021), with important economic losses and societal impact. It became evident that the study of volcanic processes and their effects on the environment need to be a priority for the Canary scientific community.

The submarine eruption at El Hierro in 2011 was the first eruption to be instrumentally monitored in the archipelago. The vast knowledge obtained from this process, along with the experience gained in emergency management and coordination, were quite useful for the later eruption at La Palma in 2021. This means that with the knowledge generated from each eruption, we are better prepared for the next one.

The Spanish Institute of Oceanography (IEO-CSIC) has been monitoring submarine volcanology in the Canary Islands for more than 12 years. Behind this

unique time series there is a large number of resources, instrumentation, people, and institutions involved. This thesis aims to contribute to this vast pool of scientific knowledge by shedding light on some of the most important physical-chemical and biological processes that take place in the ocean surrounding the Canary archipelago as a consequence of volcanic activity.

1.5.2. Thesis outline

We present three studies on the effects of the two most recent volcanic eruptions in the Canary Islands on the local marine environment. The studies explore three different types of volcano-ocean interactions: a submarine eruption; post-eruptive hydrothermal activity; and the formation of a lava delta from a subaerial eruption. All of these processes have taken place in the Canary Islands over the last decade.

Even though this work has a main focus on biogeochemistry and physical oceanography, it was intentionally designed with a marked multidisciplinary character, as the interaction of volcanoes with the ocean affects all physical, chemical, and biological parameters in the water column, and these are interconnected and affect each other.

The thesis has been structured in a chronological manner, starting with a study on the 2011 submarine eruption at El Hierro, following with a study on the same volcano during the 2011-2018 period, and ending with a study on the 2021 eruption at La Palma.

Chapter 2 explores one of the most dramatic consequences of the 2011 El Hierro submarine eruption: the loss of dissolved oxygen in a wide oceanic area surrounding Tagoro volcano. We quantify this loss and estimate its spatial extent. This work has been published in *Frontiers in Marine Science* (González-Vega et al., 2022).

Continuing on Tagoro submarine volcano, **Chapter 3** presents a comprehensive study on the emissions of dissolved inorganic nutrients during both the eruptive and post-eruptive stages. This is a unique dataset from seven years of monitoring which allowed to quantify the nutrient enrichment, spatial reach of the enriched plumes, and nutrient fluxes. This study was published in *Frontiers in Marine Science* (González-Vega et al., 2020) and complemented with a book chapter in Springer's book *El Hierro island*, from the book series *Active Volcanoes of the World* (González-Vega et al., 2023), which is summarized in **Appendix I**.

Moving on to the most recent volcanic eruption in the Canary Islands, **Chapter 4** is focused on the eruption at Cumbre Vieja (La Palma) in 2021, and the effects of the formation of lava deltas on the local marine environment. This study offers

a complete vision on the physical-chemical and biological effects of the arrival of lava flows to the ocean. This study has been submitted for publication in *Science of the Total Environment*. Supplementary material for this chapter is provided in **Appendix II**.

Finally, a brief discussion on the contributions of these three studies to the field of submarine volcanology in the Canary Islands, along with the main conclusions of the overall work, are presented in **Chapter 5**.

Deoxygenation during the eruption of Tagoro submarine volcano

Abstract

The shallow, near-shore submarine volcano Tagoro erupted in October 2011 at the Mar de las Calmas marine reserve, south of El Hierro island. The injection of lava into the ocean had its strongest episode during November 2011 and lasted until March 2012. During this time, *in situ* measurements of dissolved oxygen were carried out, using a continuous oxygen sensor constantly calibrated with water samples. A severe deoxygenation was observed in the area, particularly during October-November 2011, which was one of the main causes of the high mortality observed among the local marine ecosystem. The measured O_2 concentrations were as low as 7.71 µmol kg^{-1}, which represents a -96% decrease with respect to unaffected waters. The oxygen depletion was found in the first 250 m of the water column, with peaks between 70-120 m depth. The deoxygenated plume covered an area of at least 464 km^2, distributed particularly south and south-west of the volcano, with occasional patches found north of the island. The oxygen levels were also monitored through the following years, during the degassing stage of the volcano, when oxygen depletion was no longer observed. Additionally, during the eruption, an island-generated anticyclonic eddy interacted with the volcanic plume and transported it for at least 80 km, where the O_2 measurements still showed a -8% decrease after mixing and dilution. This feature draws attention to the permanence and transport of volcanic plumes far away from their source and long after the emission.

2.1. Introduction

The study of changes in the oceanic content of dissolved oxygen has gained relevance in recent years, as ocean models predict declines of 1 to 7% in the global ocean O_2 inventory over the next century (Plattner et al., 2001, 2002; Frölicher et al., 2009; Keeling et al., 2010). The attention has been particularly driven towards the oxygen minimum zones (OMZs), defined as mid-depth O_2 minima formed by a combination of intense respiration and weak ventilation (Sverdrup, 1938; Wyrtki, 1962; Keeling et al., 2010). These zones have been observed to be expanding due to ocean warming and increased stratification, especially in the North Pacific and tropical oceans (Ono et al., 2001; Whitney et al., 2007; Stramma et al., 2008; Keeling et al., 2010). However, other processes that can cause local declines in the dissolved oxygen content, such as the case of volcanic and hydrothermal emissions, have been less studied.

Submarine volcanism and hydrothermalism injects magma-derived volatiles into the ocean which are rich in reduced chemical compounds, such as reduced sulfur species and Fe(II) (Santana-Casiano et al., 2013), which are quickly oxidized when they come into contact with seawater (Campbell and Gieskes, 1984; Kump et al., 2001). This phenomenon can cause severe oxygen depletion and even anoxic episodes which can last from weeks to years (Campbell and Gieskes, 1984; Malahoff et al., 2006; Fraile-Nuez et al., 2012).

Volcanic-induced anoxia has been notably relevant throughout the geological history of our planet. Many paleoceanographic studies suggest that an increased rate of submarine volcanism during the mid-Cretaceous was likely the trigger for oceanic anoxic events at a global scale, which were linked to major events such as changes in marine productivity, CO_2-induced global warming, rises in sea level, and mass extinctions (Vogt, 1989; Erba, 1994; Leckie et al., 2002; Méhay et al., 2009). However, present-day volcanogenic episodes of oxygen depletion are poorly documented. Only a handful studies reporting these events have been carried out, mainly in deep-sea hydrothermal settings in the Pacific (Edmond et al., 1979; Campbell and Gieskes, 1984; Malahoff et al., 2006; Staudigel et al., 2006), usually in remote locations where intensive monitoring is not an easy task to achieve.
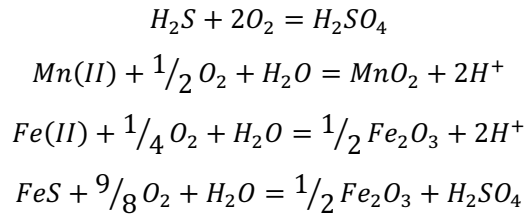
The Canary Islands, located in the north-eastern margin of the Atlantic Ocean, are an active volcanic archipelago originated from hotspot activity (Carracedo et al., 1998). El Hierro is the westernmost and youngest of these islands (Figure 2.1), with an age of 1.12 Ma (Guillou et al., 1996). Although several subaerial eruptions have occurred over the last centuries in the Canary archipelago, no submarine volcanic activity had been reported in 600 years of historical records (López et al., 2012).

On October 10th 2011, after more than 10,000 earthquakes were registered in three months at El Hierro island, a volcanic tremor marked the beginning of an underwater eruption. The newly formed submarine volcano, named Tagoro, was located 1.8 km offshore of La Restinga, the southernmost village of El Hierro, and at the *Mar de las Calmas* Marine Reserve. After several pulses of growth, the final form of the volcano presented an elongated summit in the NNW–SSE direction and an irregular base of 1–1.3 km (Fraile-Nuez et al., 2018), with a peak at 88 m depth and the main crater at 127 m depth (Figure 2.1).

The first six months of activity (October 2011 – March 2012) conformed the eruptive stage. This stage caused extreme physical–chemical perturbations in a wide area around El Hierro island, particularly south and south-west of the volcano, with visible water discoloration, bubbling and degassing (Santana-

Casiano et al., 2013). The most affected part of the water column was 75–125 m depth, but anomalies could be found from roughly 300 m depth to surface. Temperature anomalies up to +18.8°C were found, as well as salinity anomalies of –0.3 (Fraile-Nuez et al., 2012). The carbonate chemistry was also severely affected. Total dissolved inorganic carbon was as high as 12015 µmol kg^{-1}, with increases in the partial pressure of CO_2 of up to three orders of magnitude. This caused severe water acidification, reaching pH values as low as 5.2 (Santana-Casiano et al., 2013).

During the eruptive stage, Tagoro volcano released remarkable amounts of reduced chemical species into the surrounding waters, particularly reduced sulfur species (H_2S, HS^-, S^{2-}, S^0, SO_3^{2-}, S_x^{2-}, $S_2O_3^{2-}$, $S_4O_6^{2-}$) and Fe(II) (Fe^{2+}, $Fe(OH)^+$, $Fe(OH)_2$, $FeCl^+$, $Fe(HCO_3)$, FeHS). The main geochemical processes taking place were described in detail by Santana-Casiano et al. (2013) and Santana-González et al. (2017), including those responsible for oxygen consumption:

$$H_2S + 2O_2 = H_2SO_4$$

$$Mn(II) + \frac{1}{2}O_2 + H_2O = MnO_2 + 2H^+$$

$$Fe(II) + \frac{1}{4}O_2 + H_2O = \frac{1}{2}Fe_2O_3 + 2H^+$$

$$FeS + \frac{9}{8}O_2 + H_2O = \frac{1}{2}Fe_2O_3 + H_2SO_4$$

The chemical species responsible for this oxygen consumption were found in remarkable amounts during the eruption. Reduced sulfur species, which are normally below detection limit, presented concentrations as high as 476 µmol kg^{-1}. A similar pattern was observed for Fe(II), which showed an increase of up to five orders of magnitude (50 µmol kg^{-1}; reference values < 0.2 nM). The mixing of these reduced fluids with seawater caused a severe oxygen depletion, with patches of anoxia found at 100 m depth during the strongest eruptive episode (November 5th 2011) and concentrations as low as 100 µmol kg^{-1} reported during late November 2011 (Santana-Casiano et al., 2013).

These severe conditions (deoxygenation and acidification) caused a high mortality of local marine biota, particularly during the first two months of the eruption. No fish schools were acoustically detected within the affected area, and diel vertical migration was rather weak or absent 3 (Fraile-Nuez et al., 2012). Picophytoplankton groups presented distinct responses; however, heterotrophic bacteria showed a dramatic increase (Fraile-Nuez et al., 2012; Ferrera et al., 2015).

The eruption of Tagoro submarine volcano in 2011 caused water discoloration which acted as a natural tracer detectable through ocean color imagery. This was the first time that the interaction between a volcanic eruption and a mesoscale

structure could be recorded and thoroughly studied (Eugenio et al., 2014; Marcello et al., 2015). An island-generated anticyclonic eddy carrying volcanic discolored waters was monitored through satellite observations during October-November 2011 (Eugenio et al., 2014) and was sampled *in situ* on November 7th at the center of the eddy, 80 km away from the volcano.

In March 2012, the eruption came to an end and the volcano entered a new phase known as the degassing stage, which remains active. The system evolved towards a field of hydrothermal vents with release of heat, gases, metals, and inorganic nutrients (Fraile-Nuez et al., 2012; Santana-Casiano et al., 2013; González-Vega et al., 2020). The affected area was considerably reduced, reaching roughly 0.5 km around the volcano and close to the seafloor (Santana-Casiano et al., 2016). Although significant physical-chemical anomalies are still found in this area, there is a gap of knowledge about behavior of the spatial-temporal variability of the oxygen anomalies from this volcano.

The submarine volcano Tagoro has provided one of the most intensive monitoring of an ongoing underwater eruption and subsequent hydrothermal activity in the world, facilitated by its shallow and accessible location. Here we present a comprehensive study of the changes in the dissolved oxygen content of the waters affected by this volcano, with emphasis in the eruptive stage, and compare these with more recent measurements from the degassing stage. Additionally, we report and quantify the transport of the volcanic oxygen anomalies far from the source by means of an island-generated anticyclonic eddy.

2.2. Data and methods

2.2.1. Hydrography

The dataset used for this study comprises over 390 hydrographic stations and tow-yo transects, including up to 3500 discrete water samples for the calibration of the CTD-oxygen sensor data. The area was surveyed along 8 years of monitoring (2011-2018) through 13 different oceanographic cruises led by the Spanish Institute of Oceanography (IEO) (Figure 2.1). The cruises were carried out in the frame of different projects: BIMBACHE (cruises 1–2), RAPROCAN (cruises 3 and 5), CETOBAPH (cruise 4), VULCANO-I (cruises 6–7), VULCANA-I (cruises 8–10), VULCANO-II (cruises 11–12), and VULCANA-II (cruise 13). The vessels employed for the surveys were R/V *Ramón Margalef* (cruises 1, 2 and 6), R/V *Cornide de Saavedra* (cruises 3 and 4), and R/V *Ángeles Alvariño* (cruises 5 and 7–13).
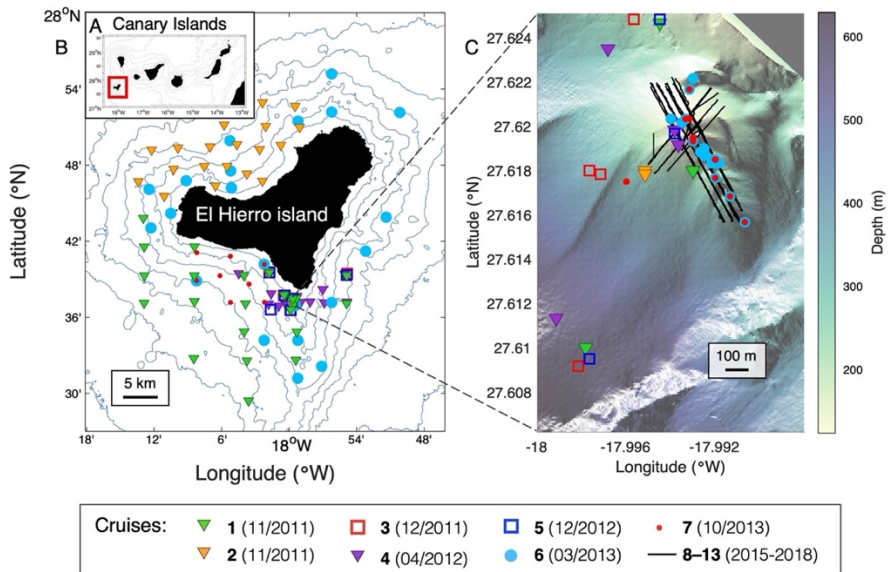
Figure 2.1. Study location. (A) Map of the Canary Islands. (B) Map of El Hierro island with the location of the vertical profiles carried out during all cruises. (C) 3D-High-resolution bathymetry of Tagoro submarine volcano, indicating the location of the hydrographic stations (cruises 1–7) and tow-yo transects (cruises 8–13).

An additional hydrographic station at 80 km south-west of the volcano was sampled during cruise 1 (November 7th 2011), when an island-generated anticyclonic eddy was transporting the discolored waters of the volcanic eruption offshore, as was observed by satellite image (Eugenio et al., 2014).

Conductivity, temperature and pressure data were acquired in every hydrographic station and tow-yo transect using a SeaBird 911-plus CTD, at a sampling interval of 24 Hz and with dual temperature and conductivity sensors with accuracies of 0.001°C and 0.0003 S/m respectively. A SBE43 dissolved oxygen sensor was coupled to the CTD system, with an accuracy of ±2% of saturation.

2.2.2. Sampling strategies

Different sampling strategies were used over the years in an effort to adapt our methodology to the evolution of the volcanic activity. During the eruptive stage (cruises 1–3), vertical profiles were carried out both in the vicinity of the volcano and in a wide area surrounding El Hierro island. This strategy continued during the early months of the degassing stage (cruises 4–5); however, seeing as the emissions at this stage reached a smaller area, a high-resolution transect across the main volcanic craters was established for cruises 6–7, with stations at few meters

of distance. A different strategy was applied during cruises 8–13 by performing tow-yo transects (Santana-Casiano et al., 2016), which consist on continuously lowering and raising the rosette between 1 and 40 m above the seafloor while the vessel moves at 0.2–0.4 kn with the Dynamic Positioning system (DP). This last methodology provides a remarkably high spatial resolution in the area affected by the hydrothermal emissions.

2.2.3. Oxygen calibration

Over 3500 discrete water samples were collected with an oceanographic rosette of 24-12-liter Niskin bottles. For the analysis of dissolved oxygen from these samples, we used the Winkler method with the subsequent modifications (Carpenter, 1965). The determination was always carried out on board, either manually or with an automated potentiometric titration. These samples were used to calibrate the continuous data from the dissolved oxygen sensor using a linear regression by least-squares. The original oxygen data in ml l-1 were converted to µmol kg^{-1} using the density values derived from the CTD data. A linear correlation was conducted for each of the cruises. All the calibrations presented a good fit (Table 2.1), with most r^2 >0.9 and all p-values <0.05.

Table 2.1. Statistics of the calibration of [O$_2$] data from the continuous sensor using water samples analyzed with the Winkler method.

Cruise	Name	Date	Number of casts*	Number of water samples	Calibration statistics	
					r^2	p-value
1	Bimbache leg 3	4-9 Nov. 2011	25	368	0.85	p<0.05
2	Bimbache leg 5	17-20 Nov. 2011	26	393	0.997	p<0.05
3	Raprocan1211	8 Dec. 2011	7	65	0.98575	p<0.05
4	Cetobaph	6-8 Apr. 2012	19	153	0.99855	p<0.05
5	Raprocan1212	9 Dec. 2012	7	676	0.97833	p<0.05
6	Vulcano0313	27 Mar.- 5 Apr. 2013	84	699	0.99703	p<0.05
7	Vulcano1013	1-7 Nov. 2013	78	319	0.9553	p<0.05
8	Vulcana0515	10-13 May 2015	8	106	0.9917	p<0.05
9	Vulcana1015	17-22 Oct. 2015	25	215	0.86041	p<0.05
10	Vulcana0316	10-15 Mar. 2016	34	159	0.91381	p<0.05
11	Vulcano1016	21-29 Oct. 2016	50	63	0.78391	p<0.05
12	Vulcano1017	23-27 Oct. 2017	17	196	0.95692	p<0.05
13	Vulcana0318	2-5 Apr. 2018	16	123	0.94201	p<0.05
Total			**396**	**3535**		

Vertical stations (cruises 1-7) or tow-yo transects (cruises 8-13).

2.2.4. Calculations

For the calculation of oxygen anomalies ($\Delta[O_2]$), for each cruise we established reference (non-affected) stations, generally located in an area around El Hierro island far away from the volcano. The classification was based on various physical-chemical parameters such as temperature, oxidation-reduction potential (ORP), pH (Santana-Casiano et al., 2016), or concentration of silicate. In the case of tow-yo transects (cruises 8–13), the reference was the down-cast or up-cast profile, depending on the direction of the local currents and the mentioned physical-chemical parameters. The anomalies were calculated as the dissolved oxygen concentration in the affected stations minus an average profile of all the reference stations for each cruise.

The theoretical saturation of O_2 in seawater was calculated for all the stations sampled during cruises 1–4 based on temperature and salinity data, as described by Weiss (1970).

2.3. Results

2.3.1. Deoxygenation in the water column

The evolution of the dissolved oxygen content during the eruptive stage in the waters affected by the volcanic emissions can be observed in Figure 2.2 as vertical profiles from cruises 1-4 (Figures 2.2A–D). Unaffected stations were also measured during each cruise to establish a reference profile for comparison.

In the first cruise (Figure 2.2A), which took place less than a month after the beginning of the eruption, severe oxygen depletion is evident in the first 150 m of the water column. A particularly deoxygenated profile is distinguished, with depletion up to -88% (minima of 25.33 µmol kg⁻¹; Table 2.2), corresponding to a station located at 1.8 km northwest from the volcano. The disparity of this profile respect to the others illustrates the unsteady nature of the eruptive event. The strongest episode occurred in late November 2011 (Figure 2.2B), during cruise 2, when conditions close to anoxia were measured (minimum of 7.71 µmol kg⁻¹, depletion of -96%) and the affection was observed in a wider range of the water column, up to 250 m depth. During this time, the volcanic plume was transported north-west of the island as observed by satellite image (Eugenio et al., 2014) and thus that northern area was measured as well, exhibiting depletion up to -25% (concentrations of 149.72 µmol kg⁻¹). During a short survey in December 2011 (Figure 2.2C), the oxygen depletion was still remarkable but less dramatic, with
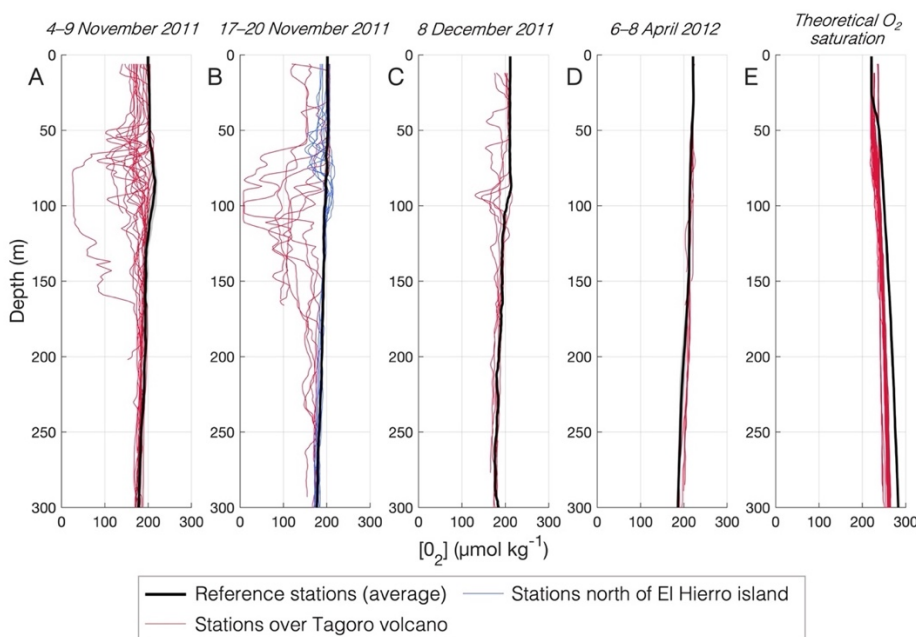
Figure 2.2. Vertical profiles of dissolved oxygen during the eruptive stage, measured during cruises 1,2,3,4 (A-D, respectively). Black line represents a reference profile, with standard deviation. Panel (E) shows the theoretical saturation of dissolved O_2 based on temperature and salinity data, for the reference profile (black line) and for the affected stations measured during cruises 1,2,3,4 (red lines).

anomalies up to -38% (129.72 μmol kg⁻¹) in a depth range of 0–140 m. Finally, oxygen was measured again in April 2012, coinciding with the time when the eruptive stage was over and the degassing stage begun. Accordingly, no evident anomalies of dissolved oxygen were observed in the vertical profiles.

Table 2.2. Minimum concentrations of dissolved oxygen during the eruptive stage at the depth of maximum depletion.

Cruise, date	Location	Depth	$[O_2]_{ref}$ ± std	Min. $[O_2]$	$\Delta[O_2]$	Depletion
		(m)	(μmol kg⁻¹)	(μmol kg⁻¹)	(μmol kg⁻¹)	(%)
1 (11/2011)	South of El Hierro	79	212.89 ± 7.41	**25.33**	-187.56	**-88.10%**
1 (11/2011)	Eddy (80km away)	79	212.89 ± 7.41	**195.39**	-17.50	**-8.22%**
2 (11/2011)	South of El Hierro	108	193.99 ± 4.56	**7.71**	-186.28	**-96.03%**
2 (11/2011)	North of El Hierro	63	200.12 ± 7.03	**149.72**	-50.40	**-25.19%**
3 (12/2011)	South of El Hierro	93	209.67 *(no std)*	**129.72**	-79.95	**-38.13%**
4 (04/2012)	South of El Hierro	119	212.44 ± 1.61	**203.34**	-9.10	**-4.28%**

A reference concentration ± standard deviation (std) from non-affected stations is shown for comparison. Anomaly ($\Delta[O_2]$) and depletion are calculated with respect to this reference.

During the eruption, an increase in temperature of +3°C and decrease in salinity of –0.3 were observed in the water column in the area affected by the volcanic plume (Fraile-Nuez et al., 2012). These physical anomalies are expected to have an impact on oxygen solubility (Weiss, 1970). For this reason, we calculated the theoretical O_2 saturation based on temperature and salinity data, for both the reference profile and all the stations affected by the volcano throughout the eruptive stage (Figure 2.2E). Although a diminution is observed respect to the reference, this difference is a -6% (average), a small percentage compared to the up to -96% depletion found. Additionally, the vertical distribution of this theoretical saturation in the affected stations follows a very stable pattern and does not show the variability observed in the $[O_2]$ data in the water column. Thus, the contribution of the chemical oxygen consumption by reaction with emitted reduced species is more relevant than the oxygen loss caused by physical anomalies.

2.3.2. Horizontal distribution of the deoxygenated plume

The oxygen anomalies observed during the eruptive stage were transported in a wide area around the volcano, particularly south-west. Figure 2.3 shows the distribution of dissolved oxygen concentration during the strongest period of the eruption, November 2011 (cruises 1 and 2). In this region and at this depth range (75–100 m), unaffected waters present O_2 concentrations above or around 200 μmol kg^{-1}. In the volcanic plume observed in Figure 2.3A at 100 m depth, we found an area of roughly 378 km^2 with $[O_2]$<200 μmol kg^{-1} (purple). Within this
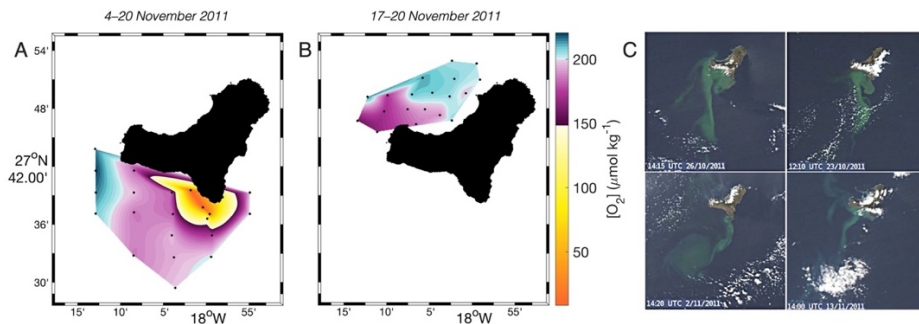

Figure 2.3. Horizontal contours of dissolved oxygen during the strongest eruptive episode. (A) Data from cruises 1 and 2, south-west of the volcano (100 m depth). (B) Data from cruise 2, when the volcanic plume was transported north of El Hierro island by the local currents (75 m depth). (C) Some examples of NASA MODIS RGB image of El Hierro island (Eugenio et al., 2014) from October-November 2011, showing the high spatial variability of the volcanic plume.

area, about 78 km² presented [O₂]<150 μmol kg⁻¹ (yellow- orange), where the minimum concentration found was 7.71 μmol kg⁻¹. In late November (Figure 2.3B) the plume reached the north of the island due to changes in local currents. This transported plume represents an additional affected area ([O₂] <200 μmol kg⁻¹) of at least 86 km². The satellite images from October-November 2011 (Figure 2.3C; Eugenio et al., 2014) show that the distribution of the colored volcanic plume was very variable depending on local currents and intensity of the eruptive event. In most cases, the plume was wider than the area sampled for oxygen (Figures 2.3A,B). Thus, our calculation of the area affected by deoxygenation is only indicative of the order of magnitude and should not be considered as an exact estimation.

On November 7th 2011, satellite images indicated the presence of an island-generated anticyclonic eddy that trapped the visibly discolored waters affected by the volcanic eruption and was being transported south-westwards for tens of kilometers (Figure 2.4). Thus, a hydrographic station (914) was sampled in the center of this eddy, 80 km away from the volcano, in order to trace and quantify the transport of the volcanic emissions (Figure 2.4A). The vertical profile of dissolved oxygen in this station is compared to a reference profile in Figure 2.4B. A local minimum was found at 79 m depth which clearly deviates from the expectable shape of a typical [O₂] profile, at exactly the same depth as the minima
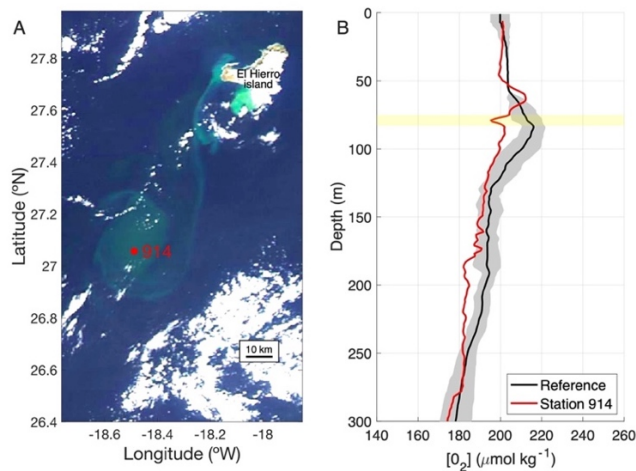

Figure 2.4. Dissolved oxygen in a plume transported 80 km southwest of the volcano by an anticyclonic eddy. (A) True color satellite image from November 5th 2011. (B) Vertical profile of dissolved oxygen within the transported plume. Black line shows a reference profile with standard deviation (grey shadow). A yellow stripe highlights the peak corresponding to the anomaly transported from the volcano.

of [O$_2$] found in the vicinities of the volcano. This peak represents a very small depletion (-8%) compared to the -88% depletion found in the volcanic area at the time, which reflects the effect of dilution and mixing with ambient waters through the 80 km journey of the eddy.

2.3.3. Post-eruptive stage

After the eruptive stage came to an end in March-April 2012, these dramatic oxygen depletions were no longer observed. However, we have continued to monitor oxygen levels all throughout the degassing stage (2012-present), as can be observed in Figure 2.5. Here, the dissolved oxygen data are shown as anomalies respect to a reference profile for each cruise (Δ[O$_2$]), in order to avoid the effects of depth and seasonality on the concentration of O$_2$. This figure should not be understood as a temporal evolution, given the disparity in sampling strategies and sample size (n) over time. The large range and the abundance of outliers during the eruptive stage (orange boxes) are representative of the huge variability and instability of the eruptive process. For the degassing stage (blue and purple boxes), the data still show a high variability, particularly in those boxes with larger sample sizes (n); however, all the observed anomalies are close to zero, suggesting that oxygen depletion is no longer observed.
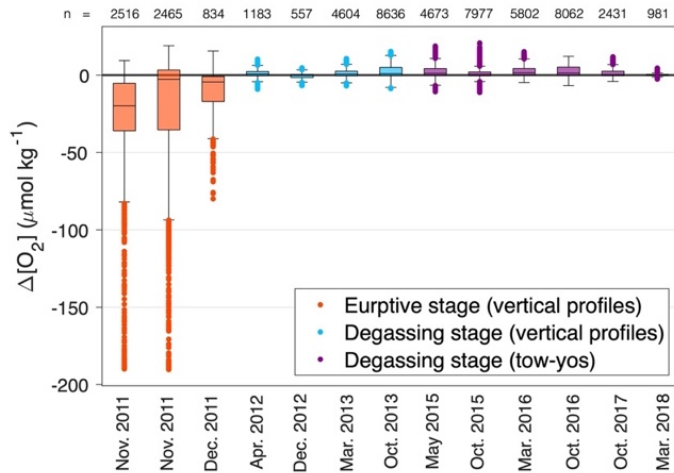

Figure 2.5. Anomalies of dissolved O$_2$ through 2011–2018 represented as boxplots, which show the median, quartiles, and outliers. Sample size (n) is specified above each box, representing the number of data collected by the continuous oxygen sensor at a sampling interval of 1 meter (vertical profiles) or 1 second (tow-yos).

2.4. Discussion

The eruption of the submarine volcano Tagoro in 2011 caused a drastic and initially negative impact on the ecosystem of the *Mar de las Calmas* marine reserve surrounding El Hierro island. Conditions close to anoxia were found during November 2011 in the first 250 m of the water column, with concentrations of dissolved oxygen as low as 7.71 µmol kg^{-1}, which represents a -96% depletion respect to the normal conditions found in reference stations. These suboxic and anoxic conditions were the cause of the high mortality observed among fish and most planktonic groups, along with other factors such as the drop of pH and the high CO_2 concentrations (Santana-Casiano et al., 2016). The cause of the deoxygenation was the emission of reduced chemical species, mainly of sulfur (H_2S, HS^-, S^{2-}, S^0, SO_3^{2-}, S_x^{2-}, $S_2O_3^{2-}$, $S_4O_6^{2-}$) and iron (Fe^{2+}, $Fe(OH)^+$, $Fe(OH)_2$, $FeCl^+$, $Fe(HCO_3)^+$, $FeHS$) (Santana- Casiano et al., 2013). Some of these species presented concentrations up to five orders of magnitude higher than unaffected stations (Santana-Casiano et al., 2013).

The patch of deoxygenated waters reached a wide area around the island of El Hierro, particularly during the strongest eruptive episodes in November 2011. The total area of reach was at least of 464 km^2 combining the south and north plumes (Figures 2.3A, B, respectively), likely even wider considering that both the south and north patches were not delimited within the sampled grid of stations as observed in the satellite images (Figure 2.3C). Note that this combined area is wider than the surface of El Hierro island (268 km^2). The spatial distribution of this suboxic patch coincides with the distribution described for other parameters that were a consequence of the eruption of Tagoro volcano, such as seawater discoloration, total dissolved inorganic carbon, pH, and inorganic nutrients (Santana-Casiano et al., 2013; Eugenio et al., 2014; González-Vega et al., 2020).

Deoxygenation caused by volcanic or hydrothermal activity has long been known, although not many studies have focused on describing this feature. Edmond et al. (1979) described anoxic conditions at the Galapagos spreading center (East Pacific Ocean). In 1984, at Guaymas Basin (Gulf of California), it was observed that even though the hydrothermal component of the sampled waters was less than 1%, the decrease in O_2 was about 10% in comparison to unaffected areas (Campbell and Gieskes, 1984). The authors deduced that the oxygen anomalies were not simply derived from mixing of O_2-deficient waters with ambient waters, but were rather a consequence of chemical oxygen consumption by the oxidation of dissolved sulfide and methane injected by the hydrothermal vents. Anoxia induced by hydrothermal discharge was also later described within the East Pit at

Lo'ihi Seamount, Hawai'i (Malahoff et al., 2006). Furthermore, at Nafanua volcano (Vailulu's Seamount, Samoa), the low oxygen values measured within the crater were suggested to be one of the causes of the observed high mortality among local nekton (Staudigel et al., 2006).

Although present-day studies showing volcanic-induced anoxia are relatively sparse, many paleoceanographic studies correlate global low-oxygen events with periods of enhanced volcanic activity in past geological periods. Particularly, the Cretaceous period (145–66 Ma) was characterized by the occurrence of several oceanic anoxic events (OAEs) and long periods of CO_2-induced global warming and climatic change (Clarke and Jenkyns, 1999), accompanied by mass extinctions in groups such as calcareous nannofossils, radiolarians, foraminifera, and mollusks (Snow et al., 2005). These events have been consistently associated with high rates of submarine volcanic activity (Vogt, 1989; Erba, 1994; Snow et al., 2005; Méhay et al., 2009), which could be linked to times of rapid oceanic plateau formation and/or increased rates of ridge crest volcanism (Leckie et al., 2002). Moreover, and going even further in the geological history of our planet, some studies have suggested a role of submarine volcanism on the establishment of an O_2-rich atmosphere (Kump et al., 2001; Kump and Barley, 2007). This hypothesis intends to explain the time gap between the rise in atmospheric O_2 levels (2400-1800 Ma) and the first records of cyanobacteria, the first oxygenic photosynthesizers, which have been identified in sediments from 2700 Ma (Brocks et al., 1999) and even associated morphologically with microfossils dated at 3500 Ma (Schopf, 1993). The authors argue that volcanism during the Archean era was predominantly submarine (which is more reducing than subaerial volcanism), acting as a sink for oxygen larger than the photosynthetic source; until a shift to a more mixed subaerial-submarine volcanism during the Archaean-Proterozoic transition allowed the establishment of a permanent oxygenated atmosphere (Kump et al., 2001; Kump and Barley, 2007).

The Canary archipelago acts as an obstacle to the flow of the Canary Current and the Trade Winds, originating mesoscale structures such as cyclonic and anticyclonic eddies, which can live >3 months and can be transported for hundreds of kilometers (Sangrà et al., 2009). The submarine volcano Tagoro represented a good opportunity to study these features, as the eruption caused water discoloration which acted as a natural tracer detectable through ocean color imagery. An island-generated anticyclonic eddy carrying volcanic discolored waters was monitored through satellite observations during October-November 2011 (Eugenio et al., 2014) and was sampled *in situ* on November 7th at the center of the eddy, 80 km away from the volcano. There, a -8% oxygen depletion was

found at the same depth (79 m) as the oxygen minima observed on top of the volcano, which were up to a -88% depletion at the time, showing that the deoxygenation in the eddy was one order of magnitude weaker. This anomaly is very small and most likely it no longer had an impact on its local environment; however, the fact that the volcanic signal is still detectable 80 km away from the site of emission is an indicative of the importance of taking into account mesoscale structures when studying the transport of volcanic plumes.

Ocean models predict declines of -1 to -7% in the global ocean O_2 inventory over the next century (Keeling et al., 2010). The eruption of Tagoro volcano caused a deoxygenation event of up to -96%. Furthermore, the fact that the signal was still detectable (although weak) 80 km away from the volcano raises attention on the permanence and transport of volcanic plumes at a larger scale. Several studies in different settings around the globe (particularly over spreading centers) have described phenomena called event plumes or "megaplumes": voluminous patches of heat and chemical anomalies caused by a brief and massive release of volcanic or hydrothermal fluids (Lupton et al., 1989; Baker and Lupton, 1990). The term "megaplume" was first used by Baker et al. (1987) to describe a 700-m-thick, 20-km- diameter plume found at the southern Juan de Fuca ridge in 1986. Even though this megaplume was formed in a few days, its heat output was comparable to ~100 black smokers venting for one year (Lupton et al., 1989). Similar events were observed at the North Fiji Basin in 1987 (Nojiri et al., 1989), at the CoAxial segment of Juan de Fuca Ridge in 1993 (Embley et al., 1995; Baker et al., 1995; Lupton et al., 1995), and at the northern Gorda Ridge in 1996 (Baker, 1998). Baker (1994) argued that the observation of several independent event plumes over a relatively short period of time suggests that these features are not exceptional. If this is true, the occurrence of these events along spreading centers, plus other intraplate events such as the case of the Tagoro eruption, would represent an enormous volume of reduced fluids that are being emitted to the ocean. This would mean that the total percentage of the global ocean undergoing deoxygenation stress could be much wider than the current assumptions based only on features like OMZs and coastal processes.

2.5. Conclusions

The eruption of the shallow submarine volcano Tagoro in 2011 at El Hierro island generated suboxic and even anoxic conditions in the first 250 m of the water column. The minimum concentration of dissolved O_2 measured was 7.71 μmol kg^{-1}, representing a -96% decrease respect to the normal conditions found in unaffected waters. The affected area was at least 464 km^2 during its strongest

eruptive episode in November 2011, an area wider than El Hierro island itself. The plume was distributed mainly to the south and south-west of the volcano, but occasional patches were also observed north of the island due to changes in the local currents. This eruption also represented a unique opportunity to observe the interaction between a volcanic plume and a mesoscale structure: an anticyclonic eddy that was monitored through satellite observations during October-November 2011. The *in situ* oxygen measurements at the center of this eddy, 80 km away from the volcano, showed a -8% decrease respect to reference stations, which is an order of magnitude weaker than the deoxygenation found above the volcano at the time. However, considering the longevity of these structures and the long distances they can reach, this feature draws attention to the importance of the transport of volcanic plumes far away from the source and their permanence in the ocean.

Release of inorganic nutrients from Tagoro submarine volcano

Abstract

Tagoro, the shallow submarine volcano that erupted south of El Hierro (Canary Islands, Spain) in October 2011, has been intensely monitored for over 7 years, from the early eruptive stage to the current degassing stage characterized by moderate hydrothermal activity. Here, we present a detailed study of the emissions of inorganic macronutrients (NO_2^- + NO_3^-, PO_4, and $Si(OH)_4$) comprising a dataset of over 3300 samples collected through three different sampling methodologies. Our results show a significant nutrient enrichment throughout the whole studied period, up to 8.8-fold (nitrate), 4.0-fold (phosphate), and 16.3-fold (silicate) in the water column, and larger enrichments of phosphate (10.5-fold) and silicate (325.4-fold), but not of nitrate, in the samples collected directly from the vents. We also provide some preliminary results showing ammonium (NH_4^+) concentrations up to 1.97 µM in the vent fluids as compared to 0.02 µM in the surrounding waters. Nutrient fluxes from the volcano during the degassing stage were estimated as 3.19 ± 1.17 mol m^{-2} year^{-1} (NO_2^- + NO_3^-), 0.02 ± 0.01 mol m^{-2} year^{-1} (PO_4), and 0.60 ± 1.35 mol m^{-2} year^{-1} ($Si(OH)_4$), comparable to other important nutrient sources in the region such as fluxes from the NW-African upwelling. Nutrient ratios were affected, with a minimum (NO_3^- + NO_2^-):PO_4 ratio of 2.36:1; moreover, a linear correlation between silicate and temperature enabled the use of this nutrient as a mixing tracer. This study sheds light on how shallow hydrothermal systems impact the nutrient-poor upper waters of the ocean.

3.1. Introduction

About 85% of Earth's volcanism occurs beneath the ocean with regard to the volume of emissions (Mitchell, 2012). Yet, submarine volcanoes are poorly characterized in comparison to their subaerial counterparts (Staudigel et al., 2006; Resing et al., 2009; Buck et al., 2018). Submarine volcanoes constitute a significant source of mantle-derived gases, solutes and heat to the ocean. Their emissions react with seawater leading to important physical-chemical anomalies with a strong potential to impact the marine ecosystems (Fraile-Nuez et al., 2012).

Volcanic inputs to the ocean have been studied mainly through hydrothermal activity. Submarine hydrothermal vents typically discharge fluids which are warm-to-hot, acidic, reducing and metal-rich, and, on a global scale, are thought to exert significant controls on the major-ion composition of seawater (Sedwick and Stüben, 1996). Studies on hydrothermal settings have been carried out mainly in

the Pacific Ocean (Edmond et al., 1979; Karl et al., 1989; Tarasov et al., 1990; Sorokin et al., 1998; Staudigel et al., 2006; Buck et al., 2018; Guieu et al., 2018), with fewer examples in the Atlantic (Thorarinsson, 1967; Sarradin et al., 1999; Desbruyères et al., 2001) and the Mediterranean (Sedwick and Stüben, 1996; Kilias et al., 2013).

Submarine volcanic activity releases nutrients into seawater, including Fe, Si, P, and N (Santana-Casiano et al., 2013). The enrichment in silicate is a general characteristic of hydrothermal vents and has been used as a geochemical thermometer due to the highly significant positive correlation between Si concentration and vent water temperature (Karl et al., 1989). Nonetheless, information about volcanoes as a source of nutrients to the ocean is very limited, and most of the existing studies have been carried out in deep hydrothermal vents (Karl et al., 1989; Sarradin et al., 1999), in comparison to fewer studies on shallow volcanic settings surrounded by nutrient-poor waters (Sedwick and Stüben, 1996; Kilias et al., 2013).

The Canary Islands, located in the north-eastern margin of the Atlantic Ocean, conform an archipelago originated from hotspot-associated volcanism (Carracedo et al., 1998). El Hierro is the youngest and westernmost of these islands (Figure 3.1), and it is surrounded by oligotrophic waters where nutrient concentrations south of the island are usually undetectable in the upper 80–100 m of the water column (Santana-Casiano et al., 2013).

On October 10, 2011, after more than 15000 earthquakes were recorded in a 3-month period, a volcanic tremor was registered south of El Hierro, suggesting the beginning of a submarine eruption (Fraile-Nuez et al., 2012). The volcano, later named Tagoro, was located 1.8 km off the southern coast of the island and presented a south-westward lava flow. The main cone grew from an initial depth of 355 m to a maximum height of 88 m below the sea surface reported in February 2012 (Fraile-Nuez et al., 2012; Santana-Casiano et al., 2013; Sotomayor-García et al., 2019).

Tagoro emitted molten material during the first 6 months, affecting a wide area southwest and northwest of the island, with peaks of intensity during late October and early November 2011. This period conformed the eruptive stage, during which the physical-chemical properties of the water column were drastically influenced by the emissions. Average temperature and salinity anomalies of +3°C and –0.3 were observed respectively, with a maximum temperature anomaly of +18.8°C (Fraile-Nuez et al., 2012). The intense bubbling and degassing caused a marked increase of CO_2 partial pressure (pCO_2) reaching values of 12000–150000

µatm at the surface, and lowering the pH by 2.9 units (Santana-Casiano et al., 2016). The volcano also released great amounts of iron [Fe(II)] (>50 µmol kg^{-1}) and reduced species of sulfur (>476 µmol kg^{-1}), which caused a fall in the redox potential, eventually reaching negative values (Santana-Casiano et al., 2013). The presence of these reduced compounds caused a drastic oxygen consumption, leading to suboxic and even anoxic conditions in subsurface waters (Fraile-Nuez et al., 2012).

After March 2012, once the eruptive stage was over, Tagoro entered an active hydrothermal phase involving the release of heat, gases, and metals. The hydrothermal discharge occurs from multiple vents dispersed around the main cone by percolation of vent fluids through the highly permeable volcanic edifice (Santana-Casiano et al., 2016). In this new stage, the wide area that had been affected north and south of the volcano quickly returned to physical and chemical conditions comparable to those observed in the surrounding waters, and the perturbations are limited to the area situated roughly 0.5 km around the main cone and quite close to the seabed (Santana-Casiano et al., 2013). However, important physical-chemical anomalies are still present in the interior of the main crater as: thermal increase of $+2.55°C$, decreases in salinity of -1.02, density decrease of -1.43 kg m^{-3}, and pH decrease of -1.25 units (Fraile-Nuez et al., 2018). Furthermore, the hydrothermal emissions exhibit a cyclic behavior, with peaks of activity every 130–170 min (Fraile-Nuez et al., 2012).

Two new habitats have been described around the summit and main craters: hydrothermal vents with microbial mats, and sulfurous-like fields mainly colonized by small hydrozoan colonies; whereas downslope the volcanic complex, other new habitats have been observed to hold a higher biodiversity, with annelids, arthropods, cnidarians, and mollusks as the first colonizers (Sotomayor-García et al., 2019). However, no clear impact has been detected on the local phytoplankton community (Gómez-Letona et al., 2018).

The exhaustive monitoring of Tagoro volcano performed over the last 7 years provides a remarkable dataset of the inorganic nutrient emissions from a shallow submarine volcano. Here we present a detailed study of the significant release of $NO_2^- + NO_3^-$, PO_4, and $Si(OH)_4$, reporting the magnitude, temporal variation, spatial distribution, fluxes and ratios of the nutrient emissions for the eruptive and degassing stages of the Tagoro submarine volcano. We discuss the implications of the different sampling methodologies used, and compare our results with different volcanic and hydrothermal settings, as well as other nutrient sources to the Canary region.

3.2. Data and methods

The activity of Tagoro submarine volcano has been intensely monitored between 2011 and 2018 through 15 oceanographic cruises led by the Spanish Institute of Oceanography (IEO) in the affected area and around the island of El Hierro (Figure 3.1). A total of about 3300 discrete water samples were analyzed for this study, obtained from 221 hydrographic stations, 43 tow-yo transects, and eight remotely operated vehicle (ROV) vent samples. The surveys were carried out on board of the research vessels *Ramón Margalef* (cruises 1, 2, 4, 5, and 7), *Cornide de Saavedra* (cruise 3), and *Ángeles Alvariño* (cruises 6 and 8–15) from the IEO.
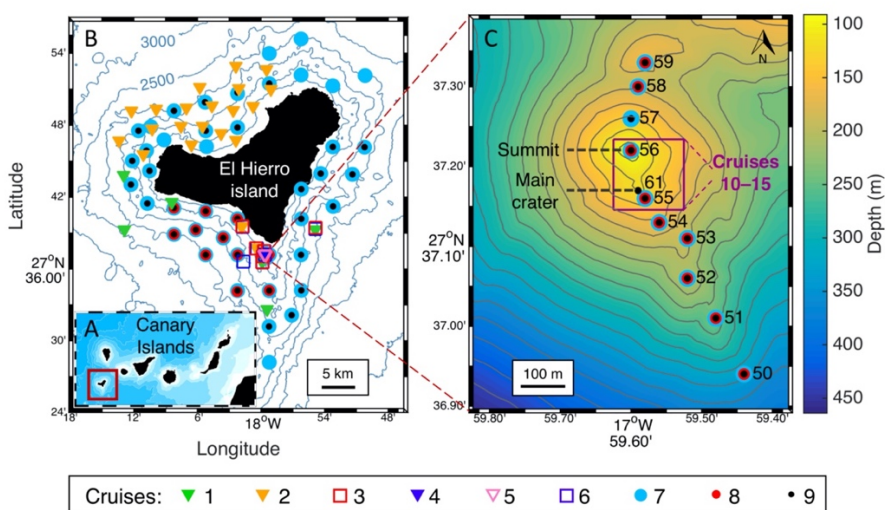
Figure 3.1. Study location. (A) Map of the Canary Islands. (B) Map of El Hierro island with stations of vertical profiles carried out during cruises 1-9. (C) Bathymetry of the volcanic edifice and high-resolution transect of vertical profiles carried out during cruises 7-9 across the main cones. The squared region shows the zone where the tow-yo samples (cruises 10-14) and vent samples (cruise 15) were collected. All maps were generated using Matlab 8.5 R2015a.

3.2.1. Sample collection

Conductivity, temperature and pressure data were collected using a SeaBird 911-plus CTD equipped with dual temperature and conductivity sensors, with accuracies of 0.001°C and 0.0003 S/m respectively, continuously recording data with a sampling interval of 24 Hz. CTD sensors were calibrated at the SeaBird laboratory before and after the cruises. Discrete water samples for nutrient analysis were obtained using a rosette of 24–12-liter Niskin bottles.

Several sampling strategies were applied throughout the 7 years of monitoring. During cruises 1–9, the sampling consisted of vertical hydrographic stations located both in the area influenced by the emissions and outside the affected area (reference stations). These were differentiated based on various physical-chemical parameters such as temperature, conductivity, oxidation-reduction potential, pH, silicate concentration and, in the case of the eruptive stage, satellite images where the water discoloration caused by the volcanic emissions could be observed (Figure 3.4D). For the degassing stage, the area affected by the emissions was drastically reduced to around 0.5 km around the main cone. A high-resolution transect was established across the main and secondary craters for the study of the degassing stage during cruises 7–9 (Figure 3.1C). The dynamic positioning (DP) system of the research vessels allowed to locate the stations at few meters of distance. The rest of the stations, located around the island, were used as reference for this stage.

For cruises 10–14, samples were collected in the area of the main craters through tow-yo transects (Figure 3.1C), which involve continuously lowering and raising the rosette between 1 and 40 m above the seabed and with the ship moving at 0.2–0.4 kn in DP, obtaining a sawtooth-shaped dataset with high spatial resolution and closer to the source of the emissions. During cruise 15, the ROV *Liropus 2000* (IEO) was used for sample collection directly from the hydrothermal vents using a piston-driven suction system. A total of eight samples (each analyzed in duplicate for nutrients) were collected from different active vents in the main craters.

3.2.2. Nutrient analysis

Nitrate+nitrite, phosphate, and silicate were analyzed by colorimetric determination using a four-channel automatized air-segmented continuous flow system SEAL AA3 AutoAnalyzer. Nitrite (NO_2^-) reacts under acidic conditions with sulfanilamide to form a diazo compound that then couples with N-Naphthylethylenediamine dihydrochloride (NEDD) to form a reddish-purple azo dye. Nitrate (NO_3^-) is reduced to nitrite by a copper-cadmium reductor column and detected likewise, giving the sum of nitrite and nitrate (Treguer and Le Corre, 1979). In the present study $NO_2^- + NO_3^-$ are analyzed jointly, which we hereafter shorten as N+N; we often refer to N+N as nitrate, since the concentrations of NO_2^- were found to be negligible with respect to NO_3^-. Phosphate (PO_4) is detected by the reaction of ortho-phosphate, molybdate ion, and antimony ion followed by reduction with ascorbic acid at a pH<1, forming a reduced blue phospho-molybdenum complex (Aminot and Kérouel, 2007). The detection of

silicate (Si(OH)$_4$) is based on the reduction of silico-molybdate in acidic solution to molybdenum blue by ascorbic acid. Oxalic acid is introduced to the sample stream before the addition of ascorbic acid to minimize interference from phosphates (Garcia et al., 2005). The detection limits are 0.02 μM for N+N, 0.01 μM for PO$_4$, and 0.040 μM for Si(OH)$_4$. The concentrations were converted to μmol kg^{-1} with density values derived from CTD data.

Ammonium was analyzed fluorometrically after reaction with ortho-phthalaldehyde (OPA) and reduction with sodium sulfite (Kérouel and Aminot, 1997) with a detection limit of 1.5 nmol l^{-1}. The implementation of this method was only possible after the period of study presented in this work, therefore we only present here data from frozen samples collected from the vents with ROV in cruise 15 (November 2018) and some samples from reference stations collected during a more recent cruise (November 2019) during which the ammonium samples were analyzed on board immediately after collection.

3.2.3. Calculations

In order to eliminate the variability of the ambient nutrient concentrations with depth from the samples affected by the volcano, nutrient anomalies were calculated. Two parameters are presented in this study: nutrient anomalies (Δ[X]), calculated as the measured concentration ([X]) minus the average reference concentration at the same depth ([X]$_{ref}$); and significant nutrient anomalies (sΔ[X]), calculated as the measured concentration minus the average and the standard deviation (std[X]$_{ref}$) at the same depth, in order to eliminate anomalies that are found within the standard deviation of the average ambient concentrations(non-significant anomalies).

$$\Delta[X] = [X] - [X]_{ref}$$

$$s\Delta[X] = [X] - [X]_{ref} - std[X]_{ref}$$

Low-temperature discharge produces localized lower density values near the source of emission, which are expected to reach density equilibrium within a few meters from the seafloor (Baker et al., 1993). In some cases, these density values near the vents could be lower than the surface values at the reference stations. For this reason, the nutrient anomalies were calculated in isobaric component instead of isopycnal component in order to avoid the localized density perturbations close to the vents and the consequent error in the estimation of the nutrient anomalies.

Nutrient fluxes were calculated from a high-resolution vertical section of nutrient anomalies above the main craters and perpendicular to the current flow, providing an optimized flux estimation (Santana-Casiano et al., 2016; Buck et al., 2018).

$$Flux\ (\mu mol\ s^{-1})$$
$$= \Delta[X](\mu mol\ kg^{-1}) \times Current\ velocity\ (m\ s^{-1})$$
$$\times\ Plume\ area\ (m^2) \times Density\ (kg\ m^{-3})$$

Hence, the fluxes were calculated by multiplying these anomaly sections by the plume area and by a mean current velocity of 0.06 m s^{-1} obtained from a 9-year time series in the Canary region (Fraile-Nuez et al., 2010). The fluxes were calculated in µmol s^{-1} and converted to mol m^{-2} year^{-1}. The plume area was delimited as the area defined by the significant anomalies (sΔ[X]). For the conversion of time units, the periodicity of the volcanic emissions was taken into account. It is estimated that the volcanic activity present pulses of emission every 140 min (this makes 3754 cycles per year), with about 40 min of activity per cycle (Fraile-Nuez et al., 2018).

The nutrient ratios were obtained from the correlations calculated by multiple linear regression by the method of least squares with a 98% confidence level. Since many of the affected datasets did not present any data near the intercept with the axis, all the regressions have been forced to intercept in 0:0 (as does the reference dataset) in order for their slopes to be comparable.

Data of mixed layer depth (MLD) and euphotic zone depth (EZD) data were provided by the Copernicus Marine Environment Monitoring Service (CMEMS). We used two products delivered by the CMEMS Iberia-Biscay-Ireland Monitoring and Forecasting Centre. The MLD data was obtained from the Physics Analysis and Forecast product, based on the NEMO ocean model (Sotillo et al., 2015); while the EZD data was obtained from the Biogeochemical Analysis and Forecast product, based on NEMO and PISCES models (Aumont et al., 2015). Both datasets have a resolution of 0.028×0.028°; we located the closest point to the coordinates of Tagoro volcano in the spatial grid of the datasets and used the monthly averaged data in this location for the periods available, 2013–2019 (MLD) and 2017–2019 (EZD).

3.2.4. Bathymetry

Three different bathymetry datasets with different spatial resolutions have been used: a global Topo15.1 bathymetry dataset with a spatial resolution of 4 km by Smith and Sandwell (1997) for the map of the Canary Islands (Figure 3.1A); a ZEE- Canary Island bathymetry with a resolution of 90 m from the IHM-IEO

for the map of El Hierro island (Figure 3.1B), and a high resolution multi-beam bathymetry dataset obtained during cruise 11 (Vulcano0316) to generate a detailed map of the submarine volcano Tagoro (Figure 3.1C). During this cruise, bathymetric data was acquired using a Kongsberg Simrad EM-710 echo sounder, which operates at sonar frequencies in the 70–100 kHz range. The data were processed with CARIS HIPS and SIPS and yields a bathymetric grid resolution of 1 m with 100% coverage.

3.3. Results

3.3.1. Quantification of the nutrient emissions

The vertical profiles of nutrient concentrations are shown in Figures 3.2A–C (N+N, PO_4, and $Si(OH)_4$) for the stations affected by the volcano during the eruptive and degassing stages and with the different sampling methodologies applied (vertical profiles for water-column samples, tow-yos for near-bottom samples, and ROV for vent samples). A reference profile was established using nutrient data from 122 non-affected stations surrounding El Hierro island, regardless of seasonality. Positive significant anomalies in all nutrients are observed with respect to the reference, underlining a nutrient discharge during both the eruptive and the degassing stages. Concentration peaks are generally found around 130 m (the depth of the main crater), although they often reached the surface during the eruptive stage. The maximum concentrations found during the eruptive stage in the water column (all in μmol kg^{-1}) were of 8.06 for N+N (reference: 1.75), 0.79 for PO_4 (reference: 0.11), and 21.76 for $Si(OH)_4$ (reference: 1.23); these were found in the 75–100 m depth range, but substantial emissions often reached the surface as well (0–50 m depth). For the degassing stage, significant emissions stayed within a more constrained depth range (75–130 m). Concentrations of phosphate and silicate increased with the proximity of the sample collection to the source: the least concentrated were the water-column samples, followed by the near-bottom samples, and finally the vent samples, with maxima of 1.60 (PO_4) and 189.40 ($Si(OH)_4$) μmol kg^{-1}. Contrastingly, the maximum concentrations of N+N were found in the water-column samples (6.21 μmol kg^{-1}), which are assumed to be the most mixed with ambient waters, and decreased in the near-bottom and vent samples.
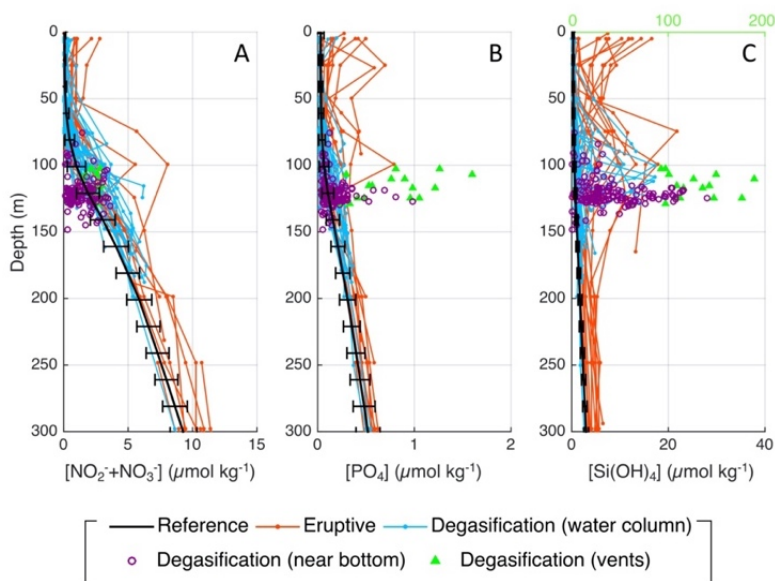
Figure 3.2. Vertical profiles of (A) nitrate+nitrite, (B) phosphate, and (C) silicate, for all the stations affected by the volcano, discerning the different stages and sampling methodologies. Black lines show the average concentrations from all the reference stations, with a standard deviation. Upper x-axis in panel (C) corresponds to silicate concentrations in the vent samples (green).

This behavior is also observed when comparing the nutrient emissions during each individual cruise (Figure 3.3). Here, in order to avoid the variability with depth, significant anomalies were calculated (sΔ[X]; see Data and Methods) and are represented as boxplots showing the median and the distribution of the data in quartiles. This representation cannot be considered a temporal evolution of the emissions due to the different sampling methodologies applied; however, it provides a more detailed comparison and shows the high variability of the data even within each methodological dataset. For the eruptive stage, all the maxima were observed in November 2011 (cruise 2). For the degassing stage, highest concentrations of phosphate and silicate were found in the samples collected with ROV (vent samples; note the difference in the axis range for these samples), but this is not the case for nitrate, which seems to decrease during degasification regardless of the sampling methodology.

Nutrient concentrations in the volcanic emissions are quantified in detail in Table 3.1. Our results demonstrate an enrichment in all nutrients during both the eruptive and degassing stages. Silicate is the most enriched, up to 16.3-fold in the water column and reaching a three orders of magnitude enrichment in the vent
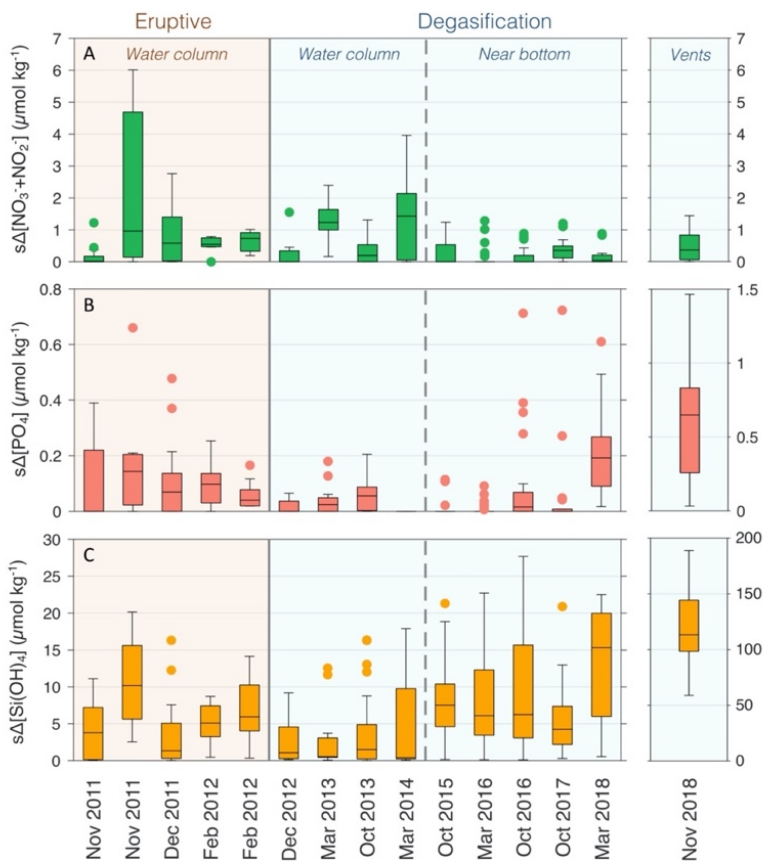
Figure 3.3. Significant anomalies of (A) nitrate+nitrite, (B) phosphate, and (C) silicate for each cruise. Boxplots show the median, quartiles, and outliers of the datasets. Volcanic stage (eruptive/degasification) and sampling type according to the sampling methodology (water column/near bottom/vents) are specified.

samples (maximum of 325.4-fold). For phosphate, a 4.0-fold enrichment was found during the eruptive stage, but it seemed to decrease in the water column during the degassing stage; however, remarkable enrichments were found when the sampling methodology was adapted for more proximity to the source, presenting a maximum of 10.5-fold in the vent samples. Nitrate was largely enriched in the water column during the eruptive stage (maximum of 8.8-fold) but drastically decreased in degasification, and unlike phosphate and silicate, the near-bottom and vent samples did not reflect higher percentages of nitrate, reaching only a 2.5-fold. Additionally, we provide some preliminary ammonium (NH_4^+) data from the ROV-collected samples (cruise 15), which show concentrations of up to 1.97 µM while reference concentrations measured at the same depth were 0.02 µM.

Table 3.1. Information from each cruise carried out in Tagoro volcano.

Cruise	Date	Stage	Sampling methodology	n_{ref}	n_{aff}	Main depth (m)	$\Delta\theta°C$	$[N+N]_{ref}$ (μmol kg^{-1})	$[N+N]_{aff}$ (μmol kg^{-1})	$[N+N]$ enrichment (fold)	$[PO_4]_{ref}$ (μmol kg^{-1})	$[PO_4]_{aff}$ (μmol kg^{-1})	$[PO_4]$ enrichment (fold)	$[Si(OH)_4]_{ref}$ (μmol kg^{-1})	$[Si(OH)_4]_{aff}$ (μmol kg^{-1})	$[Si(OH)_4]$ enrichment (fold)	$[NH_4^+]$ (μM)
1	Nov 2011	E	VP	51	14	75	+2.3	0.11±0.06	0.04–2.46	2.4	0.02±0.01	0.02–0.45	4.0	0.35±0.10	0.31–11.55	11.1	-
2	Nov 2011	E	VP	104	7	100	+2.3	1.75±0.34	0.67–8.06	3.2	0.11±0.02	0.12–0.79	3.8	1.23±0.38	3.80–21.76	4.6	-
3	Dec 2011	E	VP	51	21	10	+0.2	0.07±0.05	0.09–6.26	7.0	0.02±0.00	0.02–0.50	3.2	0.23±0.02	0.48–16.56	7.5	-
4	Feb 2012	E	VP	51	7	20	+0.6	0.05±0.02	0.55–0.83	5.8	0.02±0.00	0.05–0.27	3.0	0.23±0.00	1.13–9.22	10.0	-
5	Feb 2012	E	VP	51	18	10	+0.2	0.07±0.05	0.28–1.11	8.8	0.02±0.00	0.04–0.19	2.7	0.23±0.02	0.77–14.39	16.3	-
6	Dec 2012	D	VP	37	7	100	+1.5	1.83±1.20	0.32–3.88	2.1	0.10±0.08	0.02–0.23	1.2	0.98±0.62	0.53–10.74	2.3	-
7	Mar 2013	D	VP	593	14	90	+0.3	0.72±0.51	0.71–5.38	2.5	0.07±0.04	0.02–0.29	1.4	0.56±0.20	1.04–13.29	3.3	-
8	Nov 2013	D	VP	162	31	110	+1.5	1.54±0.72	0.34–4.08	1.7	0.06±0.03	0.02–0.29	1.7	0.82±0.12	0.60–17.22	2.9	-
9	Mar 2014	D	VP	543	11	130	+0.6	2.05±1.10	1.28–6.21	2.2	0.08±0.06	0.02–0.08	1.0	0.87±0.33	0.66–18.99	4.1	-
10	Oct 2015	D	TWY	65	51	123	+1.3	2.20±0.46	0.16–3.41	1.5	0.14±0.04	0.04–0.30	1.0	0.66±0.22	0.57–22.18	6.0	-
11	Mar 2016	D	TWY	39	54	123	+0.8	1.56±0.93	0.17–3.62	1.1	0.11±0.07	0.05–0.26	1.1	0.20±0.12	0.20–22.99	21.6	-
12	Oct 2016	D	TWY	98	35	123	+1.5	1.87±0.59	0.88–3.46	1.1	0.06±0.03	0.05–0.81	1.6	0.24±0.17	0.47–28.10	18.8	-
13	Oct 2017	D	TWY	23	26	123	+1.7	1.34±0.22	0.72–2.78	1.1	0.19±0.06	0.09–0.98	1.1	0.12±0.03	0.98–21.12	12.4	-
14	Mar 2018	D	TWY	30	16	123	+0.5	0.38±0.07	0.20–1.44	1.2	0.07±0.01	0.10–0.70	1.8	0.32±0.37	1.25–23.15	12.9	-
15	Nov 2018	D	ROV	28	2	108	+1.3	1.14±0.51	1.67–2.53	1.9	0.11±0.03	0.30–1.60	9.0	0.47±0.11	100.56–150.00	267.2	0.57±0.16
15	Nov 2018	D	ROV	28	2	126	+1.9	1.72±0.86	2.66–2.88	1.7	0.14±0.06	0.42–0.49	3.3	0.58±0.19	110.20–112.66	196.1	0.92±0.32
15	Nov 2018	D	ROV	28	2	129	+1.9	1.91±0.83	2.31–2.74	1.2	0.15±0.06	0.24–0.34	1.9	0.61±0.19	59.67–97.62	130.5	0.51±0.16
15	Nov 2018	D	ROV	28	2	118	+1.5	1.44±0.72	2.30–2.71	1.8	0.12±0.05	0.98–1.21	9.0	0.53±0.15	115.29–135.74	240.6	0.74±0.02
15	Nov 2018	D	ROV	28	2	126	+4.2	1.72±0.86	2.42–3.26	1.5	0.14±0.06	0.96–1.05	7.4	0.58±0.19	147.20–176.61	284.9	0.52±0.07
15	Nov 2018	D	ROV	28	2	116	+2.6	1.38±0.67	2.37–2.95	2.0	0.12±0.05	0.53–0.57	4.7	0.52±0.15	109.02–142.83	246.3	0.74±0.20
15	Nov 2018	D	ROV	28	2	111	+3.4	1.23±0.57	1.44–2.85	1.7	0.11±0.04	0.76–0.90	7.5	0.49±0.12	126.03–189.40	325.4	1.97±1.46
15	Nov 2018	D	ROV	28	2	103	+3.4	0.99±0.41	2.11–2.84	2.5	0.09±0.03	0.81–1.26	10.5	0.45±0.09	92.17–96.62	210.9	1.26±0.43
Other studies																	
V.I.	May 1993	-	Funnel	2	6	0.3	+44.0	0.13±0.07	0.02–0.09	0.3	0.04±0.00	0.13–1.23	20.5	87.9±0.5	631–1630	12.3	
L.S.*	Jun 1994	-	Submersible	1	4	1700	+156.0	18.2	7.79–18.10	0.8	1.22	0.10–0.87	0.4	-	-	-	
P.V.*	1987–1988	-	Submersible	1	23	1000	+26.0	42.10	14.48–42.73	0.9	2.93	1.68–3.91	0.9	102.1	102.1–721.0	2.8	

*Nutrient data are shown as: (i) Average reference concentration in the non-affected stations, with standard deviation; (ii) Concentration range at the affected stations in the affected depth range (0-150 m for eruptive stage and 60-150 m for degassing stage); (iii) Average enrichment in the affected stations respect to the reference. E = Eruptive stage; D = Degassing stage; VP = Vertical profiles (water-column samples); TWY = tow-yo transects (near-bottom samples); ROV = samples collected from the vents by remotely operated vehicle Liropus 2000 with a piston-driven suction system. n(ref.) = number of samples used as reference; n(aff.) = number of analyzed samples affected by the volcanic emissions; $\Delta\theta°C$ = maximum potential temperature anomaly. Other studies: V.I. = Beach fumaroles at Vulcano Island, Aeolian Archipelago, Italy (Sedwick and Stüben, 1996). The hot fluids were conducted directly into the sample bottle with a funnel system. L.S. = Lucky Strike at the Mid-Atlantic Ridge (Sarradin et al., 1999). Samples were collected from the vents with deep-sea submersible Nautile. P.V. = Pele's Vents in Loihi Seamount, Hawaii (Karl et al., 1989). Samples were collected from the vents with deep-sea submersibles Alvin and Pisces V. *Concentrations from these studies are in μmol l^{-1}.*

3.2.3. Extent and transport of the nutrient emissions

The spatial distribution of the emission of inorganic nutrients by the Tagoro volcano during the eruptive stage was studied using the data collected during cruises 1 (November 4–9, 2011) and 2 (November 17–20, 2011). Figures 3.4A–C show horizontal contours of nutrient anomalies during these periods. The blue tones in the contours correspond to anomalies beneath the standard deviation of the mean reference concentrations (non-significant anomalies). Satellite images from NASA MODIS are also shown for the corresponding periods, taken on November 9 and November 20, 2011 (Figure 3.4D) (Eugenio et al., 2014). Note that the observed light-green discoloration of the waters surrounding El Hierro island in these images was due to the chemicals injected by the volcano and was not related to chlorophyll concentrations (Eugenio et al., 2014) and therefore this coloring was used as a natural tracer for the extent of the volcanic plume.

During early November 2011, the plume of the volcanic emissions was transported southward and south-westward, as shown in the contours of cruise 1 (Figures 3.4A1,B1,C1) as well as in the satellite image (Figure 3.4D1). It should be noted that not all nutrients appear to be transported the same distance: silicate transport covers the widest area, followed by phosphate, and then nitrate; this could be related to the different detection limits of the nutrient analysis system. In late November 2011 (cruise 2), a plume was transported from the volcano-affected area northward by the local currents, as can be seen in the satellite images (Figure 3.4D2). This transport is also observed for the nutrient anomalies (Figures 3.4A2,B2,C2), which reached the northwest coast of El Hierro. For this area affected north of the island in late November 2011, new percentages of enrichment were calculated respect to the reference levels, obtaining enrichments up to 1.1-, 1.2-, and 2.0-fold for nitrate, phosphate, and silicate, respectively.

During the degassing stage, the effects of the volcanic emissions were detectable in a more constrained area in the vicinity of the main crater. With the purpose of studying these localized anomalies, during cruises 7–9 a high-resolution transect of vertical profiles was established across the main and secondary craters (Figure 3.1C). From these profiles, nutrient anomalies ($\Delta[X]$) for the degassing stage were calculated and are shown in Figure 3.5 as vertical contours with latitude. The blue tones in the contours represent non-significant anomalies. Due to the cyclic behavior of the hydrothermal discharge (Fraile-Nuez et al., 2018) it is not possible to obtain all the maximum anomalies during one complete transect; for this reason, the vertical profiles that showed maximum anomalies obtained during

cruises 7–9 have been selected for the contours, providing a representation of the hydrothermal discharge if it could be sampled simultaneously at all stations. Data from the vent samples of cruise 15 are also shown for phosphate and silicate
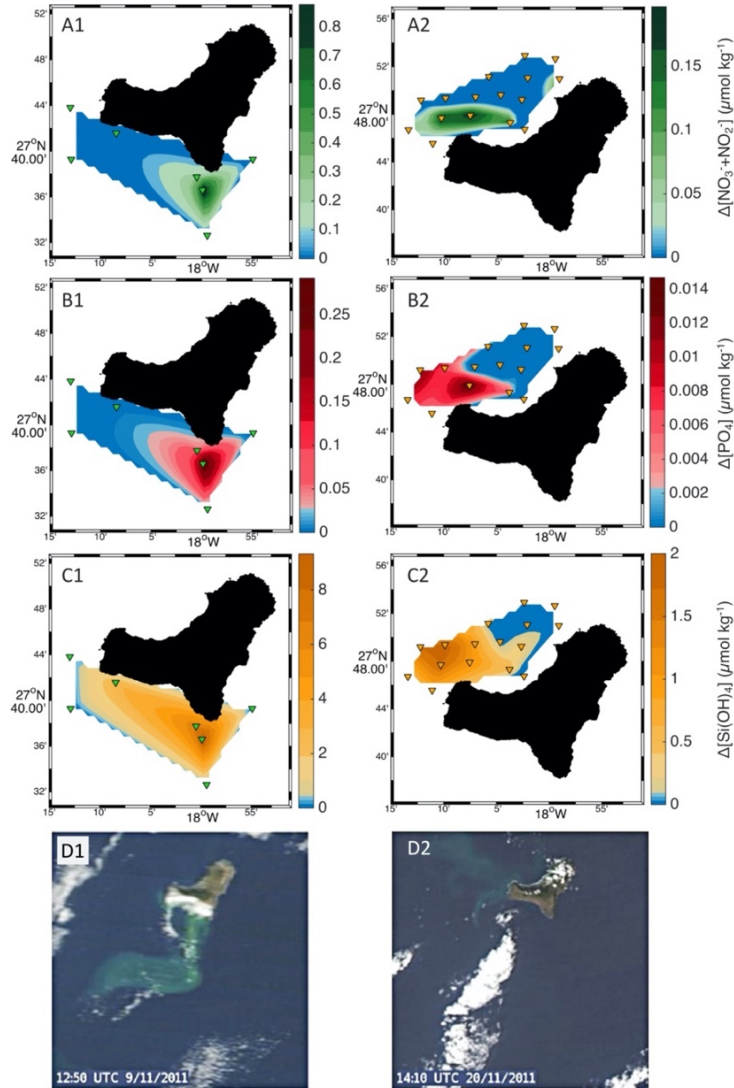

Figure 3.4. Horizontal contours of nutrient anomalies for (A1, A2) nitrate+nitrite, (B1, B2) phosphate, and (C1, C2) silicate in the eruptive stage, during cruises 1 and 2, respectively. The blue tones in the contours show anomalies below the standard deviation of the reference. (D) NASA MODIS RGB images of El Hierro island monitoring the eruptive event on (D1) November 9 and (D2) November 20, 2011. Note that the color of the plume is due to the chemicals injected by the volcano and not related to the accumulation of chlorophyll-*a* in the water column (Eugenio et al., 2014).

(Figures 3.5B,C), but not for nitrate as the vent data did not present higher values than those collected in vertical profiles. Maximum anomalies in the water column are found at stations 55–61 (main crater) and 56 (summit), with maxima of 4.87 (N+N), 0.23 (PO$_4$) and 16.36 (Si(OH)$_4$) µmol kg^{-1}, but remarkably higher anomalies are observed in the vent samples for phosphate and silicate (1.50 and
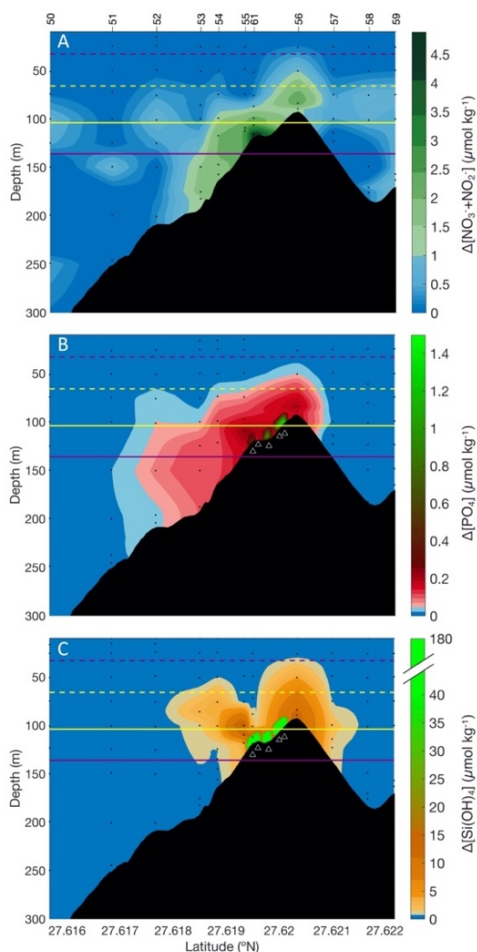
Figure 3.5. Vertical contours of anomalies of (A) nitrate+nitrite, (B) phosphate, and (C) silicate in a high-resolution transect of the main cone during the degassing stage. The blue tones show anomalies within the standard deviation of the reference (non-significant anomalies). Stations that presented maximum anomalies from cruises 7-9 were selected for the contours. Data collected in cruise 15 from several vents (marked as triangles) are also shown in panels (B,C). Horizontal lines show the depth of the mixed layer (purple) and of the euphotic zone (yellow), as minimum and maximum values (dashed lines and solid lines, respectively) obtained from monthly averaged datasets provided by the Copernicus Marine Environment Monitoring Service (see Data and Methods).

188.91 µmol kg^{-1}, respectively). The anomalies are found in the first 50–75 m above the seabed and are usually transported southward of the main cones generally until station 52 (about 250 m away from the main cone), whereas northward the anomalies reach only station 57 (about 150 m away from the summit). This is in agreement with the predominant south-southwest current direction described for this region from ADCP data (Santana-Casiano et al., 2016). In total, the nutrient emissions can be detected as enhanced concentrations in a 400 m range around (but not centered on) the main cone.

The contours in Figure 3.5 conform a high-resolution transect above the main craters and perpendicular to the main current. From these anomaly data, nutrient fluxes for the degassing stage were obtained, representing an estimate of the volcanic nutrient emissions transported to the surrounding waters. The results of the fluxes averaged for the delimited area were 3.19 ± 1.17 mol m^{-2} year^{-1} for N+N, 0.02 ± 0.01 mol m^{-2} year^{-1} for PO$_4$, and 0.60 ± 1.35 mol m^{-2} year^{-1} for Si(OH)$_4$. The substantial standard deviations account for the high variability of concentrations found along the plume, dependent on the proximity to the source, but the averaged values are a representative estimation of the magnitude of these fluxes. In Table 3.2, these results are shown in detail and can be compared with other important nutrient sources in the region such as upwelling systems, mesoscale structures and upwelling filaments.

Table 3.2. Nutrient fluxes calculated from a transect perpendicular to the main current during the degassing stage.

Setting	NO$_2^-$+NO$_3^-$ flux	PO$_4$ flux	Si(OH)$_4$ flux
Tagoro submarine volcano (mol m^{-2} year^{-1})	3.19 ± 1.17 [1.73 – 7.77]	0.02 ± 0.01 [0.01 – 0.20]	0.60 ± 1.35 [0.10 – 17.11]
NW African coastal upwelling (mol m^{-2} year^{-1})	5.87 *	0.37 **	1.81 **
Filaments reaching the Canary region (mol m^{-2} year^{-1})	0.29 *	0.02 **	0.09 **
Permanent cyclonic eddie in the Canary region (mol m^{-2} year^{-1})	1.36 *	0.09 **	0.42 **

Nitrogen fluxes reported by Barton et al. (1998)
**Phosphate and silicate fluxes estimated from the nitrogen fluxes from* Barton et al. (1998) *using the nutrient ratios obtained in this study*

3.3.3. Nutrient ratios

The correlations between all three nutrients as well as a silicate-temperature correlation are presented in Figure 3.6. First, in order to evaluate whether silicate can act as a mixing tracer of the volcanic emissions, a correlation was made with

a conservative component such as potential temperature (Figure 3.6D). In order to avoid seasonal and depth-related variability in temperature, the regression was calculated only with the data collected from the vents and some near-bottom (tow-yo) samples within the same depth range (100–130 m) and from the same season as the vent samples. The tow-yo data are quite condensed in a relatively small range of temperature and $[Si(OH)_4]$, providing an intercept for the regression line; whereas the vent data, although sparser, define a clear slope. This regression presents a $r^2 = 0.878$ and $p < 0.001$, underlining an adequate linear relationship between the concentration of silicate and the temperature of the hydrothermal fluids in the area and thus allowing to use $[Si(OH)_4]$ as a mixing tracer.
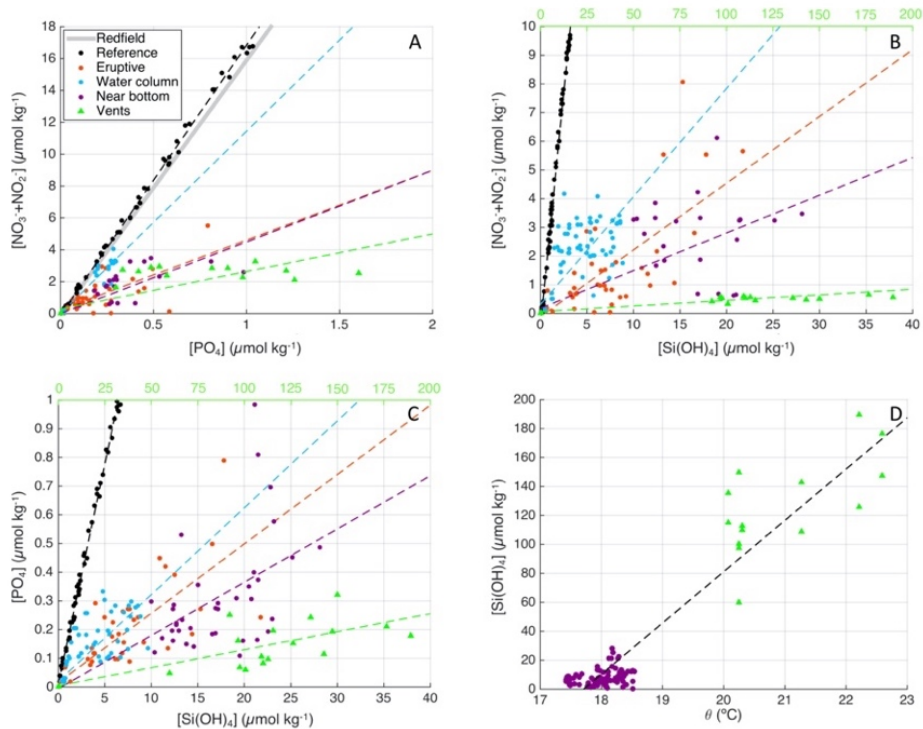
Figure 3.6. Nutrient ratios calculated as linear correlations. (A) $(NO_3^- + NO_2^-):PO_4$ ratio, abbreviated as N:P (Redfield's 16:1 ratio is shown). (B) $(NO_3^- + NO_2^-):Si(OH)_4$ as N:Si, and (C) $PO_4:Si(OH)_4$ as P:Si, for the reference stations, the eruptive stage, and the degassing stage classified according to the grade of dilution of the samples (water-column/near-bottom/vents). Upper x-axis in panels (B,C) corresponds to silicate concentration in the vent samples (green). (D) Relation between silicate and potential temperature from the closest samples to the source.

Once silicate has been correlated to a conservative parameter as temperature, the ratios of all three nutrients were studied: nitrate to phosphate (abbreviated N:P, although more accurately NO_2^- + NO_3^-:PO_4), nitrate to silicate (similarly abbreviated N:Si), and phosphate to silicate (P:Si). Figures 3.6A–C shows these correlations for reference and affected stations during both the eruptive and degassing stages, and discerning the latter according to the sample type. In this case, the data from the degassing stage were classified not only according to the sampling methodology used (vertical profiles/tow-yos) but also according to the dilution grade of the samples, using the silicate concentration as a mixing tracer. All slopes, r^2 and p-values can be consulted in Table 3.3.

In general, reference data for all three ratios presented a better fit ($r^2 > 0.99$) than the affected samples (r^2 between 0.485 and 0.925). However, although the affected datasets are more dispersed, a general trend in the slopes is evident regarding the dilution grade (proximity to the source): water-column samples (blue), which are the most diluted, present the closest ratio to the reference (black); followed by near-bottom samples (purple); and finally vent samples (green), which are the closest to the source, present the smallest ratio (2.36:1). This trend is observed for all the three ratios (Figures 3.6A–C). In Figure 3.6A (N:P ratio) the Redfield ratio is also shown, a nearly constant 16:1 correlation between nitrate and phosphate that is commonly observed in seawater as well as in phytoplankton biomass (Gruber and Deutsch, 2014); our reference data are in close agreement with this ratio (16.95:1).

Table 3.3. Slopes and statistics for the correlations shown in Figure 3.6.

Ratio	Data	Slope	r^2	p-value
N:P	Reference	16.95	0.998	$p<0.001$
N:P	Eruptive	4.38	0.485	$p<0.001$
N:P	Degasification (water column)	11.44	0.855	$p<0.001$
N:P	Degasification (near bottom)	4.49	0.812	$p<0.001$
N:P	Degasification (vents)	2.36	0.708	$p<0.001$
N:Si	Reference	3.24	0.994	$p<0.001$
N:Si	Eruptive	0.23	0.606	$p<0.001$
N:Si	Degasification (water column)	0.38	0.668	$p<0.001$
N:Si	Degasification (near bottom)	0.13	0.567	$p<0.001$
N:Si	Degasification (vents)	0.02	0.925	$p<0.001$
P:Si	Reference	0.15	0.995	$p<0.001$
P:Si	Eruptive	0.02	0.689	$p<0.001$
P:Si	Degasification (water column)	0.03	0.699	$p<0.001$
P:Si	Degasification (near bottom)	0.02	0.505	$p<0.001$
P:Si	Degasification (vents)	0.01	0.633	$p<0.001$
Si:θ	Degasification (vents + near bottom)	35.45	0.878	$p<0.001$

The interceptions of all the lines were either equal or forced to roughly 0, except for the Si:θ regression, which presented an interception of −627.78.

3.4. Discussion

The shallow submarine volcano Tagoro released significant amounts of dissolved inorganic macronutrients throughout the whole study period (2011–2018). We have quantified these emissions for the eruptive and the degassing stages of the volcano, and in the latter stage we have highlighted some noteworthy observations concerning the different sampling methodologies applied. Concentrations of phosphate and silicate increased with the proximity of the sample collection to the source: the least concentrated were the water-column samples, followed by the near-bottom samples, and finally the vent samples. Contrastingly, the maximum concentrations of N+N were found in the water-column samples (which are assumed to be the most diluted with ambient waters) and decreased in the near-bottom and vent samples. We hypothesize that dissolved inorganic nitrogen is emitted mainly in the form of ammonium (NH_4^+), as has been widely described for other hydrothermal systems (Karl et al., 1988, 1989; Sedwick and Stüben, 1996; Kilias et al., 2013). However, due to a lack of the necessary instrumentation we could not implement ammonium analyses until recently, and thus, we have only been able to measure a small number of ammonium samples collected from the vents with ROV (cruise 15). These were analyzed for ammonium long after their collection and might have been subject to losses of ammonium. Nonetheless, even with these limitations, we have found concentrations of NH_4^+ of up to 1.97 µM, in contrast to reference concentrations of 0.02 µM at the same depth. This supports our hypothesis and suggests that the higher concentrations of N+N observed in the water column with increasing distance from the vents are the result of oxidative processes, which have been observed elsewhere in hydrothermal systems from deep-sea (Lam et al., 2004, 2008; Baker et al., 2012) as well as shallow settings (Kilias et al., 2013). However, this would require a more specific study and the recollection of a larger dataset of NH_4^+ samples.

The boxplots of nutrient anomalies in Figure 3.3 also provide information regarding the changes in the emissions with the different sampling methodologies applied. When analyzing these data, it is important to keep in mind that the volcano exhibits acyclic degassing behavior (Fraile-Nuez et al., 2018), with periodic emissions that then undergo mixing and dilution through the water column. Therefore, when collecting water samples during vertical profiles or tow-yos, samples may carry recently emitted concentrated fluids, or more previously emitted fluids that have been exposed to mixing and dilution for a longer time. This feature accounts for the high variability observed in the data distribution in Figure 3.3 even within each methodological dataset. Moreover, the outliers in the

boxplots should not be interpreted as uncommonly high-concentrated episodic emissions, but rather as representatives of the most concentrated form of the hydrothermal fluids that can be detected in the water column before undergoing dilution or other withdrawal processes.

The present study provides an interesting overview on how hydrothermal emissions can have very different impacts depending on the depth at which the vents are found, as the ambient concentrations of nutrients vary markedly with depth. In Table 3.1 we provide nutrient concentrations and enrichments for Tagoro volcano and for three different hydrothermal settings: shallow active submarine warm springs off the island of Vulcano, Aeolian Archipelago, Italy (Sedwick and Stüben, 1996); Lucky Strike at 1700 m depth in the Mid-Atlantic Ridge (Sarradin et al., 1999); and Pele's Vents at 1000 m depth in Lō'ihi Seamount, Hawai'i (Karl et al., 1989). The samples in these studies were collected directly from the vents using different sampling methodologies, therefore they are comparable to the ROV-collected vent samples from Tagoro volcano. However, the comparison is not straightforward, as in the deep settings (Lucky Strike and Lō'ihi Seamount) the emitted hydrothermal fluids are mixed with nutrient-rich ambient waters. For instance, in Pele's Vents (1000 m depth), an average of 2.8-fold enrichment in silicate was obtained considering a 102.1 µM reference and a range of 102.1–721.0 µM found in the emissions. A similar $[Si(OH)_4]$ range was found in the vent samples of Tagoro volcano (126.03–189.40 µmol kg^{-1}); however, compared to the low ambient concentrations (0.49 µmol kg^{-1}) at the 111 m depth of this vent, the resulting enrichment was as large as 325.4-fold. In the same way, a $[PO_4]$ range of 0.81–1.26 µmol kg^{-1} in Tagoro volcano represented a 10.5-fold enrichment, while in the nutrient-rich deep waters of the Lucky Strike, concentrations of similar magnitude (0.10–0.87 µM) did not constitute an enrichment, but a depletion of 0.4-fold. In contrast, the enrichments found in the shallow (0.3 m depth) fumaroles of Vulcano island are more similar to our results, with a 20.5-fold enrichment for phosphate and 12.3-fold for silicate, as well as significant enrichments in NH_4^+ of roughly three times the ambient concentrations. These results underline the importance of shallow submarine volcanoes as a source of nutrient enrichment for surface waters.

Average nutrient fluxes for the degassing stage were calculated from a transect perpendicular to the current (Table 3.2). (Barton et al., 1998) estimated nitrogen fluxes related to upwelling filaments and eddies in the transition zone of the Canary Current upwelling region. With the purpose of comparing the magnitude of these different processes, we estimated phosphate and silicate fluxes from these reported nitrogen data by using the ratios obtained from the reference stations

surrounding El Hierro island (ratios in Table 3.3). The reported fluxes for upwelling and mesoscale processes in the region are of similar magnitude as compared to the hydrothermal emissions of the Tagoro volcano when compared per units of area. For instance, a 5.87 mol m^{-2} year^{-1} nitrogen flux from the African coastal upwelling was described by Barton et al. (1998), comparable to the 3.19 mol m^{-2} year^{-1} nitrate flux found in Tagoro volcano. Similarly, the phosphate flux from the filaments reaching the Canary Islands is estimated as 0.02 mol m^{-2} year^{-1}, coinciding with our results for the flux of this nutrient from the degasification of Tagoro. Additionally, the fluxes from a permanent cyclonic eddy in the Canary region (estimated silicate flux of 0.42 mol m^{-2} year^{-1}) are of similar magnitude to our results of 0.60 mol m^{-2} year^{-1} for the same nutrient. These results underline that the shallow volcano Tagoro constitutes an additional relevant source for nutrient transport in the Canary region. A comparison with other volcanic and hydrothermal settings is troublesome, since estimates of nutrient fluxes from these sorts of sources are very scarce and are mostly found as global estimates (Tréguer et al., 1995; Paytan and McLaughlin, 2007; Tréguer and De La Rocha, 2013) rather than regional approaches. Nevertheless, an interesting observation can be addressed in relation to phosphate emissions. Hydrothermal processes have often been described as a sink in the phosphorus cycle (Paytan and McLaughlin, 2007), mainly due to a net loss by formation of suspended iron oxyhydroxides and by direct uptake of phosphate through reaction with basalt (Föllmi, 1996). However, these estimations mostly account for deep hydrothermal systems where the ambient concentrations of nutrients are high. Conversely, our results show a net input of phosphate to the oligotrophic surrounding waters of El Hierro island, showing the importance of shallow hydrothermal emissions for estimating global nutrient fluxes to the surface ocean. In fact, our results show that hydrothermal nutrient emission at the Tagoro volcano occurred mostly around 50–75 m above the seabed. This means that nutrients will be occasionally injected in the mixed layer and well within the euphotic zone (Figure 3.5) where they could have a significant impact on primary production.

We aimed to study the relations among the different nutrients and the evolution of these ratios according to the dilution grade of the samples using correlation analysis. Figure 3.6A shows the commonly studied N:P ratio, although in this case it should be interpreted as $NO_2^- + NO_3^-:PO_4$ relationships. Nevertheless, our reference data exhibits a 16.95:1 ratio, in notable agreement with the Redfield ratio (16:1), and with an excellent fit ($r^2 = 0.998$; $p < 0.001$). The volcano-affected datasets are more scattered (r^2 ranging between 0.485–0.855; $p < 0.001$); however, the slopes show a clear evolution of the ratio with the dilution grade: the smallest

ratio is found at the vent samples (2.36:1), followed by the eruptive stage samples (4.38) and near-bottom degasification samples (4.49), and finally the water-column degasification samples (11.44:1).

This trend of the ratios according to the dilution grade of the samples can also be observed for the $NO_2^- + NO_3^-:Si(OH)_4$ and $PO_4:Si(OH)_4$ correlations in Figures 3.6B,C, respectively. However, these plots also offer further information about the behavior of these species after their emission, as silicate is commonly used as a mixing tracer for volcanic and hydrothermal fluids (Edmond et al., 1979; Sansone et al., 1991; Sansone and Resing, 1995; Sedwick and Stüben, 1996). When species concentrations plot linearly against dissolved Si concentration, conservative behavior is suggested for that species during mixing of the hydrothermal fluids with seawater, whereas when a non-linear relationship is observed, non-conservative mixing behavior is suggested (Sedwick and Stüben, 1996). In order to assess whether our $Si(OH)_4$ data could be used as a mixing tracer, the concentrations were plotted against potential temperature in Figure 3.6D. The data exhibited a good fit ($r^2 = 0.878$; $p < 0.001$) with a linear relationship of $y = 35.45x$ - 627.78, which is notably consistent with the relation of $y = 31.0x$ - 601 found by Sedwick and Stüben (1996) in the beach fumaroles of Vulcano island. In the same study, the N+N concentrations showed no consistent trend against dissolved Si; however, in a study in Lō'ihi Seamount (Karl et al., 1989) a linear relationship was found when N+N and PO_4 were plotted against Si. In this sense, the linear fits of our N:Si and P:Si data indicates a conservative mixing behavior of these species, but the notably lower r^2 values of these fits (roughly 0.5–0.6) should be taken into account. Considering all the observations we have discussed, in particular the notable withdrawal of phosphate indicated by a marked difference in concentration between the near-bottom and the water-column samples (Figure 3.3 and Table 3.1) as well as the nitrifying processes hypothesized previously, it is likely that the scatter in the concentrations of these nutrients could be related to a non-conservative mixing behavior caused by chemical or biological processes that cannot be assessed in this study and should be considered for further research.

In addition to the hydrothermal input of dissolved inorganic nitrogen, phosphorus, and silicate described in this work as well as in the literature (Tunnicliffe et al., 1986; Karl, McMurtry, et al., 1988; Karl et al., 1989; Sedwick and Stüben, 1996; Sarradin et al., 1999), recent studies also describe important inputs of biologically available iron [Fe(II)] from deep and shallow hydrothermal vents (Santana-Casiano et al., 2013; Resing et al., 2015; Buck et al., 2018). Consequently, the question of whether volcanic and hydrothermal emissions can

fertilize shallow waters and have an impact on the local phytoplanktonic communities becomes a relevant one (Buck et al., 2018; Gómez-Letona et al., 2018; Wilson et al., 2019). Although this question is beyond the scope of this study, the fact the nutrients are occasionally injected into the euphotic zone and into the mixed layer at the Tagoro volcano warrant further investigation in the future.

3.5. Conclusions

Through this study, we have confirmed that the submarine volcano Tagoro has emitted significant amounts of dissolved inorganic nutrients from the beginning of its eruptive process in 2011 until the latest survey carried out in 2018. We have quantified these emissions and have found maximum concentrations for the eruptive stage of 8.06 µmol kg^{-1} of NO_2^- + NO_3^- (reference: 1.75 µmol kg^{-1}), 0.79 µmol kg^{-1} of PO_4 (reference: 0.11 µmol kg^{-1}) and 21.76 µmol kg^{-1} of $Si(OH)_4$ (reference: 1.23 µmol kg^{-1}). For the degassing stage, remarkable differences in the results were observed with regard to the sampling methodology applied. The largest concentrations of phosphate and silicate were found in the samples collected directly from the vents with ROV, with maxima of 1.26 and 189.40 µmol kg^{-1}, respectively; whereas for nitrate the maximum (6.21 µmol kg^{-1}) was found in the most mixed (water-column) samples and decreased when approaching the source. From these vent samples, ammonium concentrations were analyzed, finding maximums of 1.97 µM (reference: 0.02 µM). Average enrichments were obtained, with water-column maxima of 8.8-fold (nitrate), 4.0-fold (phosphate) and 16.3-fold (silicate), and higher vent maxima of 10.5-fold (phosphate) and 325.4-fold (silicate). A preliminary analysis of ammonium (NH_4^+) in the vent samples showed maximum concentrations of 1.97µM (reference: 0.02 µM), supporting the vast compilation of studies describing the emission of this species from hydrothermal vents and suggesting the occurrence of nitrifying processes, which should be assessed in future studies.

Nutrient fluxes transported from the hydrothermal emissions into the surrounding waters during the degassing stage were estimated as 3.19 ± 1.17 mol m^{-2} year^{-1} for NO_2^- + NO_3^-, 0.02 ± 0.01 mol m^{-2} year^{-1} for PO_4, and 0.60 ± 1.35 mol m^{-2} year^{-1} for $Si(OH)_4$. These results were found to be of similar magnitude as other important nutrient transport sources in the Canary region, such as NW-African coastal upwelling, upwelling filaments, and permanent cyclonic eddies. Notably, while hydrothermal processes are often described as a sink in the phosphorus cycle, our results highlight a positive phosphate transport from the volcano into the oligotrophic surroundings.

The nutrient ratios (N:P, N:Si, and P:Si) showed an evident relationship with the grade of dilution of the samples. The N:P ratio indicated a deviation from the 16:1 Redfield proportion, progressively decreasing with the proximity of the samples to the source until finding a 2.36:1 ratio in the vent samples. The N:Si and P:Si ratios also showed this behavior, with a minimum ratio in the vent samples of 0.02:1 (N:Si; reference: 3.24:1) and 0.01:1 (P:Si; reference: 0.15:1). Furthermore, seeing as silicate can act as a mixing tracer, the notable dispersion observed in the N:Si and P:Si fits might indicate a non-conservative mixing behavior of nitrate and phosphate.

The biogeochemical impact of hydrothermal emissions has typically been studied mainly from deep hydrothermal settings. However, the unprecedented 7-year dataset from a shallow active submarine volcano presented in this study has highlighted the need to account for shallow hydrothermal emissions as important sources of nutrients to the ocean.

Impacts of the lava delta formation from the 2021 La Palma eruption on the marine environment

Abstract

The 2021 Cumbre Vieja eruption in La Palma (Canary Islands, Spain) emitted vast volumes of lava during 85 days, which reached the ocean in several occasions at the western flank of the island. Most of these flows merged to create a primary lava delta, covering an area of 48 Ha, with an additional 30 Ha underwater. Here we characterize the effects of the lava-seawater interaction on the surrounding marine environment. The area was sampled during two multidisciplinary oceanographic cruises: the first one comprised the days before the lava reached the ocean and after the first contact; and the second took place a month later, when the lava delta was already formed but still receiving lava inputs. Physical-chemical anomalies were found in the whole water column at different depths up to 300 m in all measured parameters, such as turbidity (+9 NTU), dissolved oxygen concentration (-17.17 μmol kg^{-1}), pH$_{T25}$ (-0.1), and chlorophyll-*a* concentration (-0.33 mg m^{-3}). Surface temperature increased up to +2.3ºC (28.5ºC) and surface salinity showed increases and decreases of -1.01 and +0.70, respectively, in a radius of 6 km around the lava delta. In the water column, the heated waters experimented a lava-induced upwelling, bringing deeper, nutrient-rich waters to shallower depths; however, this feature did not trigger any phytoplankton bloom. In fact, integrated chlorophyll-*a* showed an abrupt decrease of -41% in just two days and -69% a month later, compared to prior conditions. The chlorophyll-*a* depletion reached a distance larger than 2.5 km (not delimited).

4.1. Introduction

Lava-seawater interaction processes are common in volcanic islands, where the lava from subaerial eruptions flows towards the coastline, spilling over cliffs and filling the shore platforms (Soule et al., 2021; Rodriguez-Gonzalez et al., 2022). When the lava reaches the shore, the marked contrast in temperature with the seawater produces a quick solidification of the lava surface. This process can produce a geological structure known as lava delta, a platform formed over previous seafloor due to the deposition and solidification of lava and clastic materials that fill the shallower areas of the insular shelf (Moore et al., 1973; Ramalho et al., 2013; Rodriguez-Gonzalez et al., 2022). These inputs of lava to the ocean lead to significant fluxes of mass and heat to the overlying ocean on a local-to-regional basis, which have been compared in magnitude to those from ridge crest vent fields (Sansone and Resing, 1995). However, these mechanisms are rarely documented, particularly the underwater processes, due to a variety of

reasons such as the rare occurrence of these phenomena, the safety regulations during an active eruption, and the logistical challenges of organizing unforeseen emergency cruises.

Previous studies have reported surface temperature anomalies ranging from a few degrees to roughly +30ºC (Moore et al., 1973; Sansone et al., 1991; Sansone and Resing, 1995; Román et al., 2022). The lava-impacted water plumes have been observed to expand beyond 70 m depth and 2 km distance (Moore et al., 1973; Sansone and Resing, 1995). These plumes typically show a low pH due to the presence of acidic solutes and gases (Resing and Sansone, 1999; González-Santana et al., 2022). The interaction of hot lava and cold seawater can drive hydrovolcanic explosions and quench-granulation of the lava, producing small particles named hyaloclastite (Watton et al., 2013; Soule et al., 2021). The presence of these particles, along with suspended ashes from the subaerial eruption reaching the ocean, generates high levels of turbidity and light attenuation in the seawater (Sansone and Resing, 1995; Whiteside et al., 2023).

The effects of these lava-seawater interaction processes on the local marine ecosystem are very variable. At Kīlauea volcano in Hawaiʻi, a lava-induced upwelling effect has been shown to cause a phytoplankton bloom due to the ascent of deep, nutrient-rich waters to surface (Sansone and Resing, 1995; Wilson et al., 2019). However, in the recent Hunga-Tonga eruption, even though high levels of chlorophyll-*a* up to 2.7 mg m^{-3} were detected by satellite, these were not associated to phytoplankton growth but to materials expelled by the volcano into the ocean (Whiteside et al., 2023), an effect that was observed as well in the submarine eruption at El Hierro island in 2011 (Coca et al., 2014; Eugenio et al., 2014).

La Palma is the second youngest island of the Canary archipelago. This island is at the earliest and fastest shield-building stage of growth and is the fastest-growing island in the archipelago (Carracedo et al., 1999). Between March 2017 and August 2021, several seismic swarms took place around the island of La Palma. However, starting on September 11, a very strong and rapid increase in seismicity took place (Mezcua and Rueda, 2023). The last and most intense seismic swarm preceding the eruption started on 11 September 2021, with >400 events at depths up to 12 km. During the following days, earthquakes continued to grow in frequency, magnitude, and shallowness, along with ground deformation up to 15 cm (IGN, 2022). On 19 September 2021, at 15:12 local time, a strombolian eruption started in the Cumbre Vieja area (28º36'58.6''N, 17º52'0.6''W), at 900 m altitude.

The lava flow advanced over several fronts, with thicknesses of 8-15 m and variable speeds from 1 to 200 m/h. On 28 September 2021 at 23:00 local time,

the lava flow first came into contact with the seawater at the western flank of the island (28°36'38.1"N, 17°55'25.9"W), in a marine Special Conservation Zone. A first lava delta (D1) started to grow as the lava flows descended down the coastal cliffs and advanced seawards over the island shelf. Several other lava flows (D2-D4) reached the ocean on different occasions. Eventually, most of these lava flows (D1, D3 and D4) merged into one main delta, except for the northernmost flow which formed a smaller separate delta. The main delta presented a subaerial area of 48 Ha and an additional underwater area of 30 Ha (Lozano-Rodríguez et al., 2023).

The volcanic materials filled the high and medium course of some submarine ravines. The input of lava along with important deposition of ashes and hyaloclastites perturbed the marine ecosystem. No benthic or pelagic life was observed from 40 to 120 m depth (Fraile-Nuez et al., 2021), and dead pelagic fish were found floating in the surface due to the ingestion of ashes/hyaloclastites that saturated their branchial systems (Caballero et al., 2023).

First measurements in the surface waters adjacent to the frontal zone of the newly formed deltas showed increases of +5°C in surface temperature and 5 units in surface salinity (Román et al., 2022), along with pH values as low as 7.0 with important decreases in alkalinity, total dissolved inorganic carbon, and dissolved oxygen (González-Santana et al., 2022), and important increases in total dissolved nitrogen (Román et al., 2022). Satellite data revealed marked increases in turbidity in a wide area surrounding the lava delta, two orders of magnitude higher than normal conditions, while satellite-detected chlorophyll-*a* did not show any significant changes (Caballero et al., 2022).

The eruption officially ended on 13 December 2021, after 85 days of activity. One month after the end of the eruption, the surrounding marine environment was reported to return to normal conditions based on surface water sampling and satellite data (Caballero et al., 2022; González-Santana et al., 2022). The Cumbre Vieja volcano is currently in a post-eruptive stage with seismic and geochemical activity still registered and important diffuse emission of gases (IGN, 2022).

So far, the existing studies from the La Palma lava deltas are based on surface data and the first few meters of the water column, along with satellite data and unmanned aerial vehicles (UAVs) data (Caballero et al., 2022; González-Santana et al., 2022; Román et al., 2022). In this study, we characterize for the first time the effects of the lava-seawater interaction on the physical-chemical and biological properties of the whole water column, in an area up to 2.5 km distance from the lava delta shoreline. Our dataset comprises the days preceding the arrival of lava to the ocean, along with the first few days after the first lava-seawater contact, and

finally, the monitoring of the area one month later, when the lava deltas were already formed but still receiving lava inputs from the subaerial eruption.

4.2. Data and methods

The sampling strategies were always designed following the safety indications of the government authorities. A security perimeter was initially established at 1.0 km distance from the lava delta front, which was later reduced to 0.5 and finally 0.2 km.

4.2.1. Hydrography

The data were collected during two oceanographic cruises carried out in 2021 (Figure 4.1). The first cruise, VULCANA-III-0921, took place between 25 September and 4 October 2021, which allowed to study the marine environment shortly before and after the first lava flow reached the ocean (28 September). The second cruise, VULCANA-III-1021, was carried out between 18 and 29 October 2021, when lava flows were still reaching the ocean and feeding the lava delta, which allowed to monitor the evolution of the process. The cruises were conducted on board of R/V *Ramón Margalef* and R/V *Ángeles Alvariño*, respectively, both from the Spanish Institute of Oceanography (IEO-CSIC).

Conductivity, temperature, and pressure data (CTD) in the water column were acquired using a SeaBird 911-plus CTD, at a sampling interval of 24 Hz and with dual temperature and conductivity sensors with accuracies of 0.001°C and 0.0003 S/m, respectively. The CTD was also equipped with sensors of pH-ORP (oxidation-reduction potential), turbidity-fluorescence, and dissolved oxygen. Niskin bottles were used for the collection of *in situ* water samples at different depths (12 5-liter bottles on the first cruise and 24 12-liter bottles on the second cruise).

Two sampling strategies were applied. During the first cruise (VULCANA-III-0921), the area was sampled through a grid of hydrographic stations forming two parallel lines to the coast at 1.0 and 1.5 km distance (Figure 4.1B), although after the lava reached the ocean, we focused on sampling as close as possible to the lava front in the 1.0 km line. Most stations were separated less than 200 m, with maximum distances of 600 m. During the second cruise (VULCANA-III-1021), a methodology called tow-yo was applied (Baker et al., 1985; Santana-Casiano et al., 2016), consisting on a transect where the CTD is continuously moved up and down from the sea surface to 5 m above the seabed, while the vessel moves at a slow speed (0.4 kn), forming a sawtooth-shaped set of data through a transect.

This methodology offers a high spatial resolution and an almost-synoptic image of the whole water column in a transect. The transects were designed in a radial manner perpendicular to the lava delta, with a starting point at the safety perimeter (0.2 km at the time) and moving towards the open ocean (Figure 4.1B).

Reference (unaffected) stations were also sampled outside of the study area, where physical-chemical parameters were observed to be within the normal conditions of the area (Figure 4.1A). Station 2 and two repetitions of station 32 were averaged to produce a reference profile for the whole water column.

The concentration of dissolved oxygen in water samples was determined using the Winkler method with subsequent modifications (Carpenter, 1965). The determination was carried out on board with an automated potentiometric titration. These data were used to calibrate the continuous data from the dissolved oxygen sensor in the CTD, using a linear regression by least-squares. The original oxygen data in ml l^{-1} were converted to μmol kg^{-1} using the density values derived from the CTD data. The calibration presented a good fit (r^2=0.977, p-value<0.05).

Chlorophyll-*a* (chl-*a*) concentrations were also determined from the water samples and used to calibrate the fluorescence sensor. Chl-*a* was determined by the fluorometric method (Holm-Hansen et al., 1965). A correction was also applied to the fluorescence data which in some areas was affected by the turbidity signal. A multilinear regression by the method of least squares was applied to the data that presented a linear relationship between turbidity and fluorescence, and the obtained parameters were used to subtract the linear effect of turbidity from the fluorescence signal.

Additionally, surface temperature and salinity data were collected from the vessel's continuous intake of surface waters (~5 m depth) using a SBE 21 SeaCAT thermosalinograph, with a sampling interval of 4 Hz and accuracies of 0.01°C and 0.001 S/m for temperature and conductivity, respectively. These data were acquired throughout the whole trajectory of the vessel in both cruises.

During the first cruise (VULCANA-III-0921), seawater pH was measured through the CTD pH-ORP sensor, and hence, values were obtained in National Boureau Standard (NBS) scale. However, during the second cruise (VULCANA-III-1021), in addition to pH$_{NBS}$ measurements, seawater pH was analyzed by the spectrophotometric technique with m-cresol purple as indicator, following Clayton and Byrne (1993) and hence data were referred to total scale (pH$_{T25}$). Water was collected from Niskin bottles in 10 cm path-length optical glass cells and stored in an incubator at a temperature of 25°C, as it was connected to a circulating ultrathermostat (P. Selecta 6000383). Tempered samples were

subsequently measured in a spectrophotometer (model Shimadzu UV-2401PC). The precision and accuracy of the method were checked through pH measurements of Certified Reference Materials (CRMs) provided by Prof. Andrew Dickson, Scripps Institution of Oceanography, La Jolla, CA, USA (CRMs batch #199), with the pH_{T25} of the batch being calculated using the CO2SYS programme (Version v3.2.0 for MATLAB) (Van Heuven et al., 2011; Sharp et al., 2020) using nutrients, salinity and TA values provided by the supplier. Mean precision and accuracy of the pH_{T25} measurements were ±0.0049 and ±0.0055, respectively.

In order to compare pH data from both cruises, pH_{NBS} values from the first cruise (VULCANA-III-0921) were transformed to total scale through the CO2SYS program and using total alkalinity (TA) and pH_{T25} measurements performed in equivalent stations during the second cruise. TA was analyzed according to Amaya-Vías et al. (2023). Precision and accuracy of TA measurements were ±1 and ±4 µmol kg^{-1} respectively, which were determined from measurements of the above mentioned CRM batch.

4.2.2. Bathymetry and shoreline data

Several datasets were used to produce the maps shown in this work. For the Canary Islands map embedded in Figure 4.1A, the bathymetry was obtained from the Topo 25.1 global dataset. The high-resolution bathymetry of the western coast of La Palma surrounding the lava delta was obtained by the IEO-CSIC in the cruises carried out during and after the eruption, with a Kongsberg Simrad EM-710 multibeam echosounder, operating at a frequency range of 70-100 kHz and processed with CARIS HIPS and SIPS, providing a grid resolution of 1 m. An additional bathymetry was collected for the area surrounding the lava delta at >0.2 km distance, where the IEO-CSIC vessels could not navigate. In this case, a smaller vessel was used equipped with a NORBIT iWBMS narrow multibeam echosounder. These two datasets were merged to produce the bathymetry shown in Figure 4.1.

The high-definition shoreline of La Palma island was provided by the Instituto Hidrográfico de la Marina (IHM) from the Spanish Navy (in low-tide conditions). The lava flows shown in Figure 4.1 were obtained from the Copernicus Emergency Management Service (event code: EMSR546), which was activated during the 2021 volcanic eruption in La Palma.

The softwares used to produce all the maps were MATLAB R2022b and ArcGIS desktop v. 10.8.
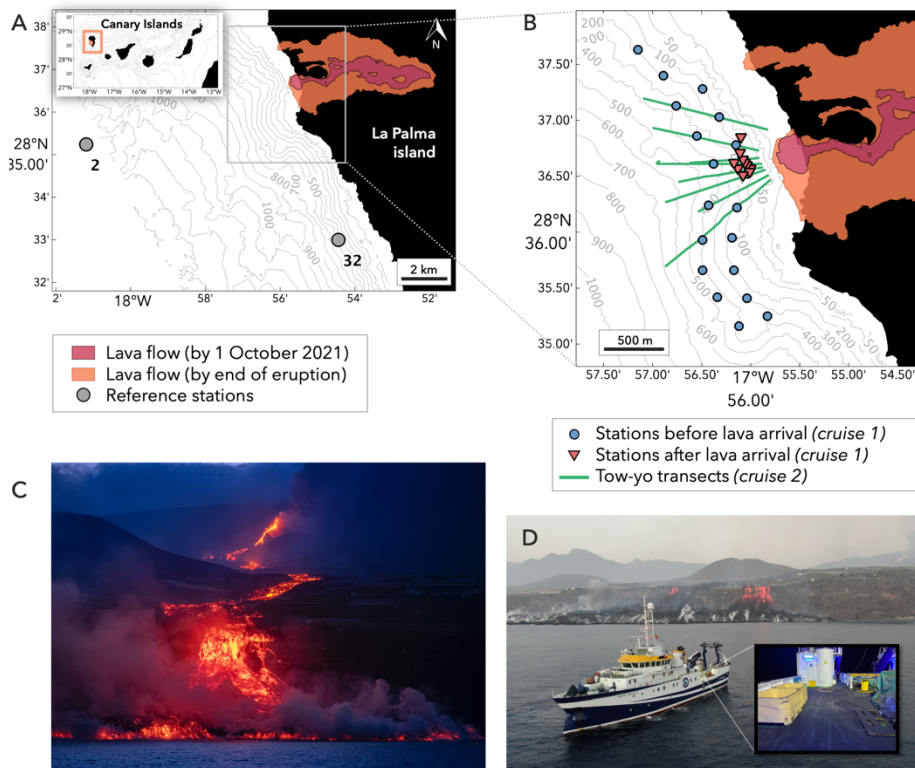
Figure 4.1. Study area in La Palma island. (A) Lava flow by 1 October 2021 (pink) and the final shape after the end of the eruption (orange). Reference stations (background conditions) are shown. Embedded: map of the Canary Islands, showing La Palma island and the location of Cumbre Vieja volcano. (B) Detail of the sampled area, with stations from the first cruise (days before and after the first lava-seawater contact) and the tow-yo transects carried out during the second cruise one month later (green lines). (C) Lava flowing downslope and off the cliff, reaching the ocean where the main lava delta was starting to form. White steam columns are observed. Credit: Arturo Rodríguez/VULCANA. (D) R/V *Ramón Margalef* working in the area, with the lava delta in the background. Embedded: deck of the vessel covered in volcanic ashes.

4.2.3. Underwater images

Recordings from the underwater lava delta were acquired with the remotely operated vehicle (ROV) *Liropus 2000* (IEO-CSIC) during the cruise VULCANA-III-1021 (18–29 October 2021). The ROV transects were carried out perpendicular to the isobaths from deeper (400 m) to shallower waters. Images were acquired with a Konsberg OE14-504 High-Definition Colour Zoom Camera. Scaling of the images was provided by two lasers located at 10 cm

distance, which were observable in the recordings; in those frames where the lasers were not visible, the scale was inferred from visible elements within the frame or from the lasers in nearby frames.

4.3. Results

4.3.1. First lava-seawater contact: initial effects on the water column

Vertical CTD profiles of turbidity, potential temperature, salinity, dissolved oxygen, pH_{NBS}, and chlorophyll-*a* are shown in Figure 4.2, along with a reference profile. The stations shown were sampled on 1 October 2021, two days after the first lava-seawater contact. All the stations presented anomalies in physical-chemical parameters in the water column when compared to reference stations. However, these anomalies were not steady with time; they were very variable within hours or even minutes, depending on a variety of factors such as the volume of lava inputs that the delta was receiving at the time, local currents, etc. Within each profile, many fluctuations and instabilities are also observed in the water column, with numerous local maximums/minimums at different depths.

Turbidity levels were extremely high in the whole water column in all sampled stations after the lava arrival (Figure 4.2A), reaching values up to 9.20 NTU in the first 30 cm in surface and 6.85 NTU in the water column (reference values under normal conditions are around 0.22 NTU). The vertical profiles show several local maximums in the water column, which indicate different fingers of lava-seawater interactions at different depths.

The same structure of fingers (local maximums/minimums at different depths) is also observed in other oceanographic variables. Dissolved oxygen presents local minimums of 213 μmol kg^{-1}, which represents a decrease of -7% respect to reference levels (Figure 4.2B). Chlorophyll-*a* showed a marked decrease especially at the deep chlorophyll maximum (DCM) depth (around 100 m in the reference profile), where the values were around 0.19 mg m^{-3} compared to the reference values of 0.52 mg m^{-3} (Figure 4.2C). The vertical profiles of temperature and salinity show a high variability as well (Figure 4.2E,F). Most of the perturbations took place between 50-150 m, which could be related to a re-structuring of the thermocline due to water column instability. At higher depths the variations are more subtle, but small local minimums/maximums are still present. The temperature and salinity anomalies in the water column can be observed in more detail in the Supplementary material (Appendix II.1).

Decreases in pH$_{NBS}$ with respect to reference values were also observed, especially in stations closer to the lava-seawater front, with a decrease up to -0.06 units (Figure 4.2G). Furthermore, comparing the pH$_{T25}$ measurements from discrete water samples between the first and second cruise (Figure 4.2H), an average decrease of roughly -0.1 was observed between the values obtained immediately after the first lava arrival (1 October) and those measured almost one month later (18-29 October). These decreases were within the range of -0.004 to -0.161 (average -0.093, standard deviation ± 0.026), with the largest anomalies found at 26 m depth.
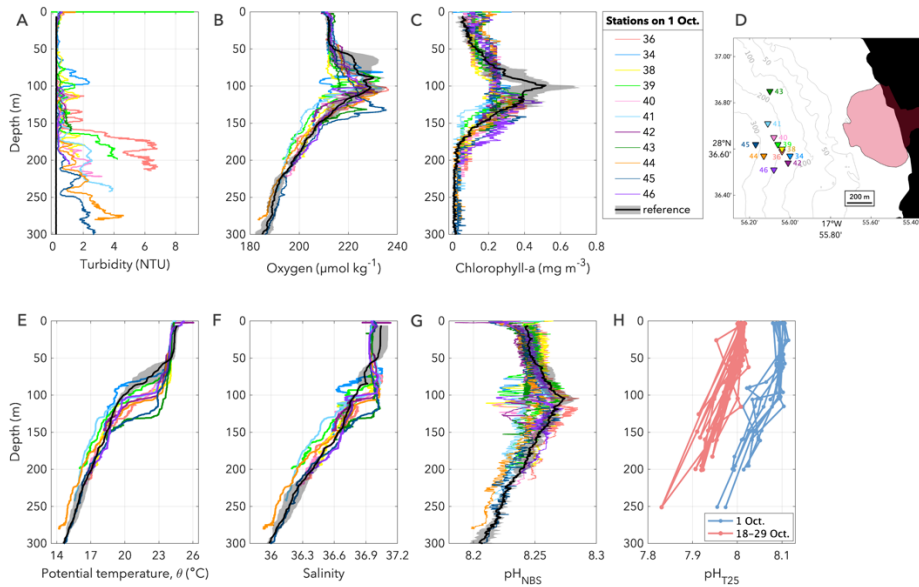
Figure 4.2. (A-C, E-G) Vertical CTD profiles of turbidity, oxygen, chlorophyll-*a*, potential temperature (θ), salinity, and pH$_{NBS}$, with depth in all stations on 1 October, 2021. A reference profile (black line) is shown representing the average of three reference stations, with standard deviation (gray shadow). (D) Location of stations sampled on 1 October. (H) Vertical profiles of pH$_{T25}$ with depth, in stations sampled on 1 October (blue), and equivalent (nearest) stations from the second cruise (18-29 October).

While the thermal and haline changes were subtle in the water column, they were much more obvious in surface. Thermosalinograph measurements from the vessel's continuous intake of surface water provided the surface temperature and salinity data shown in Figure 4.3. Here, data from the days before and after the first lava-seawater contact are shown, separated in boxes according to the distance to the shoreline. Before the lava arrival, the surface temperature was stable in a range of 25.4–26.8°C, with few variations with distance to shore. After 28 September (Figure 4.3B), a large number of high-temperature values were

recorded, with maximums up to 28.5°C (an increase of +2.3°C). These high
temperatures are observed up to 6 km distance from shore, after which they
stabilize to conditions similar to before the lava arrival. Surface salinity showed a
more variable behavior, with increases and decreases after the lava arrival.
Maximums of 37.71 (+0.70) and minimums of 36 (-1.01) were observed. The
maximums were found in the whole 0-6 km distance range, particularly at 2-4 km;
while the minimums are concentrated in the closest distances, mostly at 0-2 km.
Like temperature, salinity returned to normal conditions at >6 km distance.
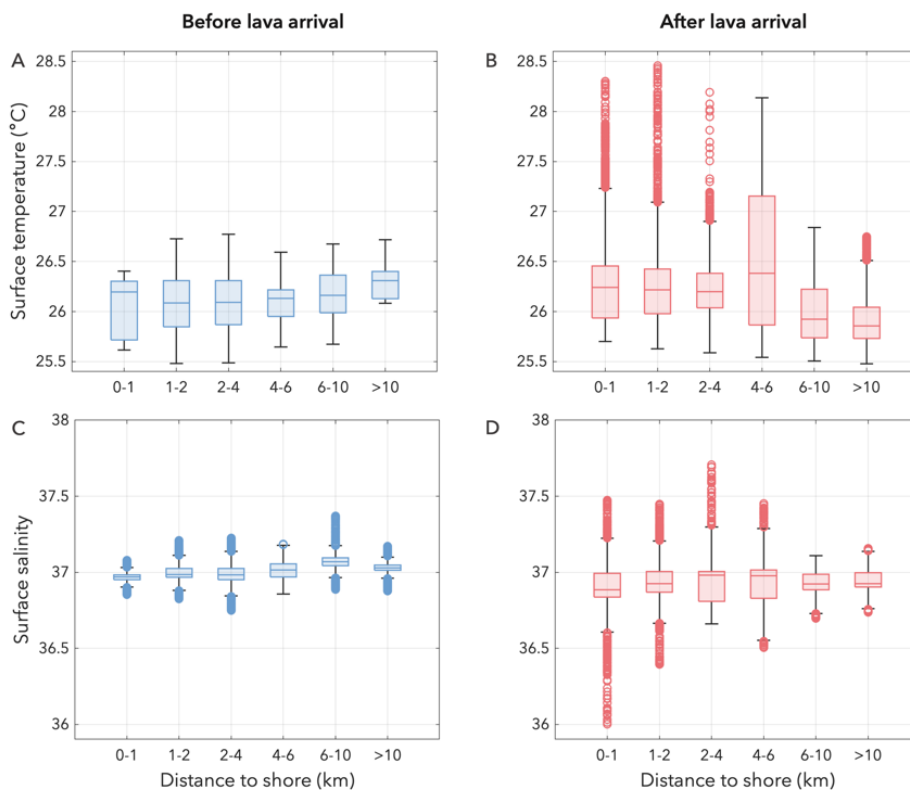
Figure 4.3. Boxplots of surface temperature and salinity data obtained from the
continuous measurements from the vessel during the first cruise (VULCANA-III-0921), the
days before (A,C) and after (B,D) the first lava-seawater contact. The data have been
classified according to the distance to the shoreline.

A quantification of the data shown in Figures 4.2 and 4.3 is provided in Table 4.1,
summarizing the effects of the lava-seawater interaction during the few days after
the first contact on 28 September 2021.

Table 4.1. Quantification of the largest anomalies found in different physical and chemical parameters during the first days after the first lava-seawater interaction. Each variable is provided with: reference value (average ± standard deviation of reference stations); the anomaly (increase/decrease) found respect to that reference; the value of the variable in that anomaly; the percentage of increase/decrease respect to the reference; and the depth at which the maximum anomaly was found.

Variable	Reference value	Largest anomaly	Value	Increase or decrease (%)	Depth (m)
Turbidity (NTU)	0.22 ± 0.00	+6.63	6.85	+2953%	209
Oxygen (µmol kg⁻¹)	230.2 ± 4.2	-17.17	213.03	-7%	89
pH (NBS scale)	8.27 ± 0.01	-0.06	8.21	-0.7%	111
pH (total scale)*	8.11*	-0.16	7.95*	-2%	26
Chlorophyll-*a* (mg m⁻³)	0.52 ± 0.15	-0.33	0.19	-64%	100
Surface temperature (ºC)	26.2 ± 0.1	+2.3	28.5	+9%	5
Surface salinity	37.01 ± 0.04	-1.01 / +0.70	36.00 / 37.71	-2.7% / +1.9%	5
Surface turbidity (NTU)	0.24 ± 0.01	+8.96	9.20	+3735%	<1

*pH$_{T25}$ values are from two days after the first lava-seawater contact (in the "reference value" column) and one month later (in the "value" column).

4.3.2. Lava-induced upwelling

An upwelling effect was observed in the tow-yo transects off the lava delta front during the second cruise (VULCANA-III-1021). Out of the 9 transects carried out, the upwelling was observed in transects twy-02, 05, 06, and 07, which coincide with the area where the submarine lava flows were propagating, according to the map of bathymetric differences shown in Figure 4.4A. All the tow-yo transects are shown in the Supplementary Material (Appendix II.2). Here we display in detail the vertical contours of transect twy-02, as it was the most representative of this feature since it followed the main direction of propagation of the lava underwater.

Vertical contours of density, potential temperature, and salinity throughout transect twy-02 are shown in Figure 4.4B-D. The isocline lines were notably lifted for all the variables in the area above the seafloor, showing an upwelling effect due to the warming and decrease in density at the points where lava inputs come into contact with seawater, forcing these waters to rise and be substituted by deeper, colder, denser waters. The effect was visible in the whole water column up to 400 m, although in temperature and salinity the effect was mostly notable from 300 m upwards. A plume of local maximums was observed at around 80 m depth and 0.5 km from the delta, which might represent where the upwelled waters begin to stabilize.
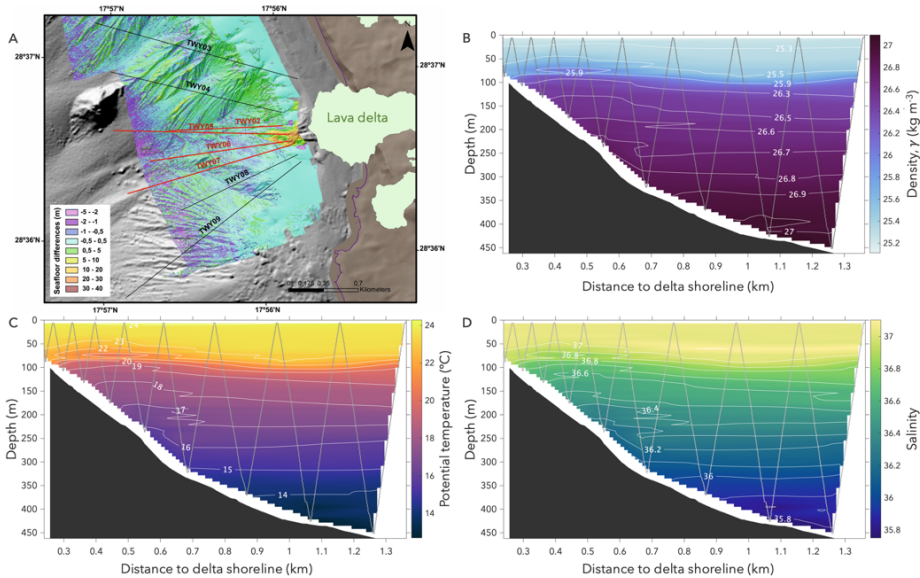
Figure 4.4. (A) Thickness map of bathymetric differences between the seafloor before the delta formation and the new seafloor by 28 October 2021. The trajectories of the tow-yo transects are displayed. The area where an upwelling effect was observed is highlighted in red. Vertical contours of density (B), potential temperature (C), and salinity (D) through transect twy-02, sampled during the second cruise (VULCANA-III-1021) one month after the first lava-seawater contact. The v-shaped gray lines represent the trajectory of the CTD, where data were acquired. Black patch shows the real bathymetry.

4.3.3. Interaction of turbidity and fluorescence signals

From the tow-yo transect twy-02, vertical sections of turbidity and fluorescence are displayed in Figure 4.5. Turbidity levels were above normal conditions (>0.2 NTU) in the whole transect (Figure 4.5A), with a maximum plume around 25 m depth and up to 0.6 km distance from the delta, showing maximums of 6.85 NTU. A weaker but more extense surface plume was observed up until 1.3 km distance, and an additional plume centered around 80 m depth extended further than the limit of the transect (>1.4 km distance).

In the fluorescence signal, we observed an unexpected plume centered around 25 m depth and 0–0.6 km distance (Figure 4.5B), coinciding with the strongest turbidity plume. Although turbidity and fluorescence were measured by the same sensor, the data should not present any correlation under normal conditions. While this was true for most of the transect, the data within that plume did show a strong linear correlation, suggesting that this fluorescence signal was not due to high concentrations of chlorophyll-*a*, but to an influence of the turbidity signal.

To correct this, we calculated the correlation found in this set of data points with a multilinear regression by least squares. We then subtracted this equation to the fluorescence signal, thus eliminating the linear dependance of fluorescence with turbidity. More information about the correction process can be found in the Supplementary Material (Appendix II.3). Finally, we calibrated the corrected fluorescence signal with *in situ* chlorophyll-*a* measurements from discrete water samples. The results are shown in Figure 4.5C, where the turbidity-influenced plume is no longer observed.
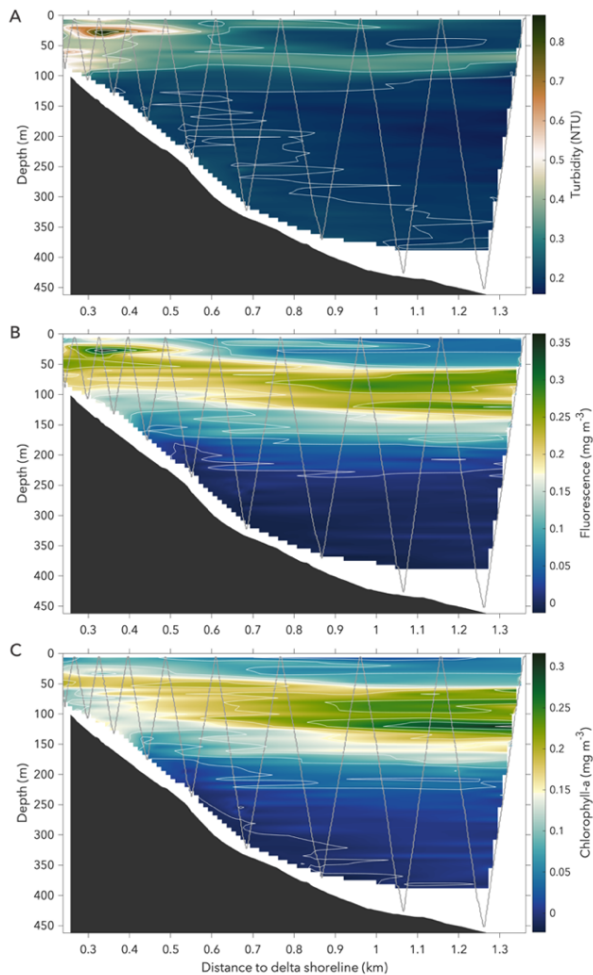
Figure 4.5. Vertical contours of turbidity (A), fluorescence (B), and chlorophyll-*a* (C) through transect twy-02. The v-shaped gray lines represent the trajectory of the CTD, where data were acquired. Black patch shows the real bathymetry. The chlorophyll-*a* contour shown in panel C was obtained from continuous fluorescence data by first applying a correction to eliminate the influence of turbidity, and then calibrating the corrected fluorescence data with *in situ* chlorophyll-*a* measurements from water samples.

4.3.4. Decrease in chlorophyll-*a* with proximity to the lava delta

An overall decrease in chlorophyll-*a* concentration was observed in the area surrounding the lava delta during its formation and growth. To quantify this decrease, chlorophyll-*a* was integrated in the first 150 m of the water column and the data were classified according to the distance to the shoreline at the time of sampling (Figure 4.6). In Figure 4.6A-B, three boxes can be observed corresponding to the parallel lines to the coast at 1.0 and 1.5 km, while in Figure 4.6C, the radial tow-yo transects allowed for a higher-resolution slicing of the distance intervals, resulting in five boxes.
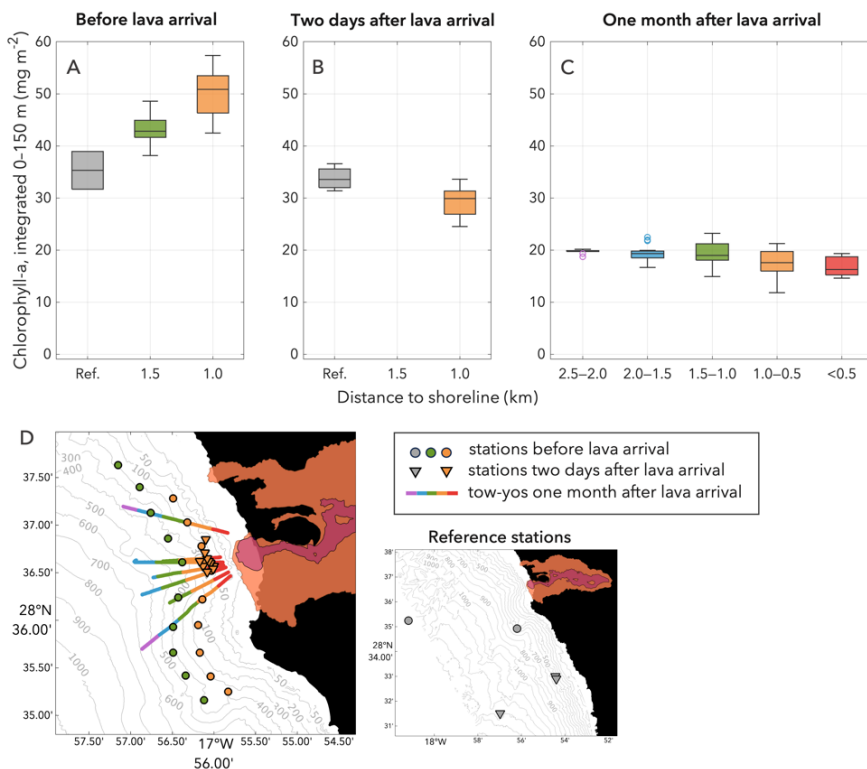
Figure 4.6. Boxplots of integrated chlorophyll-*a* in the first 150 m of the water column, categorized by proximity to the shoreline at the time (the shoreline changed as the delta grew). The data before the first lava arrival to the ocean (A) and the first few days after (B) were collected in the first cruise (VULCANA-III-0921) with vertical stations, while the data from a month after the first contact (C) was obtained in the second cruise (VULCANA-III-1021) with tow-yo transects, which allows for a higher resolution slicing of the distance intervals.

Comparing the data before and after the first lava arrival (Figure 4.6A-B), the 1.0 km distance box (yellow box) shows a remarkable decrease of -41% (from 50.85 to 29.88 mg m^{-2}; calculated from the median of the boxplots). The 1.5 km box keeps a similar median, but many lower values are observed in the lower quartile of the box. Thus, the effect of the process on the chlorophyll-*a* concentration during the first days after the first lava-seawater contact was observed up to 1.5 km distance from the shoreline.

However, the results after one month of lava delta formation are much more abrupt (Figure 4.6C). In comparable distances of around 1 km, the chlorophyll-*a* content shows a -65% decrease respect to initial conditions. The chlorophyll-*a* content seems to decrease with proximity to the lava delta, with a final -69% decrease at <0.5 km (red box) respect to initial conditions. Even more remarkable are the results from the furthest box of 2.5–2.0 km (purple box), which should be equivalent to the far-field boxes (gray boxes in Figure 4.6A-B), but they deviate significantly, showing a decrease of -44% (from 35.31 to 19.86 mg m^{-2}). This indicates that we did not reach a distance where chlorophyll-*a* levels returned to normal conditions along the transects. Therefore, we can conclude that the decrease in chlorophyll-*a* was observed to an extent larger than 2.5 km distance from the lava delta.

4.3.5. Underwater ROV images

We provide a visual overview of the underwater lava flow and deposition of ashes/hyaloclastites as seen by remotely operated vehicle (ROV) footage (Figure 4.7). The upper section of the figure (Figure 4.7A-G) shows different geological features observed in the seafloor. The lava flows were mostly located in the first 150 m depth (Figure 4.7A-D), but gravity-flow lava deposits were found up to roughly 250 m depth in the imagery, forming a breccia of grain flows with reverse gradation (Figure 4.7E). In shallow areas (about 50 m), "aa" lava flows were observed (Figure 4.7A,B), while pillow lavas and mega-pillows were common below 50 m depth (Figure 4.7C,D). Deposition of hyaloclastites and ashes was abundant up to 400 m depth and 1.2 km distance from the subaerial lava delta front (Figure 4.7F,G).

The lower section of the figure (Figure 4.7H-J) aims to highlight the impact of these deposits on the benthic habitat. A variety of organisms such as cnidarians, crabs, and lobsters were found partially or completely buried in ashes and/or hyaloclastites. Practically no pelagic organisms were observed in the area covered by new volcanic sediments while the lava flow was active.
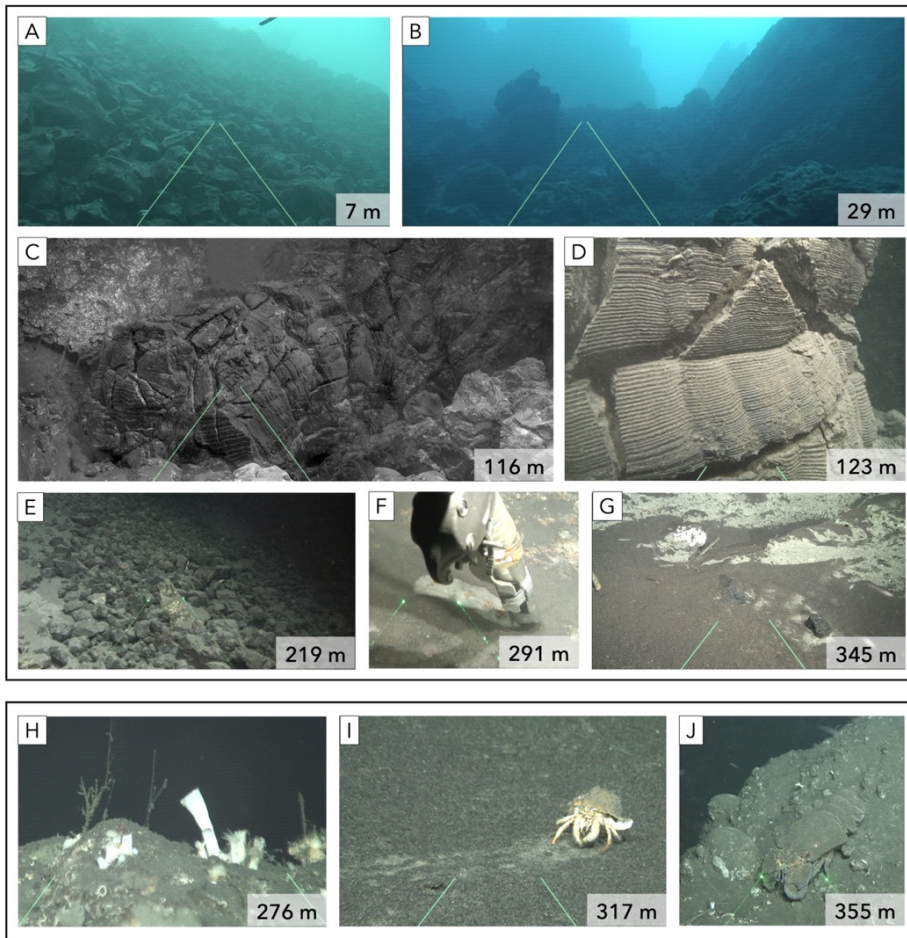
Figure 4.7. Remotely operated vehicle (ROV) imagery from transects carried out over the underwater lava delta during the second cruise in October 2021. Green lasers (real or inferred) indicate a distance of 10 cm. Upper panels (A-G) show the geological features found at different depths: A,B) "aa" lava flows in shallow areas; C) mega-pillow lavas; D) corrugation marks; E) heterogeneous breccia with reverse grading (grain flow); F,G) previous seafloor covered in ashes/hyaloclastites. Lower panels (H-J) show different benthic organisms partially or completely buried in ashes/hyaloclastites: H) cnidarians (*Anomocora fecunda*) and hydrozoans; I) hermit crab (*Dardanus arrosor*); J) lobster (*Scyllarides latus*).

4.4. Discussion

There are very few studies reporting the oceanographic conditions surrounding an active lava delta, mainly due to the logistical and safety challenges of sampling under these conditions. Most of the existing studies, including those carried out

during La Palma 2021 eruption, have focused on surface data in a very limited area surrounding the lava deltas (Thorarinsson, 1967; Sansone et al., 1991; Sansone and Resing, 1995; González-Santana et al., 2022; Román et al., 2022), with only a handful of examples covering greater depths and wider areas (Wilson et al., 2019; Soule et al., 2021; Caballero et al., 2022). Our study helps to fill this knowledge gap by providing a remarkable coverage in all dimensions: area, depth, and time. The whole water column was sampled within a distance up to 2.5 km from shore, and covering the times before, during, and after the formation of the lava delta.

We report anomalies in all measured physical-chemical parameters throughout the entire water column: turbidity, dissolved oxygen, pH, chlorophyll-*a*, temperature, and salinity (Figure 4.2; Table 4.1). All the vertical profiles had in common an unstable behavior with many fluctuations at different depths and numerous local maximums/minimums. This is likely due to the formation of several plumes of affected waters from lava-seawater interactions at different depths, caused by underwater intrusions of lava from lava tubes or by the formation process of mega-pillow lavas, as noted by Lozano-Rodríguez et al. (2023). The different plumes are particularly well observed in turbidity (Figure 4.3A), which presented values up to 30 times higher than normal conditions in the water column. This phenomenon of lava intrusions in depth had been observed before in Hawai'ian volcanism up to 725 m depth (Sansone and Resing, 1995; Wilson et al., 2019). We observed anomalies indicating lava intrusions up to 300 m depth and at distances of >1 km from the coast.

In surface waters, we found temperature increases up to +2.3ºC, consistent with previous reports in the area (Román et al., 2022) and in other lava deltas (Malmberg, 1965; Sansone and Resing, 1995); however, our study provides a wider spatial coverage, allowing to delimit the reach of these thermal anomalies. As evidenced in the boxplots shown in Figure 4.3A-B, background temperature levels were reached at >6 km distance from shore. If we consider a radius of 6 km of affection around the front of the lava delta, this gives an estimated area of 56 km² affected by the thermal increase. Furthermore, we provide water-column temperature data as well, evidencing a less drastic thermal anomaly in depth, which is also difficult to quantify due to a high instability of the thermocline depth observed in the temperature profiles (Figure 4.2E). Water-column temperature profiles near lava deltas have very rarely been documented (Wilson et al., 2019; Soule et al., 2021).

The case of salinity is more complex, as we found both positive and negative anomalies in surface, up to +0.7 and -1.0 units, respectively (Figure 4.2; Table 4.1).

At greater depths in the water column, even though the variations were more subtle, increases and decreases were also found (Figure 4.3C-D), and a high variability with many oscillations was observed in the vertical profile (Figure 4.1F). Several phenomena have been reported to affect salinity in lava delta settings: surface water evaporation; groundwater discharge; or thermal shock when the lava at >1000°C interacts with water at ~25°C, causing salt precipitation (Sansone and Resing, 1995; González-Santana et al., 2022). It is possible that some or all of these phenomena took place at some point during the lava delta formation process, resulting in the observed positive and negative anomalies and a high instability of the salinity profile in the water column.

Decreases in pH and dissolved oxygen were also observed both in surface and in depth. Other studies carried out in surface in this area and closer to the lava delta reported decreases up to -0.9 in pH and -70 µmol kg^{-1} in dissolved oxygen (González-Santana et al., 2022; Román et al., 2022). In addition to these surface anomalies, we found water-column pH$_{T25}$ decreases up to -0.16 at various depths (average -0.1), and -17 µmol kg^{-1} in dissolved oxygen. The difference in magnitude can be attributed to the smaller thermal anomalies found in the water column compared to surface, since González-Santana et al. (2022) attribute 40-55% of the pH decrease to the temperature increase. Our results enlarge the spatial reach of these anomalies both in depth and in distance. The presence of these anomalies in the whole water column is likely due to the underwater intrusion of lava through lava tubes, along with other processes such as explosions or formation of pillow lavas which can cause high turbidity (Lozano-Rodríguez et al., 2023).

An interaction of the turbidity and fluorescence signals was observed in some high-turbidity plumes surrounding the lava delta (Figure 4.5). There are several reports of satellite chlorophyll overestimations caused by dissolved materials from lava-seawater interaction events, which were not related to high *in situ* concentrations of chlorophyll-*a* (Mantas et al., 2011; Coca et al., 2014; Eugenio et al., 2014; Whiteside et al., 2023). This highlights the importance of validating observations of optical sensors with *in situ* water samples. While this is now relatively common knowledge for the case of satellite observations, we have observed a case of water-column data where the fluorescence signal was influenced by the high turbidity levels (Figure 4.5). We applied a correction to the fluorescence data that presented a linear correlation with turbidity, along with a calibration with *in situ* chlorophyll-*a* measurements. This provided a more realistic assessment of the water-column chlorophyll data.

The contours shown in Figure 4.5 evidence an upwelling effect caused by the advection of heated deep waters to the surface, in an area that coincides with the

main path of lava propagation along the seabed (Figure 4.4). This had been proposed as a hypothesis in previous studies in this area after observing surface anomalies in density (González-Santana et al., 2022) and in dissolved nitrate (Román et al., 2022), and it has been confirmed in this study with high-resolution transects perpendicular to the lava delta in the whole water column. Lava-induced upwelling is not an uncommon phenomenon in lava-seawater interaction events. In coastal Hawai'ian volcanism, Sansone and Resing (1995) described a surface "roil" of colder water (27ºC in contrast to >60ºC) observed at a few tens of meters from the shore and 5-10 m in diameter, with chemical characteristics identical to background offshore seawater. They explained this as an ascent of subsurface waters by an upward motion of the water heated by the submarine lava intrusions, and they determined an upward velocity of 0.3 m/s. Two decades later, this feature was again described by Wilson et al. (2019) during the latest Kīlauea eruption, which was accompanied by a large phytoplankton bloom due to the injection of nitrate-rich deep waters into the surface.

However, despite the occurrence of a lava-induced upwelling event and the reported high nitrate concentrations in surface (Román et al., 2022), the lava injections in La Palma did not favor any bloom, as evidenced from satellite data by Caballero et al. (2022) from satellite data. But there was not only a lack of bloom: we found that the phytoplankton community was negatively affected, as evidenced by an abrupt decrease in chlorophyll-*a* of -69% even one month after the first lava-seawater contact. The transects were carried out up to 2.5 km distance from the lava front, and at that distance there was still a -44% decrease, meaning that we did not delimit the radius of affection and we can only state that it was larger than 2.5 km.

The question of why a similar process can fuel a phytoplanktonic bloom in some cases and not in others is evident. A simple explanation would be that the upwelling might not have been strong enough to trigger this effect, but this seems unlikely due to the high total dissolved nitrogen (TDN) in surface reported by Román et al. (2022). Another hypothesis may rely on the type of eruption and lava flow. Soule et al. (2021) noted the contrast between the delta formation processes in the 2018 Kīlauea eruption, which fueled a bloom, and the deltas formed over the past decade at Pu'u 'Ō'ō (a volcanic cone on the eastern rift zone of Kīlauea), where no bloom was observed. They explain that the Kīlauea deltas are comprised largely of coarse-grained volcanic breccias and intact lava flows due to less efficient fragmentation of the lava flows; while the Pu'u 'Ō'ō deltas contained a larger fraction of fine-grained hyaloclastite, as is the case of La Palma deltas as well (Lozano-Rodríguez et al., 2023), resulting in high turbidity and low light

penetration that negatively affects photosynthetic organisms, as observed as well in the recent Tonga-Hunga eruption (Whiteside et al., 2023).

To summarize this scenario, we present a scheme showing the hypothesized processes that took place as a result of the lava-seawater interaction (Figure 4.8). This is a modification of the scheme provided by Wilson et al. (2019) where they described the upwelling effect and phytoplankton bloom caused by the lava intrusions from Kīlauea. We have adapted this scheme to the case of La Palma, with the aim of highlighting the different effects that this process can have in different settings. We hypothesize that, in the case of La Palma, the high turbidity is what caused a negative effect on phytoplankton despite the nutrient inputs from deeper waters.
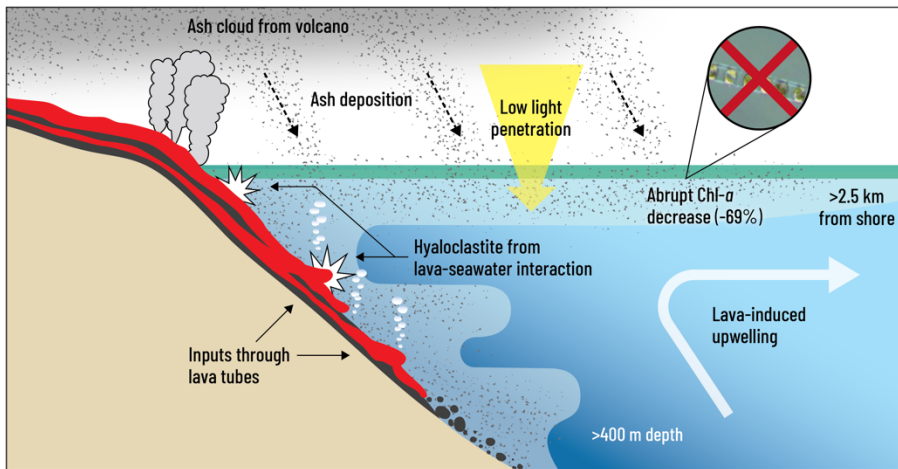
Figure 4.8. Modification of the scheme presented by Wilson et al. (2019) adapting it to the case of La Palma. We summarize the lava-seawater interaction processes that took place during the lava delta formation, including the hypothesis of high turbidity being responsible for a negative effect on phytoplankton communities despite the nutrient inputs from the lava-induced upwelling.

4.5. Conclusions

This study has explored the effects of the formation of a lava delta on the surrounding marine environment in the whole water column. The most remarkable result was an abrupt decrease (-69%) in the chlorophyll-*a* concentrations with proximity to the lava delta, suggesting a negative effect on phytoplankton communities. This effect was observed a radius of more than 2.5 km (not delimited).

Immediately after the first lava-seawater contact, anomalies respect to normal conditions were observed in all measured physical-chemical parameters (turbidity, dissolved oxygen, pH, chlorophyll-*a*, temperature, and salinity). These anomalies were often found as local maximum/minimums forming various plumes at different depths up to 300 m, likely caused by the underwater intrusion of lava as well as other processes such as explosions or small landslides.

Different processes were observed in surface and in depth. Temperature and salinity showed a strong affection in surface, while in the water column the anomalies were more subtle. Surface temperature increase was observed up to 6 km distance from the lava delta. Salinity showed both positive and negative, likely caused by several processes such as water evaporation, groundwater discharge, or precipitation by thermal shock.

The underwater lava delta was recorded. Lava flows were mostly observed in the first 150 m depth, but gravity-flow sediment deposits were found up to 250 m depth, and deposition of ashes and hyaloclastites up to 400 m depth and 1.2 km distance from the lava delta. The covering of previous seafloor by the new lava flows annihilated all benthic life, and many organisms were observed partially or completely buried in ashes/hyaloclastites.

A lava-induced upwelling process took place, where heated waters ascended to surface and were replace by deeper, colder waters. While this process brought deep nutrient-rich waters to surface, there were no signs of any phytoplankton bloom triggered by this effect. This is likely due to the high turbidity levels in the water column, which difficulted light penetration.

This study was carried out in the context of a volcanic emergency, which involved safety regulations, security perimeters for navigation, and logistical challenges. Yet, it produced a large and valuable dataset that sheds light on the poorly documented processes that take place in the oceanic environment during the formation of a lava delta.

Conclusions and final remarks

5.1. General conclusions

The main conclusions drawn from this work are the following:

- The two most recent eruptions in the Canary Islands (El Hierro, 2011 and La Palma, 2021) had abrupt effects on all measured physical and chemical parameters in the local marine environment, with high spatial and temporal variability. The local marine ecosystems were also severely impacted in both cases. The effects were often observed in the whole water column and with horizontal scopes of several kilometers.

- The eruption of the submarine volcano Tagoro (El Hierro, 2011-2012) caused a severe loss of dissolved oxygen in the surrounding oceanic area due to the emission of reduced chemical species, reaching suboxic and even anoxic conditions. During the strongest eruptive episodes, more than 460 km² were affected. Local currents and mesoscale structures such as eddies controlled the transport of these deoxygenated plumes, which at times reached distances up to 80 km from the volcano.

- The emissions from Tagoro volcano, both during the eruptive and the post-eruptive stages, carry high concentrations of inorganic nutrients, particularly silicate, which is up to 325 times more concentrated in the vent fluids than normal conditions in the area. Phosphate is also importantly enriched (10-fold). Nitrogen seems to be predominantly emitted in the form of ammonium, which is also very enriched (98-fold), and later reacts into nitrate and nitrite.

- Once Tagoro volcano evolved into a hydrothermal system with diffuse flow, these nutrient-rich emissions, still present in the area, seem to have contributed to the fast recovery of the marine ecosystem. The nutrient fluxes per unit of area at Tagoro are comparable to some of the most important nutrient inputs to the region, such as the NW-African upwelling.

- The subaerial eruption at Cumbre Vieja (La Palma, 2021) generated lava flows which reached the ocean forming new lava deltas. The process of formation of these structures generated important anomalies in the whole water column. Turbidity was particularly high (up to 30 times increased) due to the presence of ashes and hyaloclastites in the water. A general decrease in pH and dissolved oxygen was observed, while temperature increased, and salinity had a variable behavior with increases and decreases. The thermal and haline anomalies were observed in a range up to 6 km distance from the shoreline.

- These underwater inputs of lava generated an upwelling effect, which was observed in the area that coincides with the presence of new volcanic materials and no further than 1 km distance from the lava delta. However, unlike other known cases in the literature, this lava-induced upwelling did not generate a phytoplankton bloom.

- The formation of the lava deltas caused an abrupt depletion in depth-integrated chlorophyll-*a*, with a -41% decrease in just two days and a total -69% decrease one month later, in a range of more than 2.5 km distance (not delimited). This suggests a negative effect on the phytoplankton communities.

5.2. Contribution to crisis management

The research conducted in this work has helped expand our knowledge regarding the effects of different volcanic processes on the marine environment. However, it should not be understood as purely basic research: these studies have had direct applications for crisis management during the two most recent volcanic emergencies in the Canary Islands. In facts, the results shown in Chapters 2, 3, and 4 have been explicitly used and presented during the official meetings of PEVOLCA (Volcanic Emergency Plan for the Canary Islands). Hopefully, the experience gained by this working team and the collaborating institutions will strengthen the archipelago's capability to efficiently respond to future volcanic crises.

5.2.1. Recommendations for oceanographic sampling during a volcanic emergency

In oceanographic cruises, an optimal sampling plan is crucial to obtain quality data that can produce valuable scientific contributions and relevant advice for regional and national administrations. However, during a volcanic emergency, scientists often must act quickly and with little preparation time.

From the studies presented in this thesis, some recommendations can be drawn regarding the sampling during a volcanic emergency and the posterior monitoring of these volcanic settings.

- If possible, sampling the area before the volcanic inputs reach the ocean.

In the case of the submarine eruption at El Hierro, the precursory signals migrated through the whole island from north to south during several months preceding

the eruption, so it was not possible to accurately estimate the final location beforehand. However, previous observations by the IEO-CSIC in the region provided a vast background of the local oceanographic conditions before the eruption.

Contrastingly, in the case of La Palma there was a very precise prediction of where the lava flows were most likely to reach the ocean. This allowed a sampling of the area before the first lava-seawater contact, which was quite useful for some of the analyses presented in Chapter 4, allowing to establish a temporal evolution of the process.

- <u>Validating fluorescence signals with *in situ* water samples.</u>

Many studies in the literature have reported limitations in remote sensing during oceanic volcanic events, namely an overestimation of chlorophyll levels due to the presence of colored dissolved materials in the seawater (Mantas et al., 2011; Coca et al., 2014; Eugenio et al., 2014; Whiteside et al., 2023). However, in this work we have also reported for the first time a similar phenomenon from *in situ* sensor data in the water column (see section 4.3.3). During the 2021 La Palma eruption, the fluorescence sensor presented some high values that linearly correlated with turbidity and were not due to a high concentration of chlorophyll. A correction of this turbidity influence, along with a calibration with chlorophyll-*a* measurements from water samples, allowed to accurately estimate the real chlorophyll content in the water column, which turned out to be quite depleted.

Therefore, during a volcanic eruption, it is important to be cautious before reporting an apparent bloom observed by optical sensing, either from satellite data or *in situ* water-column sensors. These signals should always be validated with measurements of biological parameters from water samples.

- <u>Adapting the sampling strategies to the spatial and temporal scales of volcanic processes.</u>

Classical oceanography is mostly based around the concept of CTD vertical stations, which are typically planned to form transects or grids. This is a useful approach in most cases; in fact, it has been used in all three studies presented in this thesis. However, the rapid variability of volcanic processes in the ocean (scales of hours or even minutes) represents a limitation for this technique, because transects/grids of stations require accounting for times of navigation, sampling time between casts, etc. Another limitation is the spatial resolution, since the stations are typically at least a few tens of meters away, which may be too much for small-scale processes such as diffuse hydrothermal emissions.

In counterpart, the *tow-yo* technique provides an almost-synoptic photography of the whole water column through a transect in just one CTD cast. The term *tow-yo* comes from the words *tow* (the ship is in slow movement, towing the CTD) and *yo-yo* (the CTD is being continuously moved up and down). Although this technique presents more operational complexity than vertical stations, it offers more versatility and a remarkable spatial and temporal resolution. This methodology was quite useful for the studies presented in Chapters 3 and 4.

Additionally, the use of new technologies such as ROVs offers a whole new range of possibilities. Their use is not limited to image acquisition: they can also be used for direct sampling with specific instrumentation that can be designed *ad hoc* (e.g. the syringe system used to obtain vent fluid samples in Chapter 3). This also opens the door for instrumental engineering and innovation in this field.

5.2.2. Ecosystem resilience after a volcanic eruption

This thesis does not have a main focus on marine microbiology. However, it has provided the first steps towards understanding how the local marine ecosystem responds to volcanic inputs of any kind, and how it evolves in the following years.

In the case of Tagoro submarine volcano, the eruption in 2011-12 was quite deadly for most of the marine communities living in the area. However, the posterior monitoring over the last decade has shown a remarkable recovery, and nowadays the volcano hosts a unique and rich ecosystem (Danovaro et al., 2017; Sotomayor-García et al., 2019; Fernández de Puelles et al., 2021). The exact mechanisms that drove this recovery and the specific effects on the different communities have yet to be elucidated; however, the remarkable inputs of inorganic nutrients from the hydrothermal fluids (Chapter 3) are likely a key piece of this puzzle.

The eruption at La Palma was a completely different case. These are not direct emissions maintained in time, but rather an abrupt entry of mass and heat to the ocean with dramatic consequences for the marine ecosystem. In Chapter 4 we have evidenced a negative effect on primary producers, along with a burial of the benthos and absence of pelagic organisms. However, a regeneration can surely be expected. In more recent monitoring cruises (not included in this work), first signs of recovery have already been observed. The time frames and specific processes of this recovery will eventually become clear as long as the monitoring efforts continue.

5.3. Future works

The two unique volcanic settings studied in this thesis are still a fruitful source of scientific knowledge. Many open questions remain to be solved. Here are some key lines of research that should receive attention in the coming years.

An evident niche for further research is the rich and unique ecosystem present at Tagoro submarine volcano. Microbiological studies must be conducted to finally confirm if the volcanic emissions directly enhance phytoplankton growth. This can include *in situ* sampling as well as fertilization experiments using the vent fluids extracted from Tagoro emissions. A wide variety of biological parameters can be analyzed, such as: microbial abundance, microbial activity, community structure, DNA analysis, etc.

The physical dynamics occurring at Tagoro also offer room for future research. Some preliminary data from our research team have suggested the presence of convective cells around the volcanic cone generated by the low-density emissions. This opens a new line of work focused on the physical processes at a sub-mesoscale level. These dynamics could also be relevant for the previously mentioned studies of the fertilization process. Therefore, Tagoro continues to be an opportunity for multidisciplinary and transdisciplinary studies.

Some other examples of research lines related to Tagoro volcano that are currently active are: i) the quantification of vertical velocities and heat fluxes from the Tagoro hydrothermal vents (Martín-Díaz et al., in prep.); ii) exploring the presence of bacteria capable of producing chemical compounds with biopharmaceutical interest (García-Davis et al., 2021); or iii) Tagoro volcano as a natural laboratory to study the response of marine organisms to conditions similar to those generated by climate change, such as temperature increase or acidification.

Regarding the lava deltas from the eruption at La Palma, only two years have passed since the eruption at the time of writing this thesis, so this is still a very juvenile line of work. The phenomenon offers a wide variety of possibilities for roughly any area of marine sciences. To continue the specific work presented in Chapter 4, geological and petrological studies will help us understand the specific characteristics of this eruptive process and why it had such different effects on the marine environment compared to other settings such as Hawai'i (see section 4.4). Additionally, analyzing the evolution of the benthic communities through underwater imagery will be a crucial step towards understanding the recovery process. This is a unique opportunity to monitor the evolution of a marine ecosystem after its complete destruction and, unlike the case of Tagoro, with no additional inputs of nutrients.

Finally, we cannot forget that this is an active volcanic archipelago. Not only are more eruptions bound to occur; it is also highly possible that the seafloor of the Canary Islands already hides other undiscovered active sites. Some known examples are the Henry Seamount, a deep Cretaceous volcano located 40 km southeast of El Hierro island which has shown signs of rejuvenated volcanism (Klügel et al., 2020); or the Enmedio submarine volcano, located between the islands of Tenerife and Gran Canaria, also with signs of recent hydrothermal activity (Vázquez et al., 2021). Oceanographic research holds a great potential to shed light on the processes taking place on these settings and other possible unknown sites.

As a final remark, from a scientific point of view, the Canary Islands represent a unique opportunity to expand our knowledge on intraplate submarine volcanism; however, this line also holds a high societal value. The Canary society needs to be familiar with the volcanic nature of our archipelago, and it is a responsibility of the scientific community to bring this knowledge to the general public for a better understanding of the environment that surrounds us.

Summary of the Springer book chapter complementing Chapter 3

This appendix summarizes the contents of a book chapter published in Springer's book *El Hierro island*, from the book series *Active Volcanoes of the world*. The chapter compliments the study of the release of dissolved inorganic nutrients from Tagoro submarine volcano, presented in Chapter 3 of this thesis. The book chapter is titled "Tagoro submarine volcano as a natural source of dissolved inorganic nutrients" (González-Vega et al., 2023).

Overall, the main contribution of this book chapter compared to the information presented in Chapter 3 is the merging of the study on the nutrients N, P, Si (González-Vega et al., 2020) with the study on the emissions and kinetics of Fe (Santana-González et al., 2017). Other differences are found throughout the text, which are hereunder summarized.

First, an introductory section offers a wider overview on the role of inorganic nutrients in the ocean as a requirement for the growth of primary producers, with more emphasis on the nutrient sources and limitations. Submarine volcanic activity is presented as one important and poorly studied source of nutrients to the ocean. This is linked with a brief background on the 2011 El Hierro underwater eruption and the subsequent hydrothermal activity of Tagoro submarine volcano.

Next, a specific section about sampling strategies emphasizes the importance of the different techniques used to sample the area over the years: vertical hydrographic stations, tow-yo transects, and the use of an ROV to collect vent fluid samples.

Then, a series of sections summarize the results of the monitoring of nutrient emissions at Tagoro volcano. In contrast to the study from Chapter 3, each section here is focused on one specific nutrient: silicate, phosphate, nitrogen species (NO_3^-, NO_2^-, NH_4^+), and iron. A brief review of the role of each nutrient

in volcanic settings around the world is provided, along with the results from Tagoro volcano.

From these sections we can highlight a new representation of the data (Figure I.1), where the nutrient concentrations in the first 150 m of the water column are presented as boxplots categorized by volcanic stage and by sampling strategy. The inclusion of iron is also a novelty respect to the graphics from Chapter 3.
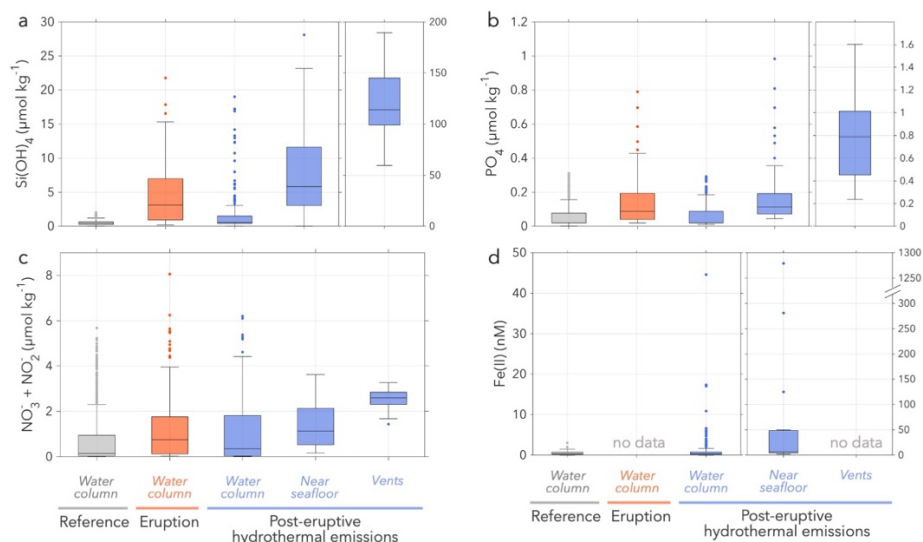
Figure I.1. Figure from Springer's book chapter (González-Vega et al., 2023). Boxplots of nutrient concentrations in reference stations (grey), eruptive stage (orange), and post-eruptive stage (blue). The boxes are also classified accoding to the sampling strategy followed: vertical profiles for water-column samples (data from the first 150 m), tow-yos for near-floor samples, and ROV for vent samples.

Results continue to be presented in the following sections, including: the horizontal and vertical extent of the nutrient plumes around Tagoro submarine volcano, the yearly nutrient fluxes, and the nutrient ratios in the different stages and with different proximities to the source. All these results are presented in a similar manner in Chapter 3, although new figures were produced for Springer's book chapter which emphasize different aspects of the results.

Finally, another important contribution of this book chapter is a more comprehensive review of the existing literature related to the possible effects of these nutrient emissions on local microbial communities. To close the chapter, the main conclusions and future works are presented, which are similar to the conclusions of Chapter 3 (section 3.5).

Supplementary material for Chapter 4

II.1. Temperature and salinity anomalies in the water column

To better observe the local minimums/maximums in temperature and salinity in the water column, in Figure II.1 we show profiles of variation of temperature and salinity with depth at intervals of 1 meter. Under normal conditions, temperature and salinity should always decrease with depth, as can be observed in the reference profiles (black line), which generally show no positive values. However, in the stations influenced by the lava-seawater interactions, positive values are observed at various depths in the water column, representing local increases of temperature and salinity. This phenomenon is particularly well observed for salinity, which shows both increases and decreases of similar magnitude.
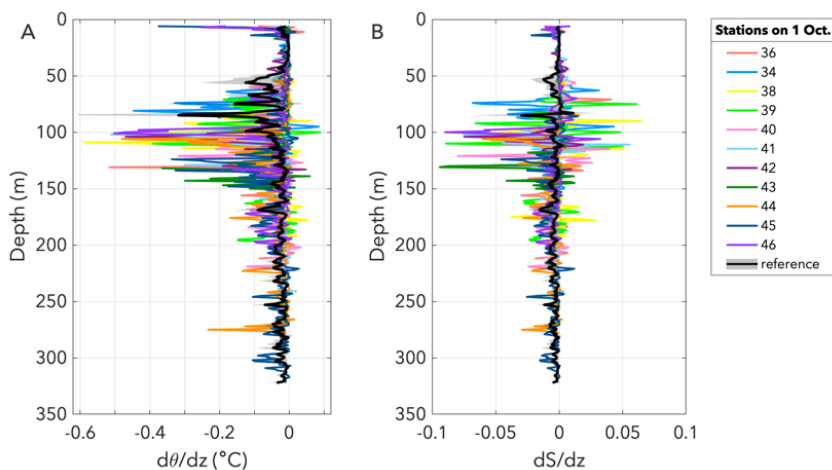
Figure II.1. Variation of potential temperature (θ) and salinity with depth in all stations from 1 October 2021, calculated as the difference at intervals of 1 meter (B, D). In all plots a reference profile is shown (black line represents the average of three reference stations, with standard deviation shown as a gray shadow).
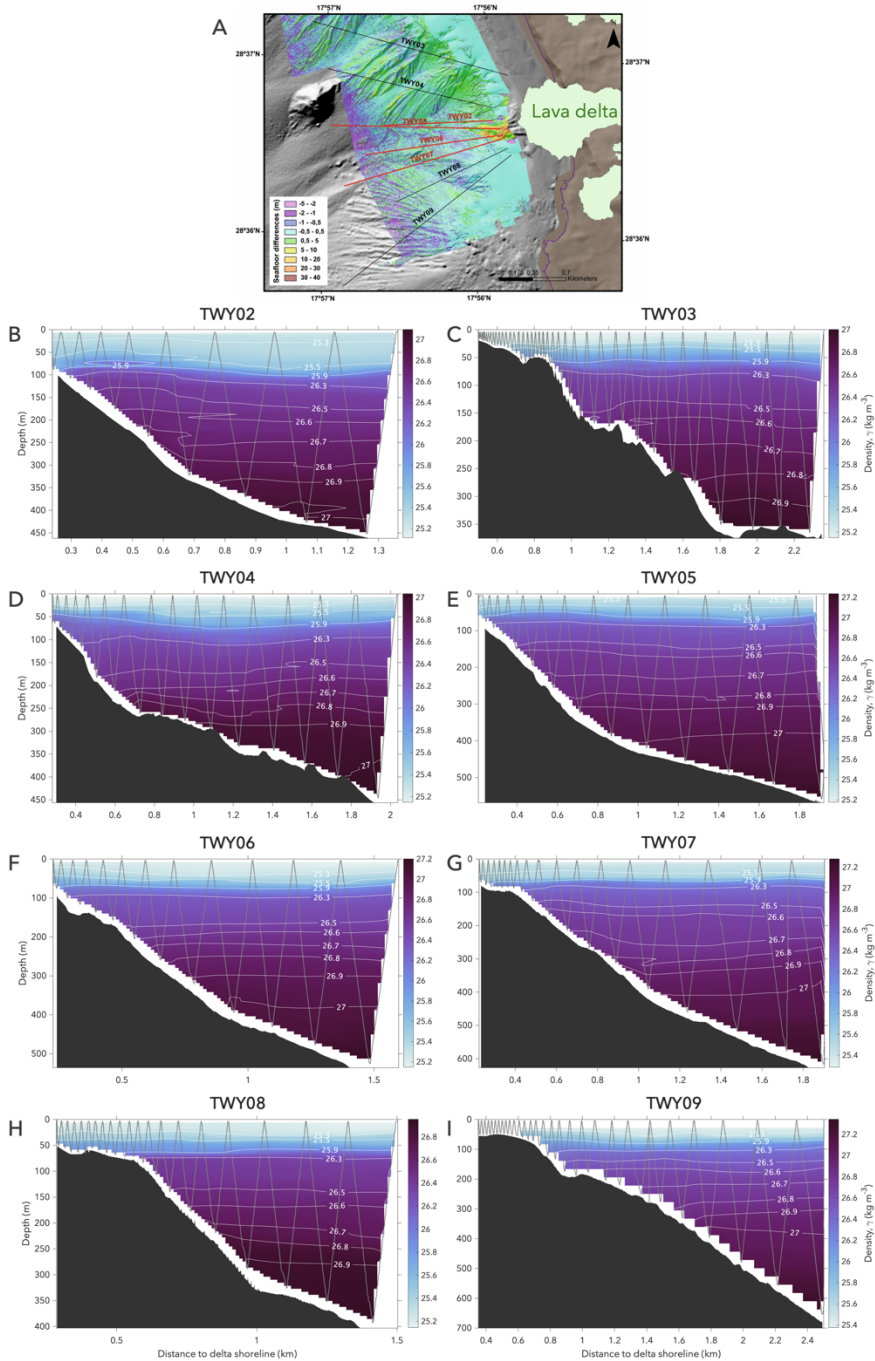
Figure II.2. (A) Map of bathymetric differences between before the lava delta formation and 28 October 2021, and trajectory of the tow-yo transects carried out in a radial manner respect to the lava delta. (B-I) All transects represented as vertical contours of density.

II.2. Lava-induced upwelling: all tow-yo transects

The vertical contours of density from all tow-yo transects are shown in Figure II.2, along with their location plotted over a map of bathymetric differences (Figure II.2-A).

The upwelling effect is more strongly observed in transects twy-02, twy-04, and twy-07; and more weakly in some isopycnals in transects twy-05 and twy-06, always in the area at <1 km distance from shore. These transects coincide with the area where the bathymetric differences are observed in Figure II.2-A. No effect is observed in other transects or at >1 km distance.

It's worth noting that twy-02 and twy-05 follow roughly the same line, but the upwelling effect is strongly observed in twy-02 (Figure II.2-B), while it's more weakly observed in twy-05 (Figure II.2-E). This is a sign of the strong variability observed during the whole process of formation of the lava delta, where the conditions widely varied depending on the amount of lava input being injected into the ocean at the time.

II.3. Correction of fluorescence with turbidity

In the transect twy-02, an apparent plume of high fluorescence appeared at 0-50 m depth and up to 0.5 km from shoreline; however, chlorophyll-*a* measurements from water samples did not show equally high values. A correction with the water samples alone was not possible because there were not enough water samples taken in that plume (it should be kept in mind that the whole tow-yo transect is just one CTD cast with 24 available Niskin bottles for collecting water samples).

As seen in Figure 4.5 in the main text, this apparent fluorescence plume coincided perfectly with a turbidity plume in surface. When fluorescence was plotted against turbidity (Figure II.3-A), a group of data with high turbidity showed an apparent linear correlation with fluorescence.

We established that the data with a turbidity higher than 0.5 NTU were the group that linearly correlated with fluorescence. To decide this limit, we ran a sensitivity test where we set the limit at different levels from 0 to the maximum turbidity in intervals of 0.05 NTU and ran linear regressions for each one, selecting the limit whose regression gave a better r^2, which was 0.5 NTU (r^2=0.724).

These data higher than 0.5 NTU were also plotted over the vertical contour of fluorescence (Figure II.3-B) and the points coincided perfectly with the surface

plume, along with a few more data outside of the plume, which according to the sensitivity test were also linearly correlated with turbidity.
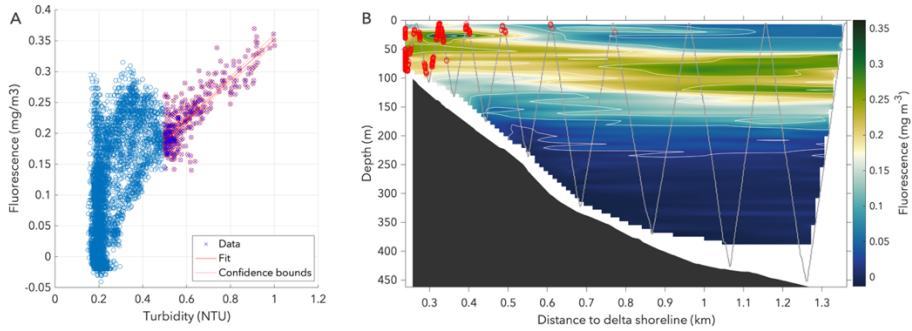
Figure II.3. Data used for linear regression to correct the influence of turbidity on the fluorescence signal from transect twy-02. (A) Fluorescence against turbidity; data selected for the regression (turbidity >0.5 NTU). (B) Same data marked in the vertical contour of fluorescence.

Once the data group of interest was established, we used the linear regression to obtain an equation of the influence of turbidity on fluorescence (fluor = m*turb + n), and then subtracted this equation from the original fluorescence signal. The result is shown in Figure II.4.
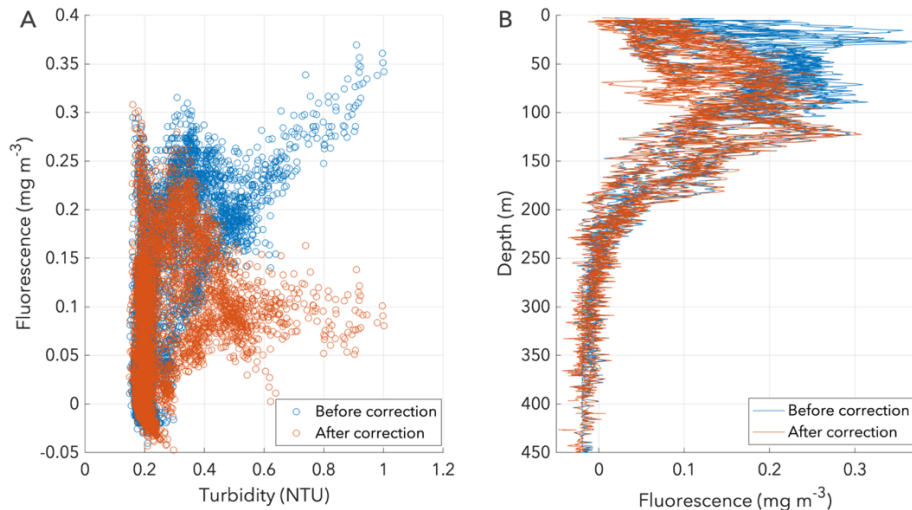
Figure II.4. Fluorescence data from transect twy-02 before and after the correction with turbidity, seen as (A) fluorescence plotted against turbidity and (B) fluorescence vertical profile with depth.

Appendix III

Lists of figures, tables, and acronyms

III.1. List of figures

III.2. List of tables

III.3. List of acronyms

BOC	Boletín Oficial de Canarias
CMEMS	Copernicus Marine Environment Monitoring Service
CTD	Conductivity, temperature, depth
EZD	Euphotic Zone Depth
IEO-CSIC	Instituto Español de Oceanografía – Consejo Superior de Investigaciones Científicas
IGN	Instituto Geográfico Nacional
IHM	Instituto Hidrográfico de la Marina
NBS	National Boureau Standard
N+N	Nitrate + nitrite (NO_3^- + NO_2^-)
MLD	Mixed Layer Depth
OMZ	Oxygen Minimum Zone
ORP	Oxydation-Reduction Potential
PEVOLCA	Plan Especial de Protección Civil y Atención de Emergencias por Riesgo Volcánico en la Comunidad Autónoma de Canarias
ROV	Remotely Operated Vehicle
ULL	Universidad de La Laguna
ULPGC	Universidad de Las Palmas de Gran Canaria
VULCANA	Vulcanología Canaria Submarina
UAV	Unmanned Aerial Vehicle

Resumen en español

IV.1. Introducción

El volcanismo es un proceso de transferencia de calor y materia entre el interior de la Tierra y su superficie (Mather, 2015). Los volcanes han sido clave en muchos eventos importantes de la historia del planeta, como cambios climáticos, extinciones masivas, e incluso el establecimiento de una atmósfera oxigenada (Leckie et al., 2002; Méhay et al., 2009). Aunque los volcanes se estudian desde muchas perspectivas (la mayoría de ellas relativas al ámbito de la geología), la interacción de estos con su entorno apela a la implicación de numerosas disciplinas. En este sentido, la oceanografía es particularmente relevante, teniendo en cuenta que el 85% del volcanismo de nuestro planeta ocurre bajo el agua (Crisp, 1984).

La interacción entre los volcanes y los océanos ocurre principalmente de dos formas: i) volcanes submarinos y fuentes hidrotermales que inyectan sus emisiones directamente al océano; y ii) volcanes subaéreos cuyas coladas de lava alcanzan la costa y entran en contacto con el océano.

La mayoría del conocimiento existente relativo a emisiones volcánicas submarinas proviene de fuentes hidrotermales profundas, sobre todo en dorsales oceánicas de separación (Von Damm et al., 1985; Baker et al., 1985; Baker, 1994; Embley et al., 1995; Sarradin et al., 1999; Desbruyères et al., 2001; Baker y German, 2004). Son particularmente bien conocidas las fumarolas de alta temperatura y gran flujo conocidas como "black-smokers" o chimeneas negras (Karl et al., 1988; Rona y Speer, 1989). Sin embargo, también existe el flujo difuso, definido como emisiones de baja temperatura (<50ºC) y baja velocidad de flujo (Baker et al., 2016). Este tipo de emisiones son de gran relevancia para los balances biogeoquímicos globales, ya que tienen la capacidad de aportar importantes concentraciones de nutrientes y metales en una forma bioasimilable (Resing et al., 2015; Santana-González et al., 2017; Lough et al., 2019; Tilliette et al., 2022). Además, en las últimas décadas, el vulcanismo submarino somero e intraplaca ha empezado a recibir más atención, ya que sus consecuencias pueden ser muy diferentes a las de

emisiones a grandes profundidades (McCarthy et al., 2005; Kilias et al., 2013; Buck et al., 2018; Esposito et al., 2018; Bellec et al., 2020).

En contraposición a las emisiones hidrotermales, respaldadas por una amplia literatura científica, las observaciones directas de erupciones magmáticas oceánicas son menos comunes, ya que suelen ocurrir en lugares remotos y su muestreo supone un gran reto logístico y de seguridad, pudiendo generar plumas corrosivas, desgasificación explosiva, e incluso tsunamis (Dziak et al., 2012; Fraile-Nuez et al., 2012; Kubota et al., 2022). Sin embargo, una vez terminada la erupción, los volcanes submarinos tienden a albergar ecosistemas ricos y únicos desde un punto de vista ecológico y de biodiversidad que los hace de especial interés para la comunidad científica (Karl et al., 1989; Sorokin et al., 1998; B. J. Baker et al., 2012; Danovaro et al., 2017).

Por su parte, los volcanes subaéreos pueden presentar otro tipo de interacciones con los océanos. La más común es la llegada de flujos de lava al mar, un fenómeno común en islas volcánicas intraplaca (Soule et al., 2021; Rodríguez-González et al., 2022). La lava se solidifica rápidamente debido al gran contraste de temperatura con el agua de mar, produciendo entradas masivas de calor y materia al océano (Sansone y Resing, 1995).

Este proceso puede generar estructuras geológicas conocidas como deltas de lava, formadas cuando la lava colmata la plataforma insular formando una nueva superficie emergida (Soule et al., 2021; Rodriguez-Gonzalez et al., 2022). Los deltas de lava conllevan una serie de riesgos asociados, como colapsos, explosiones hidrovolcánicas, o nubes de gases tóxicos (Mattox y Mangan, 1997; Chiocci et al., 2008; Bosman et al., 2014). Por este motivo, hay una escasez de estudios con muestreos directos durante la formación de los deltas de lava (Soule et al., 2021).

IV.2. Área de estudio

Canarias es un archipiélago intraplaca adyacente al margen noroeste del continente africano, a 27–29ºN de latitud y 18–13ºW de longitud. Se trata de un archipiélago de origen volcánico y actualmente activo; sin embargo, los mecanismos específicos que dieron lugar a estas islas han sido objeto de debate durante mucho tiempo. Aunque originalmente se propusieron una serie de modelos tectónicos (McDougall, 1971; Anguita y Hernán, 1975; Araña y Ortiz, 1991; Oyarzun et al., 1997), la hipótesis que ha contado con más respaldo es la del "hot spot" o punto caliente (Schmincke, 1973; Holik et al., 1991; Hoernle y Schmincke, 1993; Watts, 1994; Hoernle et al., 1995; Carracedo et al., 1998). Esta se basa en la presencia de

una pluma en el manto localizada bajo una placa litosférica en movimiento, generando erupciones que dan lugar a las islas de manera secuencial a medida que la placa se va moviendo (Wilson, 1963; Morgan, 1971). Esta hipótesis se ha ido complementando con modelos más recientes, que proponen que el ascenso de esta pluma está condicionado por la heterogeneidad de la placa litosférica; en otras palabras, el magma asciende más fácilmente por zonas de fracturas ya existentes (León et al., 2022; Negredo et al., 2022).

La formación de cada isla se caracteriza por una fase inicial de rápido crecimiento, seguido por un periodo de quiescencia y erosión, y otro periodo "post-erosional" de actividad (Carracedo et al., 1998; Negredo et al., 2022). Actualmente hay dos islas en el periodo más activo y juvenil de crecimiento, las dos islas más occidentales: El Hierro y La Palma (León et al., 2022; Negredo et al., 2022).

VI.2.1. El Hierro

El Hierro es la isla más joven del archipiélago canario, localizada en el extremo sur-occidental. Sus rocas subaéreas más antiguas están datadas en 1.12 millones de años (Guillou et al., 1996). La isla se caracteriza por la presencia de tres rifts convergentes separados por al menos tres deslizamientos gigantes, formando grandes valles que se extienden hacia el mar. Aunque la isla se encuentra en fase activa de crecimiento, pasó por más de 200 años de quiescencia desde la última erupción conocida en registros históricos, en el año 1793. Debido a su posición alejada del afloramiento costero del noroeste de África, la isla está rodeada por aguas oligotróficas (Barton et al., 1998).

En 2011 tuvo lugar una erupción submarina en la costa sur de El Hierro. La actividad pre-eruptiva comenzó en julio de 2011, con sismicidad de baja magnitud que inicialmente se localizó en el norte de la isla y posteriormente fue migrando hacia el sur. Se detectaron más de 10.000 terremotos durante esta etapa pre-eruptiva, junto con una deformación del suelo de 5 cm (López et al., 2012).

El 10 de octubre de 2011 se registró un tremor volcánico en todas las estaciones sísmicas, confirmando el inicio de una erupción submarina al sur de la isla de El Hierro. Se observaron plumas volcánicas con decoloración del mar, burbujas explosivas con elevación de la superficie del mar de hasta 10 metros de altura, y fragmentos de rocas flotando en superficie (Fraile-Nuez et al., 2012; Santana-Casiano et al., 2013).

La erupción causó perturbaciones físico-químicas extremas en toda la columna de agua en un área extensa alrededor de la isla, incluyendo aumentos de temperatura, acidificación, desoxigenación, y emisión de metales, lo que causó una gran

mortalidad de peces y grandes alteraciones en la actividad y composición de las comunidades planctónicas locales (Fraile-Nuez et al., 2012; Santana-Casiano et al., 2013).

El volcán recibió el nombre de Tagoro a petición del Instituto Español de Oceanografía (IEO-CSIC) al Instituto Hidrográfico de la Marina (IHM). Tagoro se localiza a 1.8 km al sur del pueblo de La Restinga. Su cráter principal se encuentra a 127 m bajo el nivel del mar, y su punto más alto y cráter secundario se encuentra a 88 m (Fraile-Nuez et al., 2018).

En marzo de 2012, la erupción terminó y el volcán entró en una nueva fase post-eruptiva con desgasificación y emisiones hidrotermales. Esta fase aún continúa activa, encontrándose emisiones de flujo difuso que liberan calor, gases, nutrientes inorgánicos y metales al medio marino en la zona de los cráteres principales (Santana-Casiano et al., 2013; Fraile-Nuez et al., 2018).

El Instituto Español de Oceanografía (IEO-CSIC) lleva más de una década monitorizando la actividad del volcán submarino Tagoro y sus efectos sobre el medio marino, en colaboración con las dos universidades canarias (ULPGC, ULL) así como numerosas instituciones nacionales e internacionales de ciencia marina. Se han llevado a cabo más de 30 campañas oceanográficas multidisciplinares para caracterizar los procesos físico-químicos, biológicos y geológicos que tienen lugar sobre el volcán submarino Tagoro en el contexto del proyecto multidisciplinar VULCANA, liderado desde el Centro Oceanográfico de Canarias del IEO-CSIC (Fraile-Nuez et al., 2023).

VI.2.2. La Palma

La Palma es la segunda isla más joven de Canarias, localizada en el extremo noroeste del archipiélago. Actualmente es la isla con el crecimiento más rápido del archipiélago: la mitad de todas las erupciones ocurridas en Canarias en los últimos 600 años han ocurrido en La Palma (Anguita, 2018).

La parte actualmente más activa de la isla es la zona de Cumbre Vieja, un rift volcánico poligenético formado por una serie de fisuras concentradas en una tendencia norte-sur. Presenta una altura de más de 2000 m sobre el nivel del mar, y su flanco oeste presenta acantilados costeros de hasta 700 m como resultado de la erosión (Carracedo et al., 1999).

Desde el 2017 se empezó a registrar actividad sísmica anómala al sur de la isla de La Palma, en la zona de Cumbre Vieja. Sin embargo, el último enjambre sísmico y el más intenso duró menos de dos semanas, con más de 400 eventos sísmicos registrados y una deformación del suelo de hasta 15 cm (IGN, 2022).

Finalmente, el 19 de septiembre de 2021 comenzó una erupción fisural con mecanismo estromboliano en Cumbre Vieja, a unos 900 metros de altitud (IGN, 2022). La erupción duró 85 días, con graves consecuencias para los bienes materiales de más de 2300 personas, 1600 edificios, 370 hectáreas de terreno agrícola, y 73 km de carreteras (Cabildo de La Palma).

Las coladas de lava fluyeron cuesta abajo hacia el oeste hasta alcanzar la costa 9 días más tarde, el 28 de septiembre a las 23:00 hora local, entre el puerto de Tazacorte y La Bombilla, una zona con acantilados de unos 100 metros de altura. Varios flujos de lava continuaron alcanzando el mar en distintos puntos durante las siguientes semanas. El resultado fue la formación de dos deltas de lava: uno principal con una superficie de 43 Ha en esa misma zona, formado por la unión de varios deltas de lava más pequeños; y otro delta localizado al norte de este, de 5.4 Ha de superficie (Lozano Rodríguez et al., 2023).

Los deltas de lava se propagaron bajo el agua llenando el curso de algunos barrancos submarinos y alcanzando espesores de hasta 40 metros. Los materiales volcánicos se encontraron a distancias de hasta 1.2 km de costa y >300 m bajo el nivel del mar (Lozano-Rodríguez et al., 2023). Estas entradas de lava al mar, junto con la abundante deposición de cenizas y la presencia de materiales volcánicos finos suspendidos en el agua, causaron importantes alteraciones en las propiedades físico-químicas del entorno marino circundante, incluyendo acidificación, aumento de la temperatura, y una gran turbidez (Fraile-Nuez et al., 2021; González-Santana et al., 2022; Román et al., 2022), además de una alta mortalidad de peces (M. J. Caballero et al., 2023).

VI.3. Objetivos y estructura de la tesis

Canarias es un archipiélago volcánico activo. Tras dos erupciones en un periodo de 10 años, es evidente que el estudio de los procesos volcánicos y sus efectos en el entorno deben ser una prioridad para la comunidad científica del archipiélago. La erupción submarina de El Hierro en 2011 fue la primera erupción totalmente monitorizada instrumentalmente en el archipiélago. El conocimiento y la experiencia obtenidas en este proceso fueron de gran utilidad para la siguiente erupción de La Palma en 2021. Por tanto, con el conocimiento generado en cada erupción estamos mejor preparados para la siguiente.

El Instituto Español de Oceanografía (IEO-CSIC) lleva más de una década monitorizando la volcanología submarina de Canarias. Esta serie de datos única en el mundo implica una gran cantidad de recursos, instrumentación, personal, e instituciones involucradas. La presente tesis pretende contribuir a este enorme

conjunto de conocimiento científico, arrojando luz sobre algunos de los procesos físico-químicos y biológicos más importantes que tienen lugar en el océano del archipiélago canario como consecuencia de la actividad volcánica.

Se presentan tres estudios sobre los efectos en el entorno marino de las dos erupciones volcánicas más recientes de Canarias. Estos exploran tres tipos de interacciones volcán-océano diferentes: una erupción submarina; una actividad hidrotermal post-eruptiva; y la formación de un delta de lava a partir de una erupción subaérea.

Aunque este trabajo se centra principalmente en la biogeoquímica y oceanografía física, se diseñó intencionalmente con un carácter multidisciplinar muy marcado, ya que las interacciones de los procesos volcánicos con el océano afectan a todas las propiedades físicas, químicas y biológicas en la columna de agua, y todos estos procesos interactúan entre ellos.

Tras una introducción general en el **Capítulo 1**, la tesis se estructura de manera cronológica:

El **Capítulo 2** explora una de las consecuencias más dramáticas de la erupción submarina de 2011 en El Hierro: la pérdida de oxígeno disuelto en un área extensa alrededor del volcán Tagoro. Se cuantifica esta desoxigenación y se estima su alcance espacial. Este estudio está publicado en *Frontiers in Marine Science* (González-Vega et al., 2022).

Continuando en el volcán submarino Tagoro, el **Capítulo 3** presenta un estudio detallado de las emisiones de nutrientes inorgánicos disueltos tanto durante la etapa eruptiva como la post-eruptiva, en el periodo 2011-2018. Se trata de un set de datos único, que permitió cuantificar el enriquecimiento de estos nutrientes, el alcance espacial de estas plumas enriquecidas, y los flujos de nutrientes. Este estudio se publicó en *Frontiers in Marine Science* (González-Vega et al., 2020) y se complementó con un capítulo en el libro de Springer *El Hierro island*, de la serie *Active Volcanoes of the World* (González-Vega et al., 2023), cuyo resumen puede encontrarse en el **Anexo I**.

Por último, pasando a la erupción más reciente en Canarias, el **Capítulo 4** se centra en la erupción de Cumbre Vieja (La Palma) en 2021, y los efectos de la formación de deltas de lava sobre el entorno marino local. Este estudio ofrece una visión completa de los efectos físico-químicos y biológicos de las llegadas de lava al mar. Este trabajo se ha enviado para su publicación en *Science of the Total Environment*. En el **Anexo II** se puede encontrar el material suplementario de este artículo.

Finalmente, en el **Capítulo 5** se presentan las conclusiones principales de todo el trabajo, junto con una breve discusión sobre las contribuciones de estos estudios al campo de la volcanología submarina en Canarias.

IV.4. Conclusiones generales

Las principales conclusiones de esta tesis son las siguientes:

- Las dos erupciones volcánicas más recientes de Canarias (El Hierro, 2011 y La Palma, 2021) tuvieron efectos abruptos sobre todos los parámetros físico-químicos medidos en el entorno marino, con una alta variabilidad espacial y temporal. Los ecosistemas marinos locales también se vieron severamente afectados en ambos casos. Estos efectos se observaron en toda la columna de agua y con alcances horizontales de varios kilómetros.

- La erupción del volcán submarino Tagoro (El Hierro, 2011-2012) causó una severa pérdida de oxígeno disuelto en el área oceánica circundante debido a la emisión de compuestos químicos reducidos, alcanzándose condiciones subóxicas e incluso anóxicas. Durante los episodios eruptivos más intensos, el área afectada llegó a ser de más de 460 km². Las corrientes locales y estructuras mesoescalares como remolinos controlaban el transporte de estas plumas desoxigenadas, que llegaron a detectarse a distancias de hasta 80 km del volcán.

- Las emisiones del volcán submarino Tagoro, tanto durante la etapa eruptiva como la post-eruptiva, aportan grandes concentraciones de nutrientes inorgánicos, particularmente de silicato, que está hasta 325 veces más concentrado en los fluidos hidrotermales que en las condiciones normales de la zona. El fosfato también se encuentra enriquecido (10 veces más). El nitrógeno parece emitirse predominantemente en forma de amonio, también muy enriquecido (98 veces más), y posteriormente reacciona formando nitrato y nitrito.

- Una vez que el volcán Tagoro evolucionó a un sistema hidrotermal con flujo difuso, las emisiones de nutrientes, aún presentes en la zona, parecen haber contribuido a la rápida recuperación del ecosistema marino. Los flujos de nutrientes por unidad de área en Tagoro son comparables en magnitud a algunas de las fuentes de nutrientes más importantes de la región, como el *upwelling* o afloramiento costero de la costa noroeste africana.

- La erupción subaérea de Cumbre Vieja (La Palma, 2021) generó flujos de lava que alcanzaron el océano formando nuevos deltas de lava. Este

proceso de formación generó importantes anomalías físico-químicas en toda la columna de agua. La turbidez fue particularmente alta (hasta 30 veces mayor que en condiciones normales) debido a la presencia de hialoclastitas y cenizas. También se observó un descenso en el pH y en el oxígeno disuelto, así como un aumento de temperatura, y un comportamiento variable (aumentos y disminuciones) de la salinidad. Las anomalías termohalinas se observaron en un rango de hasta 6 kilómetros de distancia a costa.

- Estas entradas de lava al océano generaron un efecto de *upwelling* o afloramiento, consistente en el ascenso de las aguas calentadas por la lava, siendo reemplazadas por aguas más profundas, frías y ricas en nutrientes. Este proceso se observó sobre el área donde las diferencias batimétricas indican la presencia submarina de nuevos materiales volcánicos, y hasta 1 km de distancia desde la nueva línea de costa. Sin embargo, al contrario que en otros casos conocidos en la literatura, este *upwelling* generado por la entrada de lava no generó un *bloom* fitoplanctónico.

- La formación del delta de lava principal causó una disminución brusca de la clorofila-*a* integrada en profundidad, con un descenso del -41% solo en los primeros dos días tras la primera llegada de lava al mar, y un -69% un mes más tarde, en un rango de más de 2.5 km de distancia (no se delimitó). Esto sugiere un efecto negativo sobre las comunidades de fitoplancton.

IV.5. Contribución a la gestión de emergencias

Aunque este trabajo ha ayudado a expandir nuestro conocimiento sobre los efectos de diferentes procesos volcánicos en el medio marino, no debería entenderse estrictamente como investigación básica. Estos estudios han tenido una aplicación directa de cara a la gestión de crisis durante las dos emergencias volcánicas más recientes de Canarias. De hecho, los resultados mostrados en los Capítulos 2, 3 y 4 se han usado explícitamente durante reuniones oficiales del Comité Científico del PEVOLCA (Plan de Emergencias Volcánicas de Canarias). Se espera que la experiencia adquirida por el grupo de trabajo involucrado en los estudios presentados fortalezca la capacidad del archipiélago para responder de manera eficiente a futuras crisis volcánicas.

IV.5.1. Recomendaciones para el muestreo oceanográfico durante una emergencia volcánica

Durante las campañas oceanográficas, una estrategia óptima de muestreo es crucial para obtener datos de calidad; sin embargo, durante una erupción volcánica, los equipos científicos deben actuar con rapidez y escaso tiempo de preparación. A partir de los estudios presentados en esta tesis, se ofrecen algunas recomendaciones de cara al muestreo oceanográfico durante una emergencia volcánica y el posterior monitoreo de estos sistemas.

- Si es posible, muestrear la zona antes de que las emisiones volcánicas alcancen el océano. En el caso de la erupción submarina de El Hierro, esto no fue posible debido a la gran migración de las señales precursoras durante los meses previos a la erupción; sin embargo, estudios previos del IEO-CSIC en esta región proporcionaron un conocimiento de las condiciones oceanográficas previas a la erupción. En cambio, en la erupción de La Palma sí hubo una predicción bastante precisa de dónde era más probable que la lava entrara en contacto con el mar, lo que permitió un muestreo previo de la zona. Esto fue de gran utilidad para algunos de los análisis presentados en el Capítulo 4, permitiendo establecer una evolución temporal del proceso.

- Validar las señales de fluorescencia con muestras *in situ* de clorofila. Muchos estudios previos ya señalaban las limitaciones de los datos satelitales de clorofila durante eventos volcánicos, normalmente sobreestimados debido a una descoloración del agua, efecto que se observó también en la erupción submarina de El Hierro en 2011 (Mantas et al., 2011; Coca et al., 2014; Eugenio et al., 2014; Whiteside et al., 2023). Sin embargo, en este trabajo hemos presentado también el caso de un fenómeno similar en columna de agua. Durante la erupción de La Palma, el sensor de fluorescencia presentó unos valores altos que se correlacionaban linealmente con la turbidez, y que no se debían a niveles altos de clorofila. Se realizó una corrección de esta influencia de la turbidez sobre la señal de fluorescencia, además de una calibración con medidas de clorofila en muestras de agua. Esto permitió estimar con precisión el contenido real de clorofila en la columna de agua, que resultó ser muy bajo. Por tanto, durante una erupción volcánica es importante tomar los datos de fluorescencia con cautela y validarlos con muestras *in situ* de clorofila antes de reportar un aparente *bloom* fitoplanctónico.

- Adaptar las estrategias de muestreo a las escalas espaciales y temporales de los procesos volcánicos. La oceanografía clásica utiliza principalmente los muestreos con estaciones verticales de CTD, normalmente formando transectos o mallas de estaciones. Sin embargo, la alta variabilidad de los procesos volcánicos en el océano (escalas de horas o incluso minutos) representa una limitación para esta técnica, ya que las estaciones implican contar con los tiempos de navegación y muestreo de la roseta entre estaciones. Otra limitación es la resolución espacial, ya que las estaciones suelen estar separadas al menos unas decenas de metros, que puede ser demasiado para procesos a pequeña escala como emisiones hidrotermales difusas. En cambio, la técnica tow-yo ofrece una fotografía casi sinóptica de toda la columna de agua a lo largo del transecto con una sola largada del CTD. Esta técnica consiste en subir y bajar constantemente el CTD mientras el barco está en movimiento lento, obteniendo un muestreo en forma de "zig-zag" en toda la columna de agua. Por otra parte, el uso de nuevas tecnologías como ROVs ofrece un nuevo abanico de posibilidades, que no se limita a la adquisición de imágenes de alta calidad: permite también el uso de instrumentación específica, que puede ser diseñada *ad hoc* para cada necesidad de muestreo.

IV.5.2. Resiliencia del ecosistema local tras una erupción

Aunque esta tesis no tiene un enfoque microbiológico, ha ofrecido los primeros pasos para comprender cómo reacciona el ecosistema marino ante aportes volcánicos de cualquier tipo, y cómo evoluciona en los años posteriores. En el caso del volcán submarino Tagoro, la erupción en 2011-12 fue mortal para gran parte del ecosistema local; sin embargo, el posterior monitoreo en la última década ha mostrado una impresionante recuperación, y hoy en día el volcán alberga un ecosistema rico y único (Danovaro et al., 2017; Sotomayor-García et al., 2019; Fernández de Puelles et al., 2021). Aunque los mecanismos específicos de esta recuperación aún están por dilucidar, el gran aporte de nutrientes inorgánicos por parte del volcán Tagoro (Capítulo 3) es muy probablemente una pieza importante para este proceso.

El caso de La Palma fue completamente diferente, ya que no se trató de emisiones directas mantenidas en el tiempo, sino una entrada abrupta de masa y calor al océano, con consecuencias dramáticas para una parte localizada del ecosistema marino de la zona. En el Capítulo 4 se ha evidenciado un efecto negativo sobre los productores primarios, además de un enterramiento de los organismos bentónicos y ausencia de organismos pelágicos durante la formación de los deltas

de lava. Sin embargo, es razonable esperar una regeneración del ecosistema. En campañas de monitoreo más recientes (no incluidas en este trabajo) ya se han observado los primeros signos de recuperación. Las escalas temporales y procesos específicos asociados a esta recuperación se irán dilucidando siempre y cuando continúe el monitoreo de la zona.

Como nota final, Canarias representa una oportunidad única desde el punto de vista científico para estudiar el volcanismo submarino intraplaca; sin embargo, esta línea de investigación también tiene un alto valor social. La sociedad canaria necesita estar familiarizada con la naturaleza volcánica del archipiélago, y es responsabilidad de la comunidad científica trasladar este conocimiento al público general para poder comprender el entorno en el que vivimos.

Agradecimientos

¿Qué hace posible una tesis doctoral? No basta con encontrar un tema que te apasione: también es necesario contar con buenos mentores que te guíen por el camino, un entorno de trabajo que te ayude a avanzar, y una red de familia y amistades en quienes apoyarte. En mi caso he tenido la increíble suerte de contar con todas estas cosas.

En primer lugar, agradezco haber tenido un director de tesis como Eugenio, que no se limita a dirigir: también apoya, aconseja, se implica, está pendiente de todo su equipo, incluso es capaz de "sacarme del agujero" cuando lo necesito. También he tenido la suerte de contar con Txetxu como codirector, cuyas revisiones y consejos enriquecen la calidad científica de cualquier estudio, y todo sin perder nunca el sentido del humor.

Por otro lado, mis compañeros y compañeras del Centro Oceanográfico de Canarias han sido un gran apoyo y me han ayudado siempre que lo he necesitado. Juan Pablo, Clàudia, Jesús, Isa, Marijn, Carmiña, José Antonio, Marisa, Pepe, Ángela, Alberto, y un largo etcétera; gracias a ellos y ellas se ha hecho más llevadero el proceso.

La tesis también ha supuesto una serie de experiencias más allá del despacho. He tenido la suerte de participar en unas 12 campañas oceanográficas. Quiero expresar mi agradecimiento a las tripulaciones de todos los buques en los que he embarcado, especialmente de los B/O *Ángeles Alvariño* y *Ramón Margalef*, donde siempre nos acogen como una segunda casa. También tuve la oportunidad de pasar tres meses en el centro de investigación GEOMAR (Kiel, Alemania). *Danke schön* to Dietrich and his team for taking me in, and to all the RD4 people for making me feel welcome.

Gracias a mis amigos y amigas que, aunque sigan sin tener muy claro de qué va mi trabajo, siempre me ayudan a desconectar cuando lo necesito. A mis amigos de Gran Canaria de toda la vida; a los que hice en Salamanca; a los que he hecho estos años en Tenerife; a todos y todas, gracias por las risas, por los memes, y por dejarme desahogarme cuando lo necesito. Y por supuesto a Bernardo, que ha tenido que aguantarme en mis peores momentos de estrés y ansiedad, y que me ha dejado el congelador lleno de comida para sobrevivir a estos últimos tiempos.

He dejado lo más importante para el final: nada de esto sería posible sin mi familia. A mis padres, que se preocuparon por estimular nuestra curiosidad y creatividad desde pequeños, y que nunca dejaron de apoyarnos en todos los caminos que

decidimos seguir. A ellos les debo todo. Gracias también a mis hermanos, Marta y Javi, que siempre fueron mi ejemplo a seguir en la vida. A todos mis tíos/as y primos/as por su cariño y apoyo. A mi abuelo Miguel, el pilar de nuestra familia, cuyos potajes de berros son capaces de curar todos los males. Y a mi abuela Maruca, que aunque se fue yendo poco a poco, no dejó de apretarnos la mano hasta el final.

A mi sobrino Nilo. Ahora eres muy pequeño, pero espero que algún día esta tesis te inspire curiosidad por cómo funciona nuestro planeta y nuestros océanos, y te anime a cuidarlos para construir un futuro mejor.

Para terminar, quiero hacer una mención a las mujeres científicas de la historia, las que tuvieron que abrirse camino en tiempos más difíciles, cuando no eran bienvenidas. Gracias por luchar hasta hacerse con el lugar que les correspondía.

Se acaba esta etapa, y como dice mi abuelo: "¡pa' lo que trajiste, bastante te llevas!".

References

Aliani, S., Bortoluzzi, G., Caramanna, G., and Raffa, F. (2010). Seawater dynamics and environmental settings after November 2002 gas eruption off Bottaro (Panarea, Aeolian Islands, Mediterranean Sea). *Continental Shelf Research*, *30*(12), 1338–1348. https://doi.org/10.1016/j.csr.2010.04.016

Aliani, S., Meloni, R., and Dando, P. R. (2004). Periodicities in sediment temperature time-series at a marine shallow water hydrothermal vent in Milos Island (Aegean Volcanic arc, Eastern Mediterranean). *Journal of Marine Systems*, *46*(1–4), 109–119. https://doi.org/10.1016/j.jmarsys.2003.11.015

Álvarez-Valero, A. M., Burgess, R., Recio, C., de Matos, V., Sánchez-Guillamón, O., Gómez-Ballesteros, M., Recio, G., Fraile-Nuez, E., Sumino, H., Flores, J. A., Ban, M., Geyer, A., Bárcena, M. A., Borrajo, J., and Compaña, J. M. (2018). Noble gas signals in corals predict submarine volcanic eruptions. *Chemical Geology*, *480*, 28–34. https://doi.org/10.1016/j.chemgeo.2017.05.013

Amaya-Vías, S., Flecha, S., Pérez, F. F., Navarro, G., García-Lafuente, J., Makaoui, A., and Huertas, I. E. (2023). The time series at the Strait of Gibraltar as a baseline for long-term assessment of vulnerability of calcifiers to ocean acidification. *Frontiers in Marine Science*, *10*. https://doi.org/10.3389/fmars.2023.1196938

Aminot, A., and Kérouel, R. (2007). *Dosage automatique des nutriments dans les eaux marines: méthodes en flux continu*. Editions Quae.

Ancochea, E., Hernám, F., Cendrero, A., Cantagrel, J. M., Fúster, J. M., Ibarrola, E., and Coello, J. (1994). Constructive and destructive episodes in the building of a young Oceanic Island, La Palma, Canary Islands, and genesis of the Caldera de Taburiente. *Journal of Volcanology and Geothermal Research*, *60*, 243–262.

Anguita, F. (2018). *Los volcanes de Canarias. Guía geológica e itinerarios*. Rueda.

Anguita, F., and Hernán, F. (1975). A propagating fracture model versus a hot spot origin for the Canary Islands. *Earth and Planetary Science Letters*, *27*(1975), 11–19.

Araña, V., and Ortiz, R. (1991). The Canary Islands: Tectonics, Magmatism and Geodynamic Framework. In *Magmatism in extensional structural settings: The phanerozoic African plate* (pp. 209–249).

Aumont, O., Ethé, C., Tagliabue, A., Bopp, L., and Gehlen, M. (2015). PISCES-v2: An ocean biogeochemical model for carbon and ecosystem studies. *Geoscientific Model Development*, *8*(8), 2465–2513. https://doi.org/10.5194/gmd-8-2465-2015

Baker, B. J., Lesniewski, R. A., and Dick, G. J. (2012). Genome-enabled transcriptomics reveals archaeal populations that drive nitrification in a deep-sea hydrothermal plume. *ISME Journal*, *6*(12), 2269–2279. https://doi.org/10.1038/ismej.2012.64

Baker, E. T. (1994). A 6-year time series of hydrothermal plumes over the Cleft segment of the Juan de Fuca Ridge. *Journal of Geophysical Research*, *99*(B3), 4889–4904. https://doi.org/10.1029/93JB01030

Baker, E. T. (1998). Patterns of event and chronic hydrothermal venting following a magmatic intrusion: New perspectives from the 1996 Gorda Ridge eruption. *Deep-Sea Research Part II: Topical Studies in Oceanography*, *45*(12), 2599–2618. https://doi.org/10.1016/S0967-0645(98)00085-X

Baker, E. T., and German, C. R. (2004). On the global distribution of hydrothermal vent fields . in Mid-Ocean Ridges: Hydrothermal Interactions Between the Lithosphere and Oceans. *Geophysical Monograph Series*, *148*, 245–266. http://www.pmel.noaa.gov/pubs/outstand/bake2544/bake2544.shtml

Baker, E. T., Lavelle, J. W., and Massoth, G. J. (1985). Hydrothermal particle plumes over the southern Juan de Fuca Ridge. *Nature*, *316*.

Baker, E. T., and Lupton, J. E. (1990). Changes in submarine hydrothermal 3He/heat ratios as an indicator of magmatic/tectonic activity. *Nature*, *346*(6284), 556–558. https://doi.org/10.1038/346556a0

Baker, E. T., and Massoth, G. J. (1987). Characteristics of hydrothermal plumes from two vent fields on the Juan de Fuca Ridge, northeast Pacific Ocean. *Earth and Planetary Science Letters*, *85*(1–3), 59–73. https://doi.org/10.1016/0012-821X(87)90021-5

Baker, E. T., Massoth, G. J., and Feely, R. A. (1987). Cataclysmic hydrothermal venting on the Juan de Fuca Ridge. *Nature*, *329*(6135), 149–151. https://doi.org/10.1038/329149a0

Baker, E. T., Massoth, G. J., Feely, R. A., Embley, R. W., Thomson, R. E., and Burd, B. J. (1995). Hydrothermal event plumes from the coaxial seafloor eruption site, Juan de Fuca Ridge. *Geophysical Research Letters*, *22*(2), 147–150. https://doi.org/10.1029/94GL02403

Baker, E. T., Massoth, G. J., Walker, S. L., and Embley, R. W. (1993). A method for quantitatively estimating diffuse and discrete hydrothermal discharge. *Earth and Planetary Science Letters*, *118*(1–4), 235–249. https://doi.org/10.1016/0012-821X(93)90170-E

Baker, E. T., Resing, J. A., Haymon, R. M., Tunnicliffe, V., Lavelle, J. W., Martinez, F., Ferrini, V., Walker, S. L., and Nakamura, K. (2016). How many vent fields? New estimates of vent field populations on ocean ridges from precise mapping of hydrothermal discharge locations. *Earth and Planetary Science Letters*, *449*, 186–196. https://doi.org/10.1016/j.epsl.2016.05.031

Barreyre, T., Escartín, J., Garcia, R., Cannat, M., Mittelstaedt, E., and Prados, R. (2012). Structure, temporal evolution, and heat flux estimates from the Lucky Strike deep-sea hydrothermal field derived from seafloor image mosaics. *Geochemistry, Geophysics, Geosystems*, *13*(4), 1–29. https://doi.org/10.1029/2011GC003990

Barton, E. D., Aristegui, J., Tett, P., Canton, M., García-Braun, J., Hernández-León, S., Nykjaer, L., Almeida, C., Almunia, J., Ballesteros, S., Basterretxea, G., Escanez, J., García-Weill, L., Hernández-Guerra, A., López-Laatzen, F., Molina, R., Montero, M. F., Navarro-Peréz, E., Rodríguez, J. M., … Wild, K. (1998). The transition zone of the Canary Current upwelling region. *Progress in Oceanography*, *41*(4), 455–504. https://doi.org/10.1016/S0079-6611(98)00023-8

Bellec, L., Cambon-Bonavita, M. A., Durand, L., Aube, J., Gayet, N., Sandulli, R., Brandily, C., and Zeppilli, D. (2020). Microbial Communities of the Shallow-Water Hydrothermal Vent Near Naples, Italy, and Chemosynthetic Symbionts Associated With a Free-Living Marine Nematode. *Frontiers in Microbiology*, *11*(August 2020), 1–16. https://doi.org/10.3389/fmicb.2020.02023

Bosman, A., Casalbore, D., Romagnoli, C., and Chiocci, F. L. (2014). Formation of an 'a'ā lava delta: Insights from time-lapse multibeam bathymetry and direct observations during the Stromboli 2007 eruption. *Bulletin of Volcanology*, *76*(7), 1–12. https://doi.org/10.1007/s00445-014-0838-2

Bosshard, E., and MacFarlane, D. (1970). Crustal structure of the western Canary Islands from seismic refraction and gravity data. *J Geophys Res*, *75*(26), 4901–4918. https://doi.org/10.1029/jb075i026p04901

Brocks, J. J., Logan, G. A., Buick, R., and Summons, R. E. (1999). Archean molecular fossils and the early rise of eukaryotes. *Science*, *285*(5430), 1033–1036. https://doi.org/10.1126/science.285.5430.1033

Buck, N. J., Resing, J. A., Baker, E. T., and Lupton, J. E. (2018). Chemical Fluxes From a Recently Erupted Shallow Submarine Volcano on the Mariana Arc. *Geochemistry, Geophysics, Geosystems*, *19*(5), 1660–1673. https://doi.org/10.1029/2018GC007470

Butterfield, D. A., Massoth, G. J., McDuff, R. E., Lupton, J. E., and Lilley, M. D. (1990). Geochemistry of hydrothermal fluids from Axial Seamount Hydrothermal Emissions Study vent field, Juan de Fuca Ridge: subseafloor boiling and subsequent fluid-rock interaction. *Journal of Geophysical Research*, *95*(B8). https://doi.org/10.1029/jb095ib08p12895

Caballero, I., Román, A., Tovar-Sánchez, A., and Navarro, G. (2022). Water quality monitoring with Sentinel-2 and Landsat-8 satellites during the 2021 volcanic eruption in La Palma (Canary Islands). *Science of the Total Environment*, *822*. https://doi.org/10.1016/j.scitotenv.2022.153433

Caballero, M. J., Perez-Torrado, F. J., Velázquez-Wallraf, A., Betancor, M. B., Fernández, A., and Castro-Alonso, A. (2023). Fish mortality associated to volcanic eruptions in the Canary Islands. *Frontiers in Marine Science*, *9*. https://doi.org/10.3389/fmars.2022.999816

Cabildo de La Palma. (n.d.). *Riesgo volcánico. Información estadística de la afección directa de la colada volcánica*. Retrieved November 2, 2023, from https://volcan.lapalma.es/

Campbell, A. C., and Gieskes, J. M. (1984). Water column anomalies associated with hydrothermal activity in the Guaymas Basin, Gulf of California Andrew C. Campbell and Joris M. Gieskes. *Earth and Planetary Science Letters*, *68*, 57–72.

Carpenter, J. I. I. (1965). The accuracy of the Winkler method for dissolved oxygen analysis. *Limonology And Oceanography*, *10*(1), 135–140. http://www.aslo.org/lo/toc/vol_10/issue_1/0135.html

Carracedo, J., Badiola, E., Guillou, H., de La Nuez, J., Perez, F., and Perez Torrado, F. (2001). Geology and volcanology of La Palma and El Hierro, Western Canaries. In *Estudios Geologicos-Madrid* (Vol. 57). https://hal.science/hal-03323419

Carracedo, J. C., Day, S., Guillou, H., Rodríguez Badiolas, E., Canas, J. A., and Pérez Torrado, F. J. (1998). Hotspot volcanism close to a passive continental margin: the Canary Islands. *Geological Magazine*, *135*, 591–604.

Carracedo, J. C., Day, S. J., Guillou, H., and Gravestock, P. (1999). Later stages of volcanic evolution of La Palma, Canary Islands: rift evolution, giant landslides, and the genesis of the Caldera de Taburiente. *GSA Bulletin*, *111*(5), 755–768.

Chiocci, F. L., Romagnoli, C., Tommasi, P., and Bosman, A. (2008). The Stromboli 2002 tsunamigenic submarine slide: Characteristics and possible failure mechanisms. *Journal of Geophysical Research: Solid Earth*, *113*(10). https://doi.org/10.1029/2007JB005172

Clarke, L. J., and Jenkyns, H. C. (1999). New oxygen isotope evidence for long-term Cretaceous climatic change in the Southern Hemisphere. *Geology*, *27*(8), 699–702. https://doi.org/10.1130/0091-7613(1999)027<0699:NOIEFL>2.3.CO;2

Clayton, T. D., and Byrne, R. H. (1993). Spectrophotometric seawater pH measurements: total hydrogen ion concentration scale calibration of m-cresol purple and at-sea results. *Deep-Sea Research*, *1*(10), 2115–2129.

Coca, J., Ohde, T., Redondo, A., García-Weil, L., Santana-Casiano, M., González-Dávila, M., Arístegui, J., Nuez, E. F., and Ramos, A. G. (2014). Remote sensing of the El Hierro submarine volcanic eruption plume. *International Journal of Remote Sensing*, *35*(17), 6573–6598. https://doi.org/10.1080/01431161.2014.960613

Crisp, J. A. (1984). Rates of magma emplacement and volcanic output. *Journal of Volcanology and Geothermal Research*, *20*(3–4), 177–211. https://doi.org/10.1016/0377-0273(84)90039-8

Danovaro, R., Canals, M., Tangherlini, M., Dell'Anno, A., Gambi, C., Lastras, G., Amblas, D., Sanchez-Vidal, A., Frigola, J., Calafat, A. M., Pedrosa-Pàmies, R., Rivera, J., Rayo, X., and Corinaldesi, C. (2017). A submarine volcanic eruption leads to a novel microbial habitat. *Nature Ecology and Evolution*, *1*(6), 1–8. https://doi.org/10.1038/s41559-017-0144

DECRETO 112/2018, de 30 de julio, por el que se aprueba el Plan Especial de Protección Civil y Atención de Emergencias por riesgo volcánico en la Comunidad Autónoma de Canarias (PEVOLCA). (2018). In *Boletín Oficial de Canarias*. https://sede.gobcan.es/boc

Desbruyères, D., Biscoito, M., Caprais, J. C., Colaço, A., Comtet, T., Crassous, P., Fouquet, Y., Khripounoff, A., Le Bris, N., Olu, K., Riso, R., Sarradin, P. M., Segonzac, M., and Vangriesheim, A. (2001). Variations in deep-sea hydrothermal vent communities on the Mid-Atlantic Ridge near the Azores plateau. *Deep-Sea Research Part I: Oceanographic Research Papers*, *48*(5), 1325–1346. https://doi.org/10.1016/S0967-0637(00)00083-2

Dziak, R. P., Baker, E. T., Shaw, A. M., Bohnenstiehl, D. R., Chadwick, W. W., Haxel, J. H., Matsumoto, H., and Walker, S. L. (2012). Flux measurements of explosive degassing using a yearlong hydroacoustic record at an erupting submarine volcano. *Geochemistry, Geophysics, Geosystems*, *13*(1), 1–14. https://doi.org/10.1029/2012GC004211

Edmond, J. M., Measures, C., McDuff, R. E., Chan, L. H., Collier, R., Grant, B., Gordon, L. I., and Corliss, J. B. (1979). Ridge crest hydrothermal activity and the balances of the major

and minor elements in the ocean: The Galapagos data. *Earth and Planetary Science Letters*, *46*(1), 1–18. https://doi.org/10.1016/0012-821X(79)90061-X

Elderfield, H., and Schultz, A. (1996). Mid-ocean ridge hydrothermal fluxes and the chemical composition of the ocean. *Annual Review of Earth and Planetary Sciences*, *24*, 191–224. https://doi.org/10.1146/annurev.earth.24.1.191

Embley, R. W., Chadwick, W. W., Jonasson, I. R., Butterfield, D. A., and Baker, E. T. (1995). Initial results of the rapid response to the 1993 CoAxial event: Relationships between hydrothermal and volcanic processes. *Geophysical Research Letters*, *22*(2), 143–146. https://doi.org/10.1029/94GL02281

Erba, E. (1994). Nannofossils and superplumes: The Early Aptian "nannoconid crisis." *Paleoceanography*, *9*(3), 483–501. https://doi.org/10.1029/94PA00258

Esposito, V., Andaloro, F., Canese, S., Bortoluzzi, G., Bo, M., Di Bella, M., Italiano, F., Sabatino, G., Battaglia, P., Consoli, P., Giordano, P., Spagnoli, F., Cono, V. La, Yakimov, M. M., Scotti, G., and Romeo, T. (2018). Exceptional discovery of a shallow-water hydrothermal site in the SW area of Basiluzzo islet (Aeolian archipelago, South Tyrrhenian Sea): An environment to preserve. *PLoS ONE*, *13*(1), 1–27. https://doi.org/10.1371/journal.pone.0190710

Eugenio, F., Martin, J., Marcello, J., and Fraile-Nuez, E. (2014). Environmental monitoring of El Hierro Island submarine volcano, by combining low and high resolution satellite imagery. *International Journal of Applied Earth Observation and Geoinformation*, *29*(1), 53–66. https://doi.org/10.1016/j.jag.2013.12.009

Fernández de Puelles, M. L., Gazá, M., Cabanellas-Reboredo, M., González-Vega, A., Herrera, I., Presas-Navarro, C., Arrieta, J. M., and Fraile-Nuez, E. (2021). Abundance and Structure of the Zooplankton Community During a Post-eruptive Process: The Case of the Submarine Volcano Tagoro (El Hierro; Canary Islands), 2013-2018. *Frontiers in Marine Science*, *8*(July). https://doi.org/10.3389/fmars.2021.692885

Ferrera, I., Arístegui, J., González, J. M., Montero, M. F., Fraile-Nuez, E., and Gasol, J. M. (2015). Transient changes in bacterioplankton communities induced by the submarine volcanic eruption of El Hierro (Canary Islands). *PLoS ONE*, *10*(2), 1–16. https://doi.org/10.1371/journal.pone.0118136

Föllmi, K. B. (1996). The phosphorus cycle, phosphogenesis and marine phosphate-rich deposits. *Earth-Science Reviews*, *40*(1–2), 55–124. https://doi.org/10.1016/0012-8252(95)00049-6

Fraile-Nuez, E., González-Dávila, M., Santana-Casiano, J. M., Arístegui, J., Alonso-González, I. J., Hernández-León, S., Blanco, M. J., Rodríguez-Santana, A., Hernández-Guerra, A., Gelado-Caballero, M. D., Eugenio, F., Marcello, J., De Armas, D., Domínguez-Yanes, J. F., Montero, M. F., Laetsch, D. R., Vélez-Belchí, P., Ramos, A., Ariza, A. V., … Benítez-Barrios, V. M. (2012). The submarine volcano eruption at the island of El Hierro: Physical-chemical perturbation and biological response. *Scientific Reports*, *2*(Figure 2), 2–7. https://doi.org/10.1038/srep00486

Fraile-Nuez, E., MacHín, F., Vélez-Belchí, P., López-Laatzen, F., Borges, R., Benítez-Barrios, V., and Hernández-Guerra, A. (2010). Nine years of mass transport data in the eastern boundary of the North Atlantic Subtropical Gyre. *Journal of Geophysical Research: Oceans*, *115*(9). https://doi.org/10.1029/2010JC006161

Fraile-Nuez, E., Santana-Casiano, J. M., González-Dávila, M., González-Vega, A., Vázquez, J. T., Sotomayor-García, A., Ferrera, I., Santana-González, C., Eugenio, F., Marcello, J., Hernández-León, S., Bakalis, E., Rueda, J. L., Gómez-Ballesteros, M., Álvarez-Valero, A. M., Sánchez-Guillamón, O., Palomino, D., Tello, O., Presas-Navarro, C., … Arrieta, J. M. (2023). Ten Years of Intense Physical–Chemical, Geological and Biological Monitoring Over the Tagoro Submarine Volcano Marine Ecosystem (Eruptive and Degassing Stages). In *Active Volcanoes of the World* (pp. 161–184). Springer Science and Business Media Deutschland GmbH. https://doi.org/10.1007/978-3-031-35135-8_8

Fraile-Nuez, E., Santana-Casiano, J. M., González-Dávila, M., Vázquez, J. T., Fernández-Salas, L. M., Sánchez-Guillamón, O., Palomino, D., and Presas-Navarro, C. (2018). Cyclic behavior associated with the degassing process at the shallow submarine Volcano Tagoro, Canary

Islands, Spain. *Geosciences (Switzerland)*, *8*(12), 1–15.
https://doi.org/10.3390/geosciences8120457

Fraile-Nuez, E., Vázquez, J. T., Gómez-Ballesteros, M., Sánchez-Guillamón, O., Naranjo, S., Ferrera, I., Arrieta, J., Huertas, E., Tovar-Sánchez, A., Roque, D., Navarro, G., Galindo, I., Mata, P., Rodríguez, A., Machín, F., Hernández-Guerra, S., Álvarez-Valero, A., Lozano, E., Presas-Navarro, C., … Martín-Díaz, J. (2021). *Informe científico-técnico para el PEVOLCA*.

Frölicher, T. L., Joos, F., Plattner, G. K., Steinacher, M., and Doney, S. C. (2009). Natural variability and anthropogenic trends in oceanic oxygen in a coupled carbon cycle-climate model ensemble. *Global Biogeochemical Cycles*, *23*(1), GB1003.
https://doi.org/10.1029/2008GB003316

Fuster, J. (1975). Las Islas Canarias: un ejemplo de evolución temporal y espacial del vulcanismo oceánico. *Estudios Geológicos*, *31*, 439–463.

Garcia, H. E., Boyer, T. P., Levitus, S., Locarnini, R. A., and Antonov, J. (2005). On the variability of dissolved oxygen and apparent oxygen utilization content for the upper world ocean: 1955 to 1998. *Geophysical Research Letters*, *32*(9), 1–4.
https://doi.org/10.1029/2004GL022286

García-Davis, S., Reyes, C. P., Lagunes, I., Padrón, J. M., Fraile-Nuez, E., Fernández, J. J., and Díaz-Marrero, A. R. (2021). Bioprospecting Antiproliferative Marine Microbiota From Submarine Volcano Tagoro. *Frontiers in Marine Science*, *8*.
https://doi.org/10.3389/fmars.2021.687701

Gómez-Letona, M., Arístegui, J., Ramos, A. G., Montero, M. F., and Coca, J. (2018). Lack of impact of the El Hierro (Canary Islands) submarine volcanic eruption on the local phytoplankton community. *Scientific Reports*, *8*(1), 1–12. https://doi.org/10.1038/s41598-018-22967-6

González-Santana, D., Santana-Casiano, J. M., González, A. G., and González-Dávila, M. (2022). Coastal carbonate system variability along an active lava–seawater interface. *Frontiers in Marine Science*, *9*. https://doi.org/10.3389/fmars.2022.952203

González-Vega, A., Arrieta, J. M., Santana-Casiano, M., González-Dávila, M., Santana-González, C., Mercado, J. M., Escánez-Pérez, J., Presas-Navarro, C., and Fraile-Nuez, E. (2023). Tagoro Submarine Volcano as a Natural Source of Significant Dissolved Inorganic Nutrients. In *Active Volcanoes of the World: Vol. Part F1209* (pp. 185–201). Springer Science and Business Media Deutschland GmbH. https://doi.org/10.1007/978-3-031-35135-8_9

González-Vega, A., Callery, I., Arrieta, J. M., Santana-Casiano, J. M., Domínguez-Yanes, J. F., and Fraile-Nuez, E. (2022). Severe Deoxygenation Event Caused by the 2011 Eruption of the Submarine Volcano Tagoro (El Hierro, Canary Islands). *Frontiers in Marine Science*, *9*(May), 1–10. https://doi.org/10.3389/fmars.2022.834691

González-Vega, A., Fraile-Nuez, E., Santana-Casiano, J. M., González-Dávila, M., Escánez-Pérez, J., Gómez-Ballesteros, M., Tello, O., and Arrieta, J. M. (2020). Significant Release of Dissolved Inorganic Nutrients From the Shallow Submarine Volcano Tagoro (Canary Islands) Based on Seven-Year Monitoring. *Frontiers in Marine Science*, *6*(January).
https://doi.org/10.3389/fmars.2019.00829

Gruber, N., and Deutsch, C. A. (2014). Redfield's evolving legacy. In *Nature Geoscience* (Vol. 7, Issue 12, pp. 853–855). https://doi.org/10.1038/ngeo2308

Guieu, C., Bonnet, S., Petrenko, A., Menkes, C., Chavagnac, V., Desboeufs, K., Maes, C., and Moutin, T. (2018). Iron from a submarine source impacts the productive layer of the Western Tropical South Pacific (WTSP). *Scientific Reports*, *8*(1), 1–9.
https://doi.org/10.1038/s41598-018-27407-z

Guillou, H., Carracedo, J. C., Pérez Torrado, F., and Rodriguez Badiola, E. (1996). K-Ar ages and magnetic stratigraphy of a hotspot-induced, fast grown oceanic island: El Hierro, Canary Islands. *Journal of Volcanology and Geothermal Research*, *73*(1–2), 141–155.
https://doi.org/10.1016/0377-0273(96)00021-2

Hoernle, K., and Schmincke, H.-U. (1993). *The Role of Partial Melting in the 15-Ma Geochemical Evolution of Gran Canada: A Blob Model for the Canary Hotspot*.
http://petrology.oxfordjournals.org/

Hoernle, K., Zhang, Y.-S., and Graham, D. (1995). Seismic and geochemical evidence for large-scale mantle upwelling beneath the eastern Atlantic and western and central Europe. *Nature*, *374*, 34–39.

Holik, J. S., Rabinowitz, P. D., and Austin, J. A. (1991). Effects of Canary hotspot volcanism on structure of oceanic crust off Morocco. *Journal of Geophysical Research*, *96*(B7). https://doi.org/10.1029/91jb00709

Holm-Hansen, O., Lorenzen, C. J., Holmes, R. W., and Strickland, J. D. H. (1965). Fluorometric Determination of Chlorophyll. *ICES Journal of Marine Science*, *30*(1), 3–15. https://academic.oup.com/icesjms/article/30/1/3/642386

IGN. (2022). *La erupción en cifras. Isla de La Palma 2021.* https://www.ign.es/resources/erupcion-la-palma-2021/Infografia-primer-aniversario.pdf

Johnson, H. P., and Embley, R. W. (1990). Axial seamount: An active ridge axis volcano on the Central Juan De Fuca Ridge. *Journal of Geophysical Research*, *95*(B8), 12689. https://doi.org/10.1029/jb095ib08p12689

Karl, D. M., Brittain, A. M., and Tilbrook, B. D. (1989). Hydrothermal and microbial processes at Loihi Seamount, a mid-plate hot-spot volcano. *Deep Sea Research Part A, Oceanographic Research Papers*, *36*(11), 1655–1673. https://doi.org/10.1016/0198-0149(89)90065-4

Karl, D. M., McMurtry, G. M., Malahoff, A., and Garcia, M. O. (1988). Loihi Seamount, Hawaii: A mid-plate volcano with a distinctive hydrothermal system. In *Nature* (Vol. 335, Issue 6190, pp. 532–535). https://doi.org/10.1038/335532a0

Karl, D. M., Taylor, G. T., Novitsky, J. A., Jannasch, H. W., Wirsen, C. O., Pace, N. R., Lane, D. J., Olsen, G. J., and Giovannoni, S. J. (1988). A microbiological study of Guaymas Basin high temperature hydrothermal vents. *Deep Sea Research Part A, Oceanographic Research Papers*, *35*(5), 777–791. https://doi.org/10.1016/0198-0149(88)90030-1

Keeling, R. F., Körtzinger, A., and Gruber, N. (2010). Ocean deoxygenation in a warming world. *Annual Review of Marine Science*, *2*(1), 199–229. https://doi.org/10.1146/annurev.marine.010908.163855

Kérouel, R., and Aminot, A. (1997). *Fluorometric determination of ammonia in sea and estuarine waters by direct segmented flow analysis.* *57*, 265–275. papers2://publication/uuid/F6C41321-4BD6-491F-A64A-11B800FD2A78

Kilias, S. P., Nomikou, P., Papanikolaou, D., Polymenakou, P. N., Godelitsas, A., Argyraki, A., Carey, S., Gamaletsos, P., Mertzimekis, T. J., Stathopoulou, E., Goettlicher, J., Steininger, R., Betzelou, K., Livanos, I., Christakis, C., Bell, K. C., and Scoullos, M. (2013). New insights into hydrothermal vent processes in the unique shallow-submarine arc-volcano, Kolumbo (Santorini), Greece. *Scientific Reports*, *3*, 1–13. https://doi.org/10.1038/srep02421

King, S. D., and Ritsema, J. (2000). African hot spot volcanism: small-scale convection in the upper mantle beneath cratons. *Science*, *290*, 1137–1140. www.sciencernag.org

Kipp, L. E., Sanial, V., Henderson, P. B., van Beek, P., Reyss, J. L., Hammond, D. E., Moore, W. S., and Charette, M. A. (2018). Radium isotopes as tracers of hydrothermal inputs and neutrally buoyant plume dynamics in the deep ocean. *Marine Chemistry*, *201*(June 2017), 51–65. https://doi.org/10.1016/j.marchem.2017.06.011

Klügel, A., Villinger, H., Römer, M., Kaul, N., Krastel, S., Lenz, K. F., and Wintersteller, P. (2020). Hydrothermal Activity at a Cretaceous Seamount, Canary Archipelago, Caused by Rejuvenated Volcanism. *Frontiers in Marine Science*, *7*. https://doi.org/10.3389/fmars.2020.584571

Kubota, T., Saito, T., and Nishida, K. (2022). Global fast-traveling tsunamis driven by atmospheric Lamb waves on the 2022 Tonga eruption. *Science*, *377*, 91–94. https://www.science.org

Kump, L. R., and Barley, M. E. (2007). Increased subaerial volcanism and the rise of atmospheric oxygen 2.5 billion years ago. *Nature*, *448*(7157), 1033–1036. https://doi.org/10.1038/nature06058

Kump, L. R., Kasting, J. F., and Barley, M. E. (2001). Rise of atmospheric oxygen and the "upside-down" Archean mantle. *Geochemistry, Geophysics, Geosystems*, *2*(1), n/a-n/a. https://doi.org/10.1029/2000gc000114

Lam, P., Cowen, J. P., and Jones, R. D. (2004). Autotrophic ammonia oxidation in a deep-sea hydrothermal plume. *FEMS Microbiology Ecology*, *47*(2), 191–206. https://doi.org/10.1016/S0168-6496(03)00256-3

Lam, P., Cowen, J. P., Popp, B. N., and Jones, R. D. (2008). Microbial ammonia oxidation and enhanced nitrogen cycling in the Endeavour hydrothermal plume. *Geochimica et Cosmochimica Acta*, *72*(9), 2268–2286. https://doi.org/10.1016/j.gca.2008.01.033

Langmann, B., Zakšek, K., Hort, M., and Duggen, S. (2010). Volcanic ash as fertiliser for the surface ocean. *Atmospheric Chemistry and Physics*, *10*(8), 3891–3899. https://doi.org/10.5194/acp-10-3891-2010

Leckie, R. M., Bralower, T. J., and Cashman, R. (2002). Oceanic anoxic events and plankton evolution: Biotic response to tectonic forcing during the mid-Cretaceous. *Paleoceanography*, *17*(3), 13-1-13–29. https://doi.org/10.1029/2001pa000623

León, R., Palomino, D., Sánchez-Guillamón, O., Fernández-Salas, L. M., and Vázquez, J. T. (2022). Tectonic control on sedimentary dynamics in intraplate oceanic settings: A geomorphological image of the eastern Canary Basin and insights on its middle-upper Miocene to quaternary volcano-tectonic-sedimentary evolution. *Marine Geology*, *445*. https://doi.org/10.1016/j.margeo.2022.106737

Little, S. A., Stolzenbach, K. D., and Von Herzen, R. P. (1987). Measurements of plume flow from a hydrothermal vent field. *Journal of Geophysical Research*, *92*(B3), 2587–2596. https://doi.org/10.1029/JB092iB03p02587

López, C., Blanco, M. J., Abella, R., Brenes, B., Cabrera Rodríguez, V. M., Casas, B., Domínguez Cerdea, I., Felpeto, A., De Villalta, M. F., Del Fresno, C., García, O., García-Arias, M. J., García-Cañada, L., Gomis Moreno, A., Gonzlez-Alonso, E., Guzmn Pérez, J., Iribarren, I., López-Díaz, R., Luengo-Oroz, N., … Villasante-Marcos, V. (2012). Monitoring the volcanic unrest of El Hierro (Canary Islands) before the onset of the 2011-2012 submarine eruption. *Geophysical Research Letters*, *39*(13), 1–7. https://doi.org/10.1029/2012GL051846

Lough, A. J. M., Connelly, D. P., Homoky, W. B., Hawkes, J. A., Chavagnac, V., Castillo, A., Kazemian, M., Nakamura, K. I., Araki, T., Kaulich, B., and Mills, R. A. (2019). Diffuse hydrothermal venting: A hidden source of iron to the oceans. *Frontiers in Marine Science*, *6*(JUL), 1–14. https://doi.org/10.3389/fmars.2019.00329

Lozano-Rodríguez, J. A., Gómez-Ballesteros, M., Vázquez, J.-T., García, M., Casillas, R., Sánchez-Guillamón, O., Arrese, B., Presas-Navarro, C., Martín-Díaz, J. P., González-Vega, A., Álvarez-Valero, A. M., Polo-Sánchez, A., and Fraile-Nuez, E. (2023). Effects of the lava flows associated to the Tajogaite volcano eruption (2021) on the insular shelf and slope of La Palma island. *10.ª Asamblea Hispano-Portuguesa de Geodesia y Geofísica - Artículos*, 690–697.

Lupton, J. E., Baker, E. T., and Massoth, G. J. (1989). Variable 3He/heat ratios in submarine hydrothermal systems: evidence from two plumes over the Juan de Fuca ridge. In *Nature* (Vol. 337, Issue 6203, pp. 161–164). https://doi.org/10.1038/337161a0

Lupton, J. E., Baker, E. T., Massoth, G. J., Thomson, R. E., Burd, B. J., Butterfield, D. A., Embley, R. W., and Cannon, G. A. (1995). Variations in water-column ^{3}He/heat ratios associated with the 1993 CoAxial event, Juan de Fuca Ridge. *Geophysical Research Letters*, *22*(2), 155–158. https://doi.org/10.1029/94GL02797

Malahoff, A., Kolotyrkina, I. Y., Midson, B. P., and Massoth, G. J. (2006). A decade of exploring a submarine intraplate volcano: Hydrothermal manganese and iron at Lōihi volcano, Hawai'i. *Geochemistry, Geophysics, Geosystems*, *7*(6), Q06002. https://doi.org/10.1029/2005GC001222

Malmberg, S. A. (1965). *A report on the temperature effect of the Surtsey eruption on the sea water.*

Mantas, V. M., Pereira, A. J. S. C., and Morais, P. V. (2011). Plumes of discolored water of volcanic origin and possible implications for algal communities. The case of the Home Reef eruption of 2006 (Tonga, Southwest Pacific Ocean). *Remote Sensing of Environment*, *115*(6), 1341–1352. https://doi.org/10.1016/j.rse.2011.01.014

Marcello, J., Eugenio, F., Estrada-Allis, S., and Sangrà, P. (2015). Segmentation and tracking of anticyclonic eddies during a submarine volcanic eruption using ocean colour imagery. *Sensors (Switzerland)*, *15*(4), 8732–8748. https://doi.org/10.3390/s150408732

Martín-Sosa, P. (2017). La pesca artesanal y la conservación de la biodiversidad: avances en la gestión integrada de la pesca y el medio ambiente en el mar de Canarias. In J. Afonso-Carrillo (Ed.), *Investigando el mar: Viaje al planeta agua. Acta XII Semana Científica Telesforo Bravo. Instituto de Estudios Hispánicos de Canarias* (pp. 71–104). www.retoqueec.com

Masson, D. G. (1996). Catastrophic collapse of the volcanic island of Hierro 15 ka ago and the history of landslides in the Canary Islands. *Geology*, *24*(3), 231–234.

Masson, D. G., Watts, A. B., Gee, M. J. R., Urgeles, R., Mitchell, N. C., Le Bas, T. P., and Canals, M. (2002). Slope failures on the flanks of the western Canary Islands. *Earth-Science Reviews*, *57*, 1–35. www.elsevier.comrlocaterearscirev

Massoth J.*, G., Butterfield A., D., Lupton E., J., McDuff E., R., Lilley D., M., and Jonasson R., I. (1989). Submarine venting of phase-separated hydrothermal fluids at Axial Volcano, Juan de Fuca Ridge. *Nature*, *340*, 702–705.

Mather, T. A. (2015). Volcanoes and the environment: Lessons for understanding Earth's past and future from studies of present-day volcanic emissions. In *Journal of Volcanology and Geothermal Research* (Vol. 304, pp. 160–179). Elsevier B.V. https://doi.org/10.1016/j.jvolgeores.2015.08.016

Mattox, T. N., and Mangan, M. T. (1997). Littoral hydrovolcanic explosions: a case study of lava-seawater interaction at Kilauea Volcano. In *Journal of Volcanology and Geothermal Research* (Vol. 75).

McCarthy, K. T., Pichler, T., and Price, R. E. (2005). Geochemistry of Champagne Hot Springs shallow hydrothermal vent field and associated sediments, Dominica, Lesser Antilles. *Chemical Geology*, *224*(1–3), 55–68. https://doi.org/10.1016/j.chemgeo.2005.07.014

McDougall, I. (1971). Volcanic island chains and sea floor spreading. *Nature Physical Science*, *231*, 141–144.

Méhay, S., Keller, C. E., Bermasconi, S. M., Weissert, H., Erba, E., Bottini, C., and Hochuli, P. A. (2009). A volcanic CO_2 pulse triggered the Cretaceous oceanic Anoxic event 1a and a biocalcification crisis. *Geology*, *37*(9), 819–822. https://doi.org/10.1130/G30100A.1

Mezcua, J., and Rueda, J. (2023). Seismic swarms and earthquake activity b-value related to the September 19, 2021, La Palma volcano eruption in Cumbre Vieja, Canary Islands (Spain). *Bulletin of Volcanology*, *85*(5). https://doi.org/10.1007/s00445-023-01646-z

Mitchell, N. (2012). Submarine volcanism: Hot, cracking rocks deep down. *Nature Geoscience*, *5*(7), 444–445. https://doi.org/10.1038/ngeo1505

Moore, J. G., Phillips, R. L., Grigg, R. W., Peterson, D. W., and Swanson, D. A. (1973). Flow of lava into the sea, 1969-1971, Kilauea volcano, Hawaii. *Geological Society of America Bulletin*, *84*, 537–546.

Morgan, W. J. (1971). Convection plumes in the lower mantle. *Nature*, *230*, 42–43.

Mortlock, R. A., Froelich, P. N., Feely, R. A., Massoth, G. J., Butterfield, D. A., and Lupton, J. E. (1993). Silica and germanium in Pacific Ocean hydrothermal vents and plumes. *Earth and Planetary Science Letters*, *119*(3), 365–378. https://doi.org/10.1016/0012-821X(93)90144-X

Negredo, A. M., van Hunen, J., Rodríguez-González, J., and Fullea, J. (2022). On the origin of the Canary Islands: Insights from mantle convection modelling. *Earth and Planetary Science Letters*, *584*. https://doi.org/10.1016/j.epsl.2022.117506

Nojiri, Y., Ishibashi, J. I., Kawai, T., Otsuki, A., and Sakai, H. (1989). Hydrothermal plumes along the North Fiji Basin spreading axis. *Nature*, *342*(6250), 667–670. https://doi.org/10.1038/342667a0

Ono, T., Midorikawa, T., Watanabe, Y. W., Tadokoro, K., and Saino, T. (2001). Temporal increases of phosphate and apparent oxygen utilization in the subsurface water of western subarctic Pacific from 1968 to 1998. *Geophysical Research Letters*, *28*(17), 3285–3288. https://doi.org/10.1029/2001GL012948

Oyarzun, R., Doblas, M., López-Ruiz, J., and Cebriá, J. M. (1997). Opening of the central Atlantic and asymmetric mantle upwelling phenomena: Implications for long-lived magmatism in western North Africa and Europe. *Geology*, *25*(8), 727–730.

Paytan, A., and McLaughlin, K. (2007). The oceanic phosphorus cycle. *Chemical Reviews*, *107*(2), 563–576. https://doi.org/10.1021/cr0503613

Plattner, G. K., Joos, F., and Stocker, T. F. (2002). Revision of the global carbon budget due to changing air-sea oxygen fluxes. *Global Biogeochemical Cycles*, *16*(4), 43-1-43–12. https://doi.org/10.1029/2001gb001746

Plattner, G. K., Joos, F., Stocker, T. F., and Marchal, O. (2001). Feedback mechanisms and sensitivities of ocean carbon uptake under global warming. *Tellus, Series B: Chemical and Physical Meteorology*, *53*(5), 564–592. https://doi.org/10.3402/tellusb.v53i5.16637

Prol-Ledesma, R. M., Canet, C., Torres-Vera, M. A., Forrest, M. J., and Armienta, M. A. (2004). Vent fluid chemistry in Bahía Concepción coastal submarine hydrothermal system, Baja California Sur, Mexico. *Journal of Volcanology and Geothermal Research*, *137*(4), 311–328. https://doi.org/10.1016/j.jvolgeores.2004.06.003

Ramalho, R. S., Quartau, R., Trenhaile, A. S., Mitchell, N. C., Woodroffe, C. D., and Ávila, S. P. (2013). Coastal evolution on volcanic oceanic islands: A complex interplay between volcanism, erosion, sedimentation, sea-level change and biogenic production. In *Earth-Science Reviews* (Vol. 127, pp. 140–170). https://doi.org/10.1016/j.earscirev.2013.10.007

Resing, J. A., Baker, E. T., Lupton, J. E., Walker, S. L., Butterfield, D. A., Massoth, G. J., and Nakamura, K. I. (2009). Chemistry of hydrothermal plumes above submarine volcanoes of the Mariana arc. *Geochemistry, Geophysics, Geosystems*, *10*(2), 1–23. https://doi.org/10.1029/2008GC002141

Resing, J. A., and Sansone, F. J. (1999). *The chemistry of lava-seawater interactions: The generation of acidity*.

Resing, J. A., Sedwick, P. N., German, C. R., Jenkins, W. J., Moffett, J. W., Sohst, B. M., and Tagliabue, A. (2015). Basin-scale transport of hydrothermal dissolved metals across the South Pacific Ocean. *Nature*, *523*(7559), 200–203. https://doi.org/10.1038/nature14577

Rivera, J., Lastras, G., Canals, M., Acosta, J., Arrese, B., Hermida, N., Micallef, A., Tello, O., and Amblas, D. (2013). Construction of an oceanic island: Insights from the El Hierro (Canary Islands) 2011-2012 submarine volcanic eruption. *Geology*, *41*(3), 355–358. https://doi.org/10.1130/G33863.1

Rodriguez-Gonzalez, A., Fernandez-Turiel, J. L., Aulinas, M., Cabrera, M. C., Prieto-Torrell, C., Rodriguez, G. A., Guillou, H., and Perez-Torrado, F. J. (2022). Lava deltas, a key landform in oceanic volcanic islands: El Hierro, Canary Islands. *Geomorphology*, *416*. https://doi.org/10.1016/j.geomorph.2022.108427

Román, A., Tovar-Sánchez, A., Roque-Atienza, D., Huertas, I. E., Caballero, I., Fraile-Nuez, E., and Navarro, G. (2022). Unmanned aerial vehicles (UAVs) as a tool for hazard assessment: The 2021 eruption of Cumbre Vieja volcano, La Palma Island (Spain). *Science of the Total Environment*, *843*. https://doi.org/10.1016/j.scitotenv.2022.157092

Rona, P. A., and Speer, K. G. (1989). An Atlantic hydrothermal plume: Trans-Atlantic Geotraverse (TAG) area, Mid-Atlantic Ridge crest near 26°N. *Journal of Geophysical Research*, *94*(B10), 879–893. https://doi.org/10.1029/jb094ib10p13879

Rona, P. A., and Trivett, D. A. (1992). Discrete and diffuse heat transfer at ashes vent field, Axial Volcano, Juan de Fuca Ridge. *Earth and Planetary Science Letters*, *109*(1–2), 57–71. https://doi.org/10.1016/0012-821X(92)90074-6

Sangrà, P., Pascual, A., Rodríguez-Santana, Á., Machín, F., Mason, E., McWilliams, J. C., Pelegrí, J. L., Dong, C., Rubio, A., Arístegui, J., Marrero-Díaz, Á., Hernández-Guerra, A., Martínez-Marrero, A., and Auladell, M. (2009). The Canary Eddy Corridor: A major pathway for long-lived eddies in the subtropical North Atlantic. *Deep-Sea Research Part I: Oceanographic Research Papers*, *56*(12), 2100–2114. https://doi.org/10.1016/j.dsr.2009.08.008

Sansone, F. J., and Resing, J. A. (1995). Hydrography and geochemistry of sea surface hydrothermal plumes resulting from Hawaiian coastal volcanism. *Journal of Geophysical Research*, *100*(C7). https://doi.org/10.1029/95jc01120

Sansone, F. J., Resing, J. A., Tribble, G. W., Sedwick, P. N., Kelly, K. M., and Hon, K. (1991). Lava-seawater interactions at shallow-water submarine lava flows. *Geophysical Research Letters*, *18*(9), 1731–1734. https://doi.org/10.1029/91GL01279

Santana-Casiano, J. M., Fraile-Nuez, E., González-Dávila, M., Baker, E. T., Resing, J. A., and Walker, S. L. (2016). Significant discharge of CO 2 from hydrothermalism associated with

the submarine volcano of El Hierro Island. *Scientific Reports*, *6*(May), 1–9. https://doi.org/10.1038/srep25686

Santana-Casiano, J. M., González-Dávila, M., Fraile-Nuez, E., De Armas, D., González, A. G., Domínguez-Yanes, J. F., and Escánez, J. (2013). The natural ocean acidification and fertilization event caused by the submarine eruption of El Hierro. *Scientific Reports*, *3*, 5–12. https://doi.org/10.1038/srep01140

Santana-González, C., Santana-Casiano, J. M., González-Dávila, M., and Fraile-Nuez, E. (2017). Emissions of Fe(II) and its kinetic of oxidation at Tagoro submarine volcano, El Hierro. *Marine Chemistry*, *195*(Ii), 129–137. https://doi.org/10.1016/j.marchem.2017.02.001

Sarradin, P.-M., Caprais, J.-C., Riso, R., Kerouel, R., and Aminot, A. (1999). Chemical environment of the hydrothermal mussel communities in the Lucky Strike and Menez Gwen vent fields, Mid Atlantic Ridge. *Cahiers de Biologie Marine*, *40*(February), 93–104.

Schmincke, H. (1973). Magmatic evolution and tectonic regime in the Canary, Madeira, and Azores islad groups. *Geological Society of America Bulletin*, *84*, 633–648.

Schopf, J. W. (1993). Microfossils of the early Archean apex chert: New evidence of the antiquity of life. *Science*, *260*(5108), 640–646. https://doi.org/10.1126/science.260.5108.640

Sedwick, P., and Stüben, D. (1996). Chemistry of shallow submarine warm springs in an arc-volcanic setting: Vulcano Island, Aeolian Archipelago, Italy. *Marine Chemistry*, *53*(1–2), 147–161. https://doi.org/10.1016/0304-4203(96)00020-5

Sharp, J., Pierrot, D., Humphreys, M., Epilaton, J., Orr, J., and Lewis, E. (2020). *CO2SYSv3 for MATLAB*. Zenodo. https://doi.org/10.5281/ZENODO.3950563

Snow, L. J., Duncan, R. A., and Bralower, T. J. (2005). Trace element abundances in the Rock Canyon Anticline, Pueblo, Colorado, marine sedimentary section and their relationship to Caribbean plateau construction and ocean anoxic event 2. *Paleoceanography*, *20*(3), 1–14. https://doi.org/10.1029/2004PA001093

Sobradelo, R., Martí, J., Mendoza-Rosas, A. T., and Gómez, G. (2011). Volcanic hazard assessment for the Canary Islands (Spain) using extreme value theory. *Natural Hazards and Earth System Science*, *11*(10), 2741–2753. https://doi.org/10.5194/nhess-11-2741-2011

Sorokin, Y. I., Sorokin, P. Y., and Zakuskina, O. Y. (1998). Microplankton and its functional activity in zones of shallow hydrotherms in the Western Pacific. *Journal of Plankton Research*, *20*(6), 1015–1031. https://doi.org/10.1093/plankt/20.6.1015

Sotillo, M. G., Cailleau, S., Lorente, P., Levier, B., Aznar, R., Reffray, G., Amo-Baladrón, A., Chanut, J., Benkiran, M., and Alvarez-Fanjul, E. (2015). The myocean IBI ocean forecast and reanalysis systems: Operational products and roadmap to the future copernicus service. *Journal of Operational Oceanography*, *8*(1), 63–79. https://doi.org/10.1080/1755876X.2015.1014663

Sotomayor-García, A., Rueda, J. L., Sánchez-Guillamón, O., Urra, J., Vázquez, J. T., Palomino, D., Fernández-Salas, L. M., López-González, N., González-Porto, M., Santana-Casiano, J. M., González-Dávila, M., Presas-Navarro, C., and Fraile-Nuez, E. (2019). First macro-colonizers and survivors around tagoro Submarine Volcano, Canary Islands, Spain. *Geosciences (Switzerland)*, *9*(1). https://doi.org/10.3390/geosciences9010052

Soule, S. A., Zoeller, M., and Parcheta, C. (2021). Submarine lava deltas of the 2018 eruption of Kīlauea volcano. *Bulletin of Volcanology*, *83*(4). https://doi.org/10.1007/s00445-020-01424-1

Speer, K. G., and Rona, P. A. (1989). A model of an Atlantic and Pacific hydrothermal plume. *Journal of Geophysical Research*, *94*(C5), 6213. https://doi.org/10.1029/jc094ic05p06213

Staudigel, H., Hart, S. R., Pile, A., Bailey, B. E., Baker, E. T., Brooke, S., Connelly, D. P., Haucke, L., German, C. R., Hudson, I., Jones, D., Koppers, A. A. P., Konter, J., Lee, R., Pietsch, T. W., Tebo, B. M., Templeton, A. S., Zierenberg, R., and Young, C. M. (2006). Vailulu'u seamount, Samoa: Life and death on an active submarine volcano. *Proceedings of the National Academy of Sciences of the United States of America*, *103*(17), 6448–6453. https://doi.org/10.1073/pnas.0600830103

Stetter, K. O. (1982). Ultrathin mycelia-forming organisms from submarine volcanic areas having an optimum growth temperature of 105 °C. *Nature*, *300*(5889), 258–260. https://doi.org/10.1038/300258a0

Stramma, L., Brandt, P., Schafstall, J., Schott, F., Fischer, J., and Körtzinger, A. (2008). Oxygen minimum zone in the North Atlantic south and east of the Cape Verde Islands. *Journal of Geophysical Research: Oceans*, *113*(4), 1–15. https://doi.org/10.1029/2007JC004369

Sverdrup, H. U. (1938). On the explanation of the oxygen minima and maxima in the oceans. *ICES Journal of Marine Science*, *13*(2), 163–172. https://doi.org/10.1093/icesjms/13.2.163

Tarasov, V. G., Gebruk, A. V., Mironov, A. N., and Moskalev, L. I. (2005). Deep-sea and shallow-water hydrothermal vent communities: Two different phenomena? *Chemical Geology*, *224*(1–3), 5–39. https://doi.org/10.1016/j.chemgeo.2005.07.021

Tarasov, V. G., Propp, M. V., Propp, L. N., Zhirmunsky, A. V., Namsakakv, B. B., Gorlenko, V. M., and Starynin, D. A. (1990). Shallow-Water Gasohydrothermal Vents of Ushishir Volcano and the Ecosystem of Kraternaya Bight (The Kurile Islands). *Marine Ecology*, *11*(1), 1–23. https://doi.org/10.1111/j.1439-0485.1990.tb00225.x

Thorarinsson, S. (1967). The Surtsey eruption and related scientific work. *Polar Record*, *13*(86), 571–578. https://doi.org/10.1017/S0032247400058113

Tilliette, C., Taillandier, V., Grima, N., Maes, C., and Montanes, M. (2022). *Dissolved Iron Patterns Impacted by Shallow Hydrothermal Sources Along a Transect Through the Tonga-Kermadec Arc Global Biogeochemical Cycles*. 1–27. https://doi.org/10.1029/2022GB007363

Tréguer, P. J., and De La Rocha, C. L. (2013). The world ocean silica cycle. *Annual Review of Marine Science*, *5*(January 2013), 477–501. https://doi.org/10.1146/annurev-marine-121211-172346

Treguer, P., and Le Corre, P. (1979). The ratios of nitrate, phosphate, and silicate during uptake and regeneration phases of the Moroccan upwelling regime. *Deep Sea Research Part A, Oceanographic Research Papers*, *26*(2), 163–184. https://doi.org/10.1016/0198-0149(79)90074-8

Treguer, P., Tréguer, P., Nelson, D. M., Van Bennekom, A. J., DeMaster, D. J., Leynaert, A., and Quéguiner, B. (1995). The silica balance in the world ocean: a reestimate. *Science*, *268*, 375–379.

Tunnicliffe, V., Botros, M., De Burgh, M. E., Dinet, A., Johnson, H. P., Juniper, S. K., and McDuff, R. E. (1986). Hydrothermal vents of Explorer Ridge, northeast Pacific. *Deep Sea Research Part A, Oceanographic Research Papers*, *33*(3), 401–412. https://doi.org/10.1016/0198-0149(86)90100-7

Urgeles, R., Canals, M., and Masson, D. (2001). Flank stability and processes off the western Canary Islands: a review from El Hierro and La Palma. *Scientia Marina*, *65*, 21–31.

Van Heuven, S., Pierrot Rae, J., Lewis, E., and Wallace, D. (2011). *MATLAB program developed for CO₂ System Calculations. ORNL/CDIAC-105b*. Carbon Dioxide Information Analysis Center (Oak Ridge, Tenn: Oak Ridge Natl. Lab., US Dep. of Energy).

Vázquez, J. T., Palomino, D., Sánchez-Guillamón, O., Martínez-Carreño, N., Fernández-Salas, L. M., Gómez-Ballestero, M., Lozano, P., Meletlidis, S., Presas-Navarro, C., Tello, O., and Fraile-Nuez, E. (2021). Análisis de las características morfoestructurales del volcán de Enmedio (Islas Canarias). In J. Errandonea Martín, I. Gárate Olave, S. García de Madinabeitia, and F. Sarrionaindia Eguidazu (Eds.), *X Congreso Geológico de España* (pp. 350–350). Sociedad Geológica de España. http://www.sociedadgeologica.orghttp://www.sociedadgeologica.org

Villasante-Marcos, V., and Pavón-Carrasco, F. J. (2014). Palaeomagnetic constraints on the age of Lomo Negro volcanic eruption (El Hierro, Canary Islands). *Geophysical Journal International*, *199*(3), 1497–1514. https://doi.org/10.1093/gji/ggu346

Vogt, P. R. (1989). Volcanogenic upwelling of anoxic, nutrient-rich water: a possible factor in carbonate-bank/reef demise and benthic faunal extinctions? *Geological Society of America Bulletin*, *101*(10), 1225–1245. https://doi.org/10.1130/0016-7606(1989)101<1225:VUOANR>2.3.CO;2

Von Damm, K. L., Edmond, J. M., Grant, B., Measures, C. I., Walden, B., and Weiss, R. F. (1985). Chemistry of submarine hydrothermal solutions at 21 °N, East Pacific Rise. *Geochimica et Cosmochimica Acta*, *49*(11), 2197–2220. https://doi.org/10.1016/0016-7037(85)90222-4

Watton, T. J., Jerram, D. A., Thordarson, T., and Davies, R. J. (2013). Three-dimensional lithofacies variations in hyaloclastite deposits. *Journal of Volcanology and Geothermal Research*, *250*, 19–33. https://doi.org/10.1016/j.jvolgeores.2012.10.011

Watts, A. B. (1994). Crustal structure, gravity anomalies and flexure of the lithosphere in the vicinity of the Canary Islands. *Geophysical Journal International*, *119*(2), 648–666. https://doi.org/10.1111/j.1365-246X.1994.tb00147.x

Weiss, R. F. (1970). The solubility of nitrogen, oxygen and argon in water and seawater. *Deep-Sea Research and Oceanographic Abstracts*, *17*(4), 721–735. https://doi.org/10.1016/0011-7471(70)90037-9

Wenzhofer, F., Holby, O., Glud, R. N., Nielsen, H. K., and Gundersen, J. K. (2000). In situ microsensor studies of a shallow water hydrothermal vent at Milos, Greece. *Marine Chemistry*, *69*, 43–54.

Whiteside, A., Dupouy, C., Singh, A., Bani, P., Tan, J., and Frouin, R. (2023). Impact of ashes from the 2022 Tonga volcanic eruption on satellite ocean color signatures. *Frontiers in Marine Science*, *9*. https://doi.org/10.3389/fmars.2022.1028022

Whitney, F. A., Freeland, H. J., and Robert, M. (2007). Persistently declining oxygen levels in the interior waters of the eastern subarctic Pacific. *Progress in Oceanography*, *75*(2), 179–199. https://doi.org/10.1016/j.pocean.2007.08.007

Wilson, J. T. (1963). A possible origin of the Hawaiian Islands. *Canadian Journal of Physics*, *41*, 863–870. www.nrcresearchpress.com

Wilson, S. T., Hawco, N. J., Armbrust, E. V., Barone, B., Björkman, K. M., Boysen, A. K., Burgos, M., Burrell, T. J., Casey, J. R., DeLong, E. F., Dugenne, M., Dutkiewicz, S., Dyhrman, S. T., Ferrón, S., Follows, M. J., Foreman, R. K., Funkey, C. P., Harke, M. J., Henke, B. A., … Karl, D. M. (2019). Kīlauea lava fuels phytoplankton bloom in the North Pacific Ocean. *Science*, *365*(6457), 1040–1044. https://doi.org/10.1126/science.aax4767

Witt, V., Ayris, P. M., Damby, D. E., Cimarelli, C., Kueppers, U., Dingwell, D. B., and Wörheide, G. (2017). Volcanic ash supports a diverse bacterial community in a marine mesocosm. *Geobiology*, *15*(3), 453–463. https://doi.org/10.1111/gbi.12231

Wyrtki, K. (1962). The oxygen minima in relation to ocean circulation. *Deep-Sea Research and Oceanographic Abstracts*, *9*(1–2), 11–23. https://doi.org/10.1016/0011-7471(62)90243-7